



STRUCTURAL AND METAMORPHIC RELATIONS  
BETWEEN LOW, MEDIUM AND HIGH GRADE  
ROCKS, MT FRANKS - MUNDI MUNDI AREA,  
BROKEN HILL, N.S.W.

by

Richard Arthur Glen, B.Sc.(Hons.) (Sydney)

PART II

of two parts plus Appendices

Department of Geology and Mineralogy  
University of Adelaide  
April, 1978.

*Awarded December 1978*

## 6.1 INTRODUCTION.

This chapter describes the macroscopic geometry of the Mt Franks - Mundi Mundi area. In the following chapter, Chapter 7, the scope of this discussion is extended northwards, and macroscopic features, together with meso- and microscopic features of areas to the north are described so that a structural and metamorphic synthesis of the northwestern part of the Willyama Complex can be attempted. This synthesis suggests that rocks in the northwestern part of the Willyama Complex share a common structural and metamorphic history because of their position in the western limb of a regional  $F_1$  syncline.

6.1.1 Principles of Mapping

The principles of structural mapping in a complexly deformed terrain have been recently summarised by Hobbs et al (1976, pp.371-375). In the Mt Franks - Mundi Mundi area, the existence and distribution of major structures were determined in four ways:

- 1) by following out marker horizons where possible,
- 2) by changes in bedding orientation in uniform lithologies,
- 3) by changes in younging directions, and
- 4) by changes in the vergence of different generations of mesoscopic structures discussed in Chapter 3.

In the virtual absence of refolded folds and lineations, the main criteria for the establishment of different generations of macroscopic folds are changes in vergence of mesoscopic structures and the overprinting of schistosity.

The establishment of sedimentary younging direction as discussed in Section 2.3.3 provides a powerful tool in the positioning of major fold hinges. For the purpose of finding "way upness," sedimentary structures were divided into three classes - good, moderately good and doubtful. Both 'good' and 'moderately good' structures show unequivocal directions of

younging, but 'moderately good' structures are less convincing. 'Doubtful' structures yield uncertain directions. Altogether, 116 younging directions from 101 different localities were determined throughout the area. Slightly over half of these were located in the Mt Franks facies.

### 6.1.2 Data Presentation

The following discussion of macroscopic structure will not be accompanied by a 'routine' description of homogeneous sub areas and orientation data on equal area plots. Rather, these are presented in Appendix III. However, key data from these orientation plots and plots of data themselves from critical areas are discussed in, and interleaved with, the text. The map of sub area boundaries from Appendix II, is reproduced as Map 2 in the back pocket of this thesis, so that it can be used as a reference for the location of critical structures described in the text.

The following maps and figures will be used as bases for the ensuing discussion:

- Map 1 - pocket, back of Volume II
  - Map 2 - sub area boundaries and  $S_{1P}$ ,  $S_{1N}$  boundary, pocket, back of Volume II
  - Map 3 - Relations in the Mt Franks Area, pocket, back of Volume II
  - Map 4 - Relations on Mt Franks, pocket, back of Volume II
- Interleaved with the text
- Fig. 6.1 - Sedimentary younging directions and bedding trend
  - Fig. 6.2 - Structural Map,  $D_1$  event
  - Fig. 6.3 - Structural Map,  $D_3$  event
  - Fig. 6.4 - Structural Map,  $D_2$  and  $D_4$  events

Other figures will be cited as they are referred to in the text.

## 6.2 MACROSCOPIC STRUCTURE.

Sedimentary younging directions together with the broad geometry of bedding ( $S_0$ ) are shown in Fig. 6.1. Despite the disruption of the area into three blocks - eastern, central and western - by the northeast trending

Apollyon Valley and Mt Franks Retrograde Schist Zones, bedding is consistently eastward younging in the western and central blocks and there is a possibility that it is eastward younging in the eastern block. Bedding trends and dips indicate the influence of only two regional folds throughout the area. In the central block between the two retrograde schist zones, bedding outlines steeply north plunging folds which are parasitic on a major synformal hinge lying to the east, but which is now obscured by the Apollyon Valley Retrograde Schist Zone. In the western part of the western block, bedding is folded around a major southwest plunging synform. Younging directions indicate that whereas the first synform is upward facing, the second synform is downward facing. This problem of two oppositely facing adjacent synforms without any obvious intervening antiform, as well as other aspects of the geometry in the area are analysed in terms of superposed deformations. It will be shown that the major upward facing synform is  $F_1$  in age, and that the downward facing synform is  $F_3$  in age.

The major folds in bedding outlined in Fig. 6.1 are classified into different generations in Figs. 6.2, 6.3 and 6.4. Both the  $D_1$  and the  $D_3$  events are major fold forming and schistosity forming events.  $D_2$  and  $D_4$  events (Fig. 6.4) on the other hand, are relatively minor fold forming events and of these only  $D_2$  is associated with schistosity formation, and then on a very localised scale. Most of the obvious macroscopic folds in the eastern and western blocks are  $F_3$ ;  $F_1$  folds predominate in the central block.

Figure 6.2 also demonstrates the presence of large domains characterised by different bedding/schistosity relations. Bedding-parallel schistosity ( $S_{1P}$ ) occurs in the eastern block and in much of the western block. Non parallel relations ( $S_{1N}$ ) dominate the central block, and also occur in the western block. In the western block,  $S_{1N}$  relations are best seen just west of the Mt Franks Retrograde Schist Zone, but they also occur in a small area in the centre of the block. One boundary between  $S_{1P}$  and  $S_{1N}$  domains lies along the Apollyon Valley Retrograde Schist Zone. All the other

boundaries are localised wholly within the Robe Beds. The major  $S_{1P}$  and  $S_{1N}$  domains are not directly related to any macroscopic fold in the area. Relations between  $S_{1P}$  and  $S_{1N}$  are discussed in Section 6.2.3.4 where two models are discussed: overprinting of  $S_{1P}$  by  $S_{1N}$  and equivalence of  $S_{1P}$  and  $S_{1N}$ . Anderson (1966) suggested that  $S_{1P}$  and  $S_{1N}$  of this study are equivalent.

The macroscopic structure of the whole area will now be discussed starting from the eastern block (east of the Apollyon Valley Retrograde Schist Zone) and moving west to the central block between the Apollyon Valley and Mt Franks Retrograde Schist Zones and then only the western block west of the Mt Franks Retrograde Schist Zone.

#### 6.2.1 Macroscopic Structure of the Parnell Beds in the Eastern Block

(subarea 25, Map 2)

Limited traversing in the pseudomorphically retrogressed Parnell Beds has indicated that it is dominated by a pervasive schistosity ( $S_1$ ) which strikes northeast and which dips at about  $60^\circ$  to the southeast. Bedding, where visible, lies parallel to  $S_1$ , and also lies parallel to a disrupted amphibolite marker unit which occurs in the northern part of the block. Because of the pseudomorphous  $M_3$  retrogression, graded bedding is hard to recognise, and even where it is present, it is difficult to assign an unequivocal direction of younging to them. Nevertheless, 'doubtful' younging directions from two scattered areas (Loc. 5332 4856 and Loc. 5324 4833 ) may possibly suggest that bedding youngs to the southeast and is therefore right way up.

With the exception of late stage  $F_3$  parasitic folds, no closures have been recognised.  $F_3$  folds are upright with a northeast trend and are either dextral southwest plunging or sinistral northeast plunging. They are thus parasitic on an  $F_3$  synform lying east of the area mapped and are consistent with the sense and plunge of minor  $D_3$  structures in bedding across the Apollyon Valley Retrograde Schist Zone (northeast plunging, sinistral).

### 6.2.2 Macroscopic Structure of the Apollyon Beds in the Central Block

(subareas 1, 2, 8, 9, Map 2)

A series of steeply north plunging folds in the southern part of the Apollyon Beds is outlined by:

- 1) calc silicate bands,
- 2) bedding in quartz mica schist, and
- 3) the boundary between carbonaceous schist and quartz mica schist (which locally lies along a narrow retrograde zone).

From north to south, these folds consist of two sinistral fold pairs and a complimentary synform/-antiform pair which is best outlined by calc silicates. This last fold pair can be traced along the axial surface trend to the northeast where it intersects hinges in the quartz mica schist/carbonaceous schist boundaries (Fig. 6.5). Because of strong retrogression around the antiformal hinge, and because this hinge is cut off by the Apollyon Valley Retrograde Schist Zone, it is not known whether:

1. this synform/antiform pair constitutes a sinistral fold pair in the western limb of a major synform obscured by the retrograde zone, or
2. the synformal hinge represents the major synformal axis and the antiform is actually part of a dextral fold pair in its eastern limb.

The shape of small scale structures in the antiformal hinge is not considered indicative of either model because it is not known if the most easterly hinge which controls the shape of the eastern limb is visible or obscured by retrogression or alluvium. Similarly, the presence of a fault sliver of calc silicates at Locality 5325 4863 may be accounted for by either model since neither the amount of horizontal or vertical displacement across the retrograde zone is known. Until definite evidence in favour of model 2 is brought forward, model 1 is used as a working hypothesis, viz., that these folds are all parasitic on a major synform obscured by the retrograde zone. In reality, there is little difference between these models in any regional structural reconstruction since the axial trace of the synform in model 2 is

is also truncated by the Apollyon Valley Retrograde Schist Zone.

Scattered younging data in Fig. 6.5 and younging data north of this area suggest that these folds are upward facing. The antiformal hinge plunges steeply north (Fig. 6.5a) and the shared limb of the major synform/antiform pair is best outlined by a continuous band of west dipping calc silicates (Fig. 6.5). A second more easterly band of calc silicates may also outline this limb but is marked by mesoscopic plunge reversals. Equal area plots around the synformal axis (Fig. 6.5b) indicate a steep northerly plunge. In the western limb of the synform, calc silicates are discontinuous and grade into quartz mica schists with a decrease in the amount of calc silicate minerals. At least three separate calc silicate horizons can be distinguished in this limb. In addition, a pod of calc silicates occurs within the Mt Franks Retrograde Schist Zone, along the inferred strike of other calc silicate bands.

In the western limb of the major synform, two congruent parasitic fold pairs are also steeply north plunging but may be marked by overturning of the shared limb (Fig. 6.5). These folds are characterised by the emplacement of granitoid sheets along axial surfaces and locally along bedding. Establishment of these structures as  $F_1$  in age is best made around the most southerly of these parasitic folds. It is only here that clear bedding/schistosity relations are present, and it is only here that the superposed schistositities can be separated. This separation is best made using congruency/incongruency relations to the fold since both  $S_1$  and  $S_3$  are low grade muscovite + quartz schistositities which may show evidence of the crenulation of earlier oriented growth. (Sections 4.2.1 and 4.5.2.2). Separation of fabrics further south and east is hindered by pseudomorphous retrogression. These folds are regarded as  $F_1$  in age because:

- 1)  $S_3$  does not lie parallel to the mapped axial surface of the folds, and cuts across both limbs so that  $S_0/S_3$  relations are everywhere sinistral northeast plunging, even in the overturned limb,

2)  $S_0/S_1$  relations change from sinistral north plunging to dextral north plunging about the folds,

3) in the overturned limb,  $S_1$  dips more gently east than  $S_0$  whereas  $S_3$  is steeper than  $S_0$  and therefore incongruent to the fold, and

4)  $S_1$  trends lie parallel to the constructed axial surfaces joining the major hinges, and it is overprinted by  $S_3$ .

Plunges of the antiformal and synformal hinge are shown in Fig. 6.5c and d, and indicate steep northerly plunges. Steep south plunging mesoscopic folds may occur in locally overturned bedding.  $L_1$  in this area is consistently south plunging (Fig. 6.5d) and thus lies at an angle to the major hinges.

Relations in the south of this area are discussed in detail in Section 6.2.3.6.

In subareas 1, 2 and 9 north of these folds, bedding is generally planar - strike  $030^\circ$ , dip  $70^\circ$ SE. Where  $S_1$  can be identified, it trends  $020^\circ$  with subvertical dips, and  $S_0/S_1$  relations are dextral south plunging. There is thus a south to north change in plunge of  $F_1$  folds and  $S_0/S_1$  relations through the horizontal from sinistral north plunging to dextral south plunging. Dextral south plunging  $S_0/S_1$  intersections may lie parallel to  $L_1$ .

Macroscopic south plunging  $F_1$  folds are restricted to subarea 9 (Fig. 6.6), where a broad antiform and tighter synform are best outlined by the boundaries of a poorly outcropping carbonaceous schist. This fold is regarded as an  $F_1$  structure because:

1) its plunge lies parallel to  $S_1/S_0$  intersections in the area (Fig. 6.6a),

2)  $S_1/S_0$  relations change from dextral to sinistral to dextral across the fold,

3)  $S_3/S_0$  relations are sinistral north plunging,

4)  $S_3$  crosses both limbs of the fold in the same sense, crenulates  $S_1$ , and is therefore incongruent to the fold, and



5) a parasitic  $F_3$  fold developed on the western dextral limb of the  $F_1$  fold is sinistral north plunging.

The cusp fold in Fig. 6.6 trends ESE with a steep ( $70^\circ$ ) plunge to the SE. This orientation, and the orientation of co-axial crenulations in the hinge zone, lie parallel to the trend of  $F_4$  folds throughout the area, and thus suggest an  $F_4$  age for this structure. The southern limb of this fold is marked by a rotation of  $S_0$  from a NE to NNW orientation. The sinistral schistosity near this hinge is undifferentiated  $S_{1-3}$  although microscopic evidence suggests it may be a rotated  $S_3$ .

### Synthesis

The Apollyon Beds in the central block between the retrograde schist zones are dominated by macroscopic  $F_1$  folds which change orientation from south plunging in the north to north plunging in the south.  $F_1$  folds and  $S_1$  are overprinted by  $S_3$ . Variations in the plunge of  $F_1$  structures are related to variable plunges of the reconstructed regional  $F_1$  syncline (Section 6.3). These folds also have a variable relation to  $L_1$  - an elongation lineation in  $S_1$  - defined by the shape alignment of mineral aggregates. Borradaile (1972) and Roberts and Sanderson (1974) have suggested that fold axes are able to rotate within the XY plane towards the X direction, represented by the elongation direction. If such a situation has occurred in the Apollyon Beds,\* it would appear that folds characterised by  $F_1//L_1$  represent a higher state of strain than folds in which  $F_1 \times L_1$ . This further implies that all folds were originally formed at an angle to  $L_1$  in the early stages of the deformation.

#### 6.2.3 Macroscopic Structure of the Robe Beds and of the Apollyon Beds in the Western Block (subareas 3-7, 10-24, Map 2)

An analysis of macroscopic structures west of the Mt Franks Retrograde

---

\* this would have occurred unless there has been rotation of the strain ellipsoid, or unless there has been variation in the orientation of local strain ellipsoids.

Schist Zone is complicated by the presence of major folds of different generations, and by the presence of large domains characterised by different bedding/schistosity relations (Fig. 6.2). In order to discuss the macroscopic relations, the western block has been divided into four areas, three of which occur in the  $S_{1P}$  domain. The boundaries between these areas lie along sub areas and are shown in Map 2 and Fig. 6.1, and are listed below:

Area 1. Dominated by a southwest plunging  $F_3$  synform and complimentary antiform in  $S_{1P}$  rocks. Subareas 15, 16, 17.

Area 2. Dominated by an open southwest plunging  $F_3$  synform in west dipping  $S_{1P}$  rocks which is parasitic to the folds in Area 1. Subareas 11b, 13, 14, 19 and includes a small area of  $S_{1N}$  relations in Subarea 18.

Area 3. Dominated by  $F_3$  folds in east and southwest dipping  $S_{1P}$  rocks which are congruent to the folds in area 1. Subareas 20, 21, 22, 23.

Area 4. Dominated by  $S_{1N}$  relations in  $S_0$  which is generally southeast dipping but also southwest dipping. Subareas 3, 4, 5, 6, 7, 10, 11a, 12.

The macroscopic structure of areas 1, 2, and 3 are discussed first. A discussion of relations in area 4 is followed by a discussion of  $S_{1N}/S_{1P}$  relations - relations between area 4 and areas 2 and 3 - which draws heavily on previous mesoscopic (Section 3.5.2.3) and microscopic (Section 4.3.6) treatments of this topic.

#### 6.2.3.1 Area 1 in the Western Block (Subareas 15, 16, 17, Map 2)

This area is dominated by a large southwest plunging  $F_3$  synform outlined by  $S_0//S_1$  in the Robe sillimanite schist (subarea 15), and by a smaller southwest plunging synform, also  $F_3$  in age which is outlined by  $S_0//S_1$  in the Mundi Mundi carbonaceous facies, and in part by the boundary of that unit (subarea 17). Between these two synforms, changes in bedding indicate the presence of a tight, cusp-like  $F_3$  antiform. The western boundary of the Mundi Mundi facies cuts across bedding just in the eastern limb, or near the hinge of this antiform and is regarded as a fault. The  $F_3$  antiform and the synform in the Mundi Mundi facies die out along the axial trace of the axial

surface to the northeast.

Although no younging directions were found in subarea 15, younging data along Mundi Mundi Creek from four separate localities spanning the hinge and eastern limb of the synform in the Mundi Mundi facies (see Map 1) indicate that this fold is downward facing on  $S_3$ .

Outcrops along Mundi Mundi Creek indicate that whereas relations in the eastern limb of the fold are planar and marked by mesoscopic, sinistral, southwest-plunging  $F_3$  folds, the hinge zone and the western limb are marked by the presence of parasitic  $F_3$  folds which change shape from symmetrical to dextral southwest plunging. Further north, bedding in the Mundi Mundi facies outlines a simple synformal hinge which is marked by the development of an axial planar retrograde zone.  $S_3$  is not common in this area but trends NNE with subvertical dips. Minor  $F_3$  folds plunge to the southwest at  $20^\circ$ - $60^\circ$ ; the calculated axis of the major synform plunges at about  $60^\circ$  to the southwest.

The hinge and western limb of the synform in subarea 15 is outlined by  $S_0//S_1$ . The eastern limb is outlined by  $S_0//S_1$  as well as by a lenticular carbonaceous schist, the termination of which is interpreted as a facies variation. The axis of this synform lies parallel to small  $F_3$  folds in the area (plunging at about  $40^\circ$ - $60^\circ$  to the southwest) which change sense from sinistral to dextral across the hinge from east to west. The axial surface is marked by a muscovite bearing  $S_3$  which trends northeast with subvertical dips. The major fold is therefore  $F_3$  in age. To the south, this simply defined hinge is marked by the formation of the antiform-synform pair discussed above.

Correlation of structures developed in the Mt Franks - Mundi Mundi area with structures further north in the Mt Robe area (Section 7.2.3.3) suggests that the major southwest plunging synform in subarea 15 represents a continuation of the Mt Robe Synform, and is so named. The eastern limb of this synform in subarea 15 is marked by the presence of an  $F_4$  fold pair

(Loc. 5268 4893) which plunges steeply ( $70^\circ$ ) to the WNW. The axial surface of this structure trends WNW, dipping very steeply ( $80^\circ$ ) south and lies parallel to the orientation of  $S_4$  throughout the area.

Subarea 16, west of the Mt Robe Synform, is dominated by bedding with a southerly enveloping dip. This is interpreted as the hinge area of a variably southwest plunging  $F_3$  antiform, the western limb of which is cut off by the Mundi Mundi Retrograde Schist Zone. Small southwest plunging  $F_3$  folds change shape from dextral to symmetrical passing westwards across this structure.

It is suggested that this hinge represents the extension of the Mt Robe Antiform recognised further north by Anderson (1971) (see Section 7.2.3.3).

#### 6.2.3.2 Area 2 in the Western Block (subareas 11b, 13, 14, Map 2)

This area lies east and southeast of the Mt Robe Synform and is dominated by a macroscopic  $F_3$  southwest plunging, synform in  $S_0//S_1$  which is open in style. The change in  $S_0//S_1$  orientation around this hinge is reflected by changes in orientation of an amphibolite marker unit. In the eastern, sinistral limb of this fold (subarea 11b) the enveloping surface of  $S_0//S_1$  strikes northeast and dips at  $40^\circ$ - $60^\circ$  to the northwest. The trend of bedding in this area is also outlined by two amphibolite marker horizons which have been partially disrupted by boudinage during  $D_1$ . Minor  $F_3$  folds are southwest plunging sinistral lying (sub)parallel to  $L_1$ , and are parasitic on the  $F_3$  synformal hinge in subarea 14 which is outlined by amphibolite horizons and by changes in the orientation of  $S_0//S_1$ . This hinge is  $F_3$  in age since

- 1) its axis lies parallel to small  $F_3$  folds and  $S_1/S_3$  intersections ( $35^\circ$  to the southwest),
- 2) small  $F_3$  folds and  $S_1/S_3$  relations change sense from sinistral to symmetrical about the axis, and
- 3)  $S_3$  lies axial planar to the mapped axial surface.

The western limb of this fold (subarea 13) trends northwest and dips to the southwest ( $30^{\circ}$ - $50^{\circ}$ ). It is outlined by bedding trends, air photo lineaments and by disrupted amphibolites. Thickly bedded psammites in several areas (e.g. Loc. 5284 4871) demonstrate the large scale continuity of bedding.  $F_3$  folds in this limb plunge  $20^{\circ}$ - $30^{\circ}$  to the southwest and lie parallel to  $S_1/S_3$  intersections.  $S_3$  is locally developed as a crenulation schistosity and trends northeast with subvertical dips. The area west of subarea 13 has not been examined, and the orientation of amphibolites and bedding in this area, and between this subarea and subarea 15 is not known. However at the northern margin of subarea 13,  $S_0//S_1$  passes into an  $S_{1N}$  domain (subarea 18), as well as into subarea 19, marked by  $S_0//S_1$  relations.

In the north of subarea 19 bedding trends to the northeast, and dips to the northwest. Further south, bedding trends northwest and dips to the southwest and is believed to be continuous with subarea 13. It is thus suggested that there is an  $F_3$  antiformal hinge in this subarea.

The hinge in subarea 19 plunges at about  $30^{\circ}$ - $40^{\circ}$  to the southwest and lies parallel to  $S_1/S_3$  intersections,  $F_3$  small folds and parallel also to  $L_1$ .  $F_3$  small folds change sense from symmetrical to sinistral southwest plunging about the axis. The northwestern limb is outlined by a disrupted amphibolite as well as by  $S_0//S_1$  which trends northeasterly and dips at moderate angles to the northwest.  $S_1/S_3$  relations vary from sinistral southwest plunging to parallel in strike and steeper in dip and a regional retrograde  $S_3$  is strongly developed.  $F_3$  mesoscopic folds are parasitic on the Mt Robe Synform to the west. Some shallow plunging mesoscopic  $F_3$  folds in this limb refold  $L_1$ .

Younging evidence from three localities in the short limb (Map 1) suggest that bedding is overturned (i.e. youngs to the northeast), and as a result, is downward facing on  $S_3$ . Just near this antiformal hinge, the shared limb of this fold pair contains a local domain characterised by  $S_{1N}$  relations (Fig. 6.7). In the south of the area,  $S_{1N}$  lies parallel to  $S_0$  in

strike, but dips more gently southwest than  $S_0$ . In the main part of this domain,  $S_0/S_{1N}$  relations are sinistral west plunging and  $S_{1N}$  generally dips more gently west than  $S_0$ .

In the following equal area plots, it is shown that:

- 1) poles to  $S_0$  plot around  $330^{\circ}65^{\circ}W$  although there is a tendency to be redistributed around an  $F_3$  axis (Fig. 6.7a),
- 2) poles to  $S_{1N}$  plot as a maximum about  $360^{\circ}60^{\circ}W$  (Fig. 6.7b) and thus indicate that  $S_0$  is sinistral to, and dips more steeply than  $S_{1N}$ ,
- 3)  $S_0/S_{1N}$  intersections plunge to the west within  $S_{1N}$  (Fig. 6.7c), and
- 4)  $S_3$  trends about  $040^{\circ}90^{\circ}$ , and  $S_1/S_3$  intersections plunge to the west, close to  $L_1$  in orientation and that  $F_3$  folds plunge to the southwest (Fig. 6.7d).

The change in bedding/schistosity relation from  $S_{1P}$  just south of Fig. 6.7 to  $S_{1N}$  in Fig. 6.7 (firstly by a change in dip angle and then by a change in strike angle) may be due either to  $S_{1N}$  overprinting  $S_{1P}$  or to variations in the orientation of  $S_1$  so that it may lie both parallel and non parallel to bedding. Lack of definitive evidence does not permit a choice to be made between these two possibilities.\* However, it is significant that  $S_0/S_{1N}$  relations here indicate that  $S_0$  is generally overturned on  $S_{1N}$  and this is confirmed by a single younging direction (Fig. 6.7). This relationship is consistent with a position in the overturned limb of a major fold related to  $S_{1N}$  in the main  $S_{1N}$  domain further east.

#### 6.2.3.3 Area 3 in the Western Block (subareas 20, 21, 22, 23)

##### *F<sub>3</sub> Structures*

Area 3 is dominated by an  $F_2$  fold pair (subarea 23c) and by variably plunging, macroscopic  $F_3$  folds which are parasitic on the Mt Robe Synform. The southwestern part of this area (subareas 20 and 21) project into area 2

---

\*  $S_{1P}/S_{1N}$  relations are discussed in Section 6.2.3.4.

and will be discussed first.

Along the southeastern side of this projection,  $S_0//S_1$  strikes east-northeast and dips to the southeast at about  $55^\circ$ . Amphibolite bodies also outline this trend.  $S_3$  is not common in this area but has a northeasterly strike and subvertical dip and  $S_1/S_3$  relations are thus dextral, southwest plunging. Minor  $F_3$  folds in this limb and small macroscopic folds (e.g. Loc. 5296 4889) are dextral southwest plunging. They indicate the presence of an  $F_3$  antiform to the west.

Along the northwestern side of this projection,  $S_0//S_1$  and a segmented amphibolite trend northeast, but, in contrast to the southeastern side, dip to the northwest at about  $50^\circ$ . Dips in this area lie parallel to dips in the northern part of subarea 19. Minor  $F_3$  folds in this area are sinistral southwest plunging and indicate the presence of an  $F_3$  antiform to the southeast. These observations are consistent with the presence of a southwest plunging antiformal hinge in subareas 20 and 21. Although a closure is difficult to locate in this area because of strong retrogression, and because of  $M_1$  migmatite formation, this view is supported by:

- 1) southwesterly enveloping dips to granitoid sheets parallel to  $S_1$ ,
- 2) the presence of numerous southwest ( $20^\circ$ - $30^\circ$ ) plunging symmetrical  $F_3$  synforms and antiforms, the enveloping surface of which dips to the southwest,
- 3) the southward termination of amphibolites in this area which can be accounted for by an antiformal hinge, and
- 4) the consistency of this interpretation with the southwesterly enveloping dip of  $S_0//S_1$  immediately to the southwest in subarea 19.

This southwest plunging  $F_3$  antiform can be traced to the northeast into subarea 22, and is accompanied by a shallowing of plunge. Plunge variations probably account for the unusual outcrop pattern of calc silicates at Loc. 5305 4895 whereas the southwest plunging hinge at Loc. 5307 4898 is probably a reflection of this antiform also. Nearby (Loc. 5311 4903), this antiform

is associated with the development of variable, shallowly plunging parasitic folds. From Loc. 5313 4998 to the northeast,  $F_3$  folds become northeast plunging, and there is thus an  $F_3$  culmination in this area. Thus  $F_3$  folds at Loc. 5317 4990 plunge at  $20^\circ$ - $35^\circ$  to the northeast and are outlined by poorly outcropping calc silicates, one bed of which may be connected to the calc silicate mentioned above at Loc. 5305 4895.

The northwestern limb of this antiform in subarea 20 is generally planar. In contrast, the northwest limb of this fold further along strike to the northeast (subareas 22, 23) outlines a parasitic  $F_3$  fold pair which must be faulted off to the south against subarea 19. These two folds consist of an eastern, northeasterly plunging antiform and a complimentary neutral fold west of it. The eastern limb of these folds in subarea 23 dips to the southeast and is outlined by  $S_0//S_1$  and by a segmented amphibolite layer. A synformal hinge can be located in a heavily retrogressed, poorly outcropping area between this limb and the antiform lying to the southeast.

The  $F_3$  northeast plunging antiform and complimentary neutral fold have been traced along axial surface strike to the northeast and are best considered by looking at subarea 23 - Fig. 6.8, "Structural Relations in the Black Prince - Eldee Creek Area." Here, both the  $F_3$  antiform - called the Black Prince Antiform - and the  $F_3$  neutral fold - the Black Prince Neutral Fold - are displaced by the northeast trending Shepherds Hut Fault. Bedding changes dip through the vertical from southeast to northwest around these folds and mesoscopic and macroscopic structures in the western limb of the Black Prince Neutral Fold are parasitic on the Mt Robe Synform.

The eastern limb and hinge of the Black Prince Antiform are outlined by changes in orientation of  $S_0//S_1$  and by:

- 1) amphibolites and partly by calc silicates just south of Eldee Creek (subarea 23a),
- 2) amphibolites and the andalusite/sillimanite isograd in the centre of subarea 23b, and



3) amphibolites along the northern margin of subarea 23b, ESE of the Black Prince Mine.

The antiformal hinge also occurs on a strongly outcropping ridge in the south of subarea 23a, but rocks are highly retrogressed in this area and  $S_0/S_3$  relations are hard to find.

In subarea 23a, the southeastern limb of this fold is marked by dextral northeast plunging  $F_3$  folds (e.g. Loc. 5319 6491, Fig. 6.8) and  $S_1/S_3$  intersections. Mesoscopic  $F_3$  folds are symmetrical in the hinge area, and where  $S_3$  is developed,  $S_1/S_3$  relations are high angle.  $F_3$  crenulations may plunge to the southwest where  $S_0/S_1$  is locally overturned, but are generally northeast plunging, parallel to the calculated plunge of  $50^\circ$  for the major hinge (Fig. 6.8c). The antiformal hinge can be traced across Eldee Creek to the northeast into subarea 23b where it passes through poor outcrop and migmatized metasediments until it runs into, and is localised along, the Shepherds Hut Fault (Fig. 6.8). From here north, hinge relations are generally destroyed except at Loc. 5339 64934, Fig. 6.8 where poles to  $S_0/S_1$  indicate a plunge of  $85^\circ$  to the northeast (Fig. 6.8d).

In the western limb of the Black Prince Antiform (the shared limb of the fold pair),  $S_0/S_1$  trends ESE or E-W with subvertical north or south dips.  $F_3$  folds are symmetrical and  $S_1/S_3$  relations are high angle, plunging to the northeast or southwest depending on the sheet dip of the limb. This limb is best developed ESE of the Black Prince Mine where the antiform is more open than in subarea 23a.

Sedimentary structures in subarea 23b in the eastern limb of the antiform (Fig. 6.8) young to the east and indicate that the antiform is upward facing on  $S_3$ .

The hinge of the Black Prince Neutral Fold is best seen in subarea 23a and in subarea 23b ESE of the Black Prince Mine. In the latter area, the hinge is characterised by a rotation of vertical bedding and therefore has a vertical plunge (Fig. 6.8h). Away from the hinge, northwest dips prevail

in the northwestern limb, and sedimentary structures younging to the southeast (Fig. 6.8) indicate that these beds are overturned. The northeast trend of this limb is outlined by  $S_0//S_1$  and by amphibolites and continues along strike where it defines the eastern limb of the Mt Robe Synform (Section 7.2.3.3).

If the axial surface trace of this neutral fold is drawn between subarea 23a and the area just discussed, it becomes displaced by the Shepherds Hut Fault (left lateral). South of this fault, the fold is defined by changes in orientation of  $S_0//S_1$  from E-W or WSW to N or NE, and  $S_0//S_1$  in the northwestern limb dips to the northwest.  $S_1/S_3$  relations in this limb are generally sinistral southwest plunging but  $S_3$  may locally lie parallel to  $S_0//S_1$  in strike. Between the Black Prince Mine area and the Shepherds Hut Fault, the axial trace of the neutral fold is poorly defined. It is suggested that it accounts for changes in orientation of  $S_0//S_1$  and the andalusite/sillimanite isograd at Loc. 5331 64941 (Fig. 6.8).

The northwestern limb of the Black Prince Neutral Fold is planar immediately ESE of the Black Prince Mine. Further south, however, this limb is dominated by a macroscopic  $F_2$  fold pair (see below) and by a southwest plunging  $F_3$  fold pair which is cut off to the north by an inferred  $F_4$  fault (see below).

This parasitic  $F_3$  fold pair consists of an eastern synform and western antiform in  $S_1//S_0$  and is parasitic on the Mt Robe Synform to the west. The northeast trending axial trace of the eastern synform is clearly defined (Fig. 6.8), and the plunge of this structure has been calculated in subarea 23c, the Shepherds Hut Area, ( $50^\circ$  to  $250^\circ$ , Fig. 6.9a) and from a few readings further to the northeast ( $40^\circ$  to  $240^\circ$ , Fig. 6.8i). The complimentary antiform to the west is represented only by a broad warp in subarea 23c, the Shepherds Hut area, but is defined further to the northeast up plunge by a disrupted amphibolite unit.

A plot of  $L_1$  around the  $F_3$  synform in the Shepherds Hut area, (Fig.

6.9b) shows a random distribution between readings from the short limb, hinge and long limb. The  $F_3$  axis to  $S_0$  and  $S_1$  (Fig. 6.9b) plots in the same general area as  $L_1$  and in the absence of any well defined redistribution pattern, it is concluded that the spread of  $L_1$  is a primary feature, and that  $F_3$  axes have a similar orientation to  $L_1$ . In one small area however, horizontal or shallowly north plunging  $F_3$  folds fold the sillimanite lineation.

#### *The Shepherds Hut Fold Pair - An $F_2$ Structure*

A macroscopic dextral  $F_2$  pair in subarea 23c is outlined by the boundaries of a segmented and  $D_1$  boudinaged amphibolite as well as by  $S_0//S_1$  in metasediments (Fig. 6.9). The long limbs of this fold are northwest trending, southwest dipping and contain dextral mesoscopic  $F_2$  folds which generally plunge to the west. The shared limb, on the other hand, is not planar but contains a sinistral fold pair, and mesoscopic  $F_2$  folds in this limb change sense around these folds. A plot of poles to  $S_0$  and  $S_1$  (Fig. 6.9c) shows that the macroscopic  $F_2$  axis plunges at about  $50^\circ$  to the west and is parallel to small  $F_2$  folds in the sinistral limb of the  $F_3$  synform. A plot of  $L_1$  (sillimanite lineation) taken around the macroscopic Shepherds Hut Fold shows no obvious redistribution about the  $F_2$  axis (Fig. 6.9d). Even where lineation orientations are classified into positions on long limb, hinge and short limb of the  $F_2$  fold there is no obvious subdivision according to location around the  $F_2$  fold and the  $F_2$  axis lies within the field of  $L_1$  plots.

#### *Relations Between $F_2$ and $F_3$ Folds*

Evidence that  $F_3$  folds overprint  $D_2$  structures is provided by:

- 1) the microscopic evidence (Section 4.4) that sericite clots defining  $S_2$  contain laths of sericite which have been crenulated about  $S_3$  or which have been recrystallised parallel to  $S_3$ ,
- 2) the small variation in orientation of mesoscopic  $F_2$  folds depending upon location in major  $F_3$  folds. Thus, dextral  $F_2$  folds in the sinistral limb of the  $F_3$  synform in Fig. 6.8 (Loc. 5316 64925) have a different

orientation to dextral  $F_2$  folds near the hinge area of an  $F_3$  fold in Fig. 6.9 (Loc. 5303 64918). Unfortunately, no definite  $F_2$  folds were recognised in the  $F_3$  short limb of the Shepherds Hut Fold. Equal area plots of small  $F_2$  folds (Fig. 6.9d) show a spread of readings but no obvious  $F_3$  refolding.

3) the rotation of the major synformal hinge towards the plane of  $S_3$  as indicated in Fig. 6.9.

Changes in the orientation of  $S_0//S_1$  in Fig. 6.9 indicate that the  $F_2$  Shepherds Hut Fold lies in the southeast, sinistral limb of the  $F_3$  synform. Equal area plots (Fig. 6.9e) show that  $F_3$  axes do not lie parallel to  $F_2$  axes, but there is no obvious redistribution of axes.

#### $F_4$ Structures

Anderson (1966) first suggested that a NW trending fault was located in the Black Prince area. The present study has also suggested the presence of a fault in this general area, but further south than that of Anderson.

The existence of a NW - WNW trending structure southwest of the Black Prince Mine (Fig. 6.8) is inferred from the change in structural relations in the west limb of the Black Prince Neutral Fold north and south of this line. South of here, two southwest plunging  $F_3$  folds can be established. North of here,  $S_0//S_1$  and bands of amphibolites define the eastern limb of the Mt Robe Synform which is generally planar NE except just north of the fault where it is rotated into a WNW orientation tangential to the fault itself.

The presence of a fault in this area also explains the local non parallelism between  $S_0//S_1$  and the andalusite/sillimanite isograd.

The general orientation of this fault lies parallel to axial planes of  $F_4$  crenulations in this area and is regarded as an  $F_4$  feature. An  $F_4$  age is also assigned to the warp in  $S_0//S_1$ , just north of the fault because the axis of warping, although established with difficulty, lies parallel to small  $F_4$  folds (Fig. 6.8j).

Summary of Area 3

The southern part of area 3 is dominated by a southwest plunging  $F_3$  antiform. The northern part is dominated by northeast plunging  $F_3$  folds, and it is suggested that an antiformal culmination occurs in this area.

Around the Black Prince Fold Pair,  $S_0//S_1$  changes orientation from northeasterly dipping right way up to northwesterly dipping and overturned. This change in dip about the vertical is probably pre- $D_3$  in age and is reflected by the gradual change in plunge of  $F_3$  folds from northeasterly (Black Prince Antiform) to southwesterly (parasitic  $F_3$  folds and Mt Robe Synform to the northwest) as bedding changes dip from easterly to westerly. It is thus suggested that  $S_0//S_1$  became overturned about an E-W trace which after  $D_3$  folding, lies in the hinge area of the Black Prince Fold pair. The presence of westerly dipping  $F_2$  folds in the Shepherds Hut Area, coupled with a possible easterly younging, might suggest that this overturn is pre- $D_2$  in age.

Further south there must be a similar change in bedding orientation between the western limb of the  $F_3$  antiform and bedding in Area 2; but in this case, dips are not oppositely directed because bedding in Area 3 is folded around only one hinge whereas bedding in Area 2 is folded around two hinges. It has not been possible to verify this latter change in bedding younging direction because of the absence of sedimentary structures. The trace of younging change in the northern and southern parts of this area are probably related across a NW trending fault at the south of subarea 23a.

6.2.3.4 Area 4 in the Western Block (subareas 3, 4, 5, 6, 7, 10, 11a, 12, Map 2)

In contrast to areas 1, 2 and 3 discussed above which are dominated by  $S_{1P}$  relations, area 4 is dominated by  $S_{1N}$  relations. Although microscopic data indicate that  $S_{1N}$  overprints an earlier fabric (Section 4.2.2), it lies axial planar to the earliest recognised mesoscopic (Sections 3.3.1, 3.3.2) and macroscopic folds ( $F_1$  folds) in this area.

This section describes the macroscopic geometry of Area 4. The next section discusses the correlation between  $S_{1N}$  in Area 4 and  $S_{1P}$  in Areas 2 and 3.

Macroscopic folds in Area 4 occur around Mt Franks (subareas 3, 4, 5, 6) and in subarea 12.

#### MACROSCOPIC FOLDS IN THE MT FRANKS AREA

The Mt Franks Area is shown in Map 3. This map spans the boundaries between Areas 3 and 4. The western and northwestern parts of the map contain  $S_{1P}$  relations whereas the other parts are dominated by  $S_{1N}$  relations. Macroscopic relations in the  $S_{1N}$  part of this map (area 4) will be discussed here.

#### Macroscopic $F_3$ Folds

The Mt Franks Area is dominated by an  $F_3$  synform outlined by  $S_{1N}$  (Map 3 and Map 4).  $S_{1N}$  is rotated from a N/S trending, steep westerly dip in the sinistral limb of this synform (southern part of Map 3) into a NW trend SW dip or into an ENE trend, SSE dip in the dextral limb of this variably tight synform (Map 3). North of Mt Franks itself, the hinge of this synform (defined by change in orientation of  $S_{1N}$  in psammites) can be represented by a single axial trace (Map 4). Further north again (north of map 3), this synform develops into a zone of strong  $F_3$  crenulation and schistosity formation. The overall plunge of this synform is  $35^\circ$  to the southwest.

Two critical features of this synform need emphasising:

1)  $S_0$  is unfolded by the synform. This is seen best in two sketches of detailed traverses across the fold hinge - (Fig. 6.10 and Fig. 6.11). The location of these is shown on Map 3.

2) The hinge of this synform defined by changes in orientation of  $S_{1N}$  in psammites does not correspond to the hinge defined by a change in orientation of  $S_{1P}$  in pelites which lies further to the west. The area between these two hinges contains oppositely dipping  $S_{1N}$  in different beds - type III herringbone structures (Section 3.5.2.2). These relations are best

seen in Fig. 6.11.

Both points 1) and 2) are explicable in terms of the discussion of herringbone structures (Section 3.5.2.2) and merely represent an extension of these relations to the macroscopic scale. The findings of this section were:

1.  $S_0$  is not folded about  $S_3$  when its orientation after  $D_1$  folding lies parallel to the orientation of  $S_3$  of the new deformation.

2. The formation of herringbone structures is due to different responses of  $S_{1N}$  in pelite and psammite layers to the  $D_3$  deformation.  $S_{1N}$  (psammite) undergoes bulk rotation whereas  $S_1$  (pelite) undergoes small scale crenulation, the enveloping surface of which still lies parallel to the unfolded orientation.

3. the rotation of  $S_{1N}$  (psammite) about  $S_0$  results in a change of  $S_0/S_{1N}$  relations from dextral southwest plunging to sinistral southwest plunging. Rotated  $S_{1N}$  (psammite) dips to the southeast more gently than  $S_0$ .

#### Macroscopic $F_1$ Folds

In the sinistral limb of this  $F_3$  synform,  $S_{1N}$  lies axial planar to a variably plunging  $F_1$  dextral fold pair - the Mt Franks fold pair (Map 3). In the dextral limb  $S_{1N}$  lies axial to a sinistral steeply east plunging  $F_1$  fold pair which is not obviously related to the Mt Franks fold pair. Each of these  $F_1$  structures will be discussed in turn.

#### *The Mt Franks Fold Pair (Maps 3 and 4)*

This fold pair is best outlined by bold outcrop of Mt Franks facies: the western and northern ridges of Mt Franks define the western and shared limbs (Fig. 2.12) while the eastern limb is outlined by a northeast trending ridge east of Eldee Creek. The fold pair is also outlined by the boundary between the Apollyon Beds and Robe Beds, and also by the boundary between the Apollyon chiastolite schist and the Apollyon andalusite schist. This latter boundary is not strongly folded, however, because of gentle  $F_1$  fold plunges. Although outcrop is poor in the Cascade Creek Area (see Map 3)

lack of folding of lithological boundaries here is attributed to shallow  $F_1$  plunges.

The Mt Franks fold pair is characterised by the following features:

- 1) an eastern antiformal hinge and a western synformal hinge,
- 2) consistent eastward stratigraphic younging especially from the Mt Franks facies which indicate that easterly dipping bedding is right way up, that folds are upward facing on  $S_{1N}$  and that there is no small scale pre- $F_1$  folding (Fig. 6.13),
- 3) an overturning of the western dextral limb from east dipping to west dipping south of Waterfall Gully (see Map 3),
- 4) a rotation of axial surfaces and  $S_{1N}$  from north south trending, steeply west dipping near Cascade Creek to northwest trending, southwest dipping near Mt Franks. This is attributed to  $F_3$  folding since the axis of  $S_1$  folding lies parallel to the plunge of small  $F_3$  folds and the orientation of  $S_1/S_3$  intersections,
- 5) a north to south shallowing of plunge, and
- 6) a north to south tightening of the fold pair and decrease in distance perpendicular to axial surface traces.\*

An  $F_1$  age for the Mt Franks fold pair is indicated by:

1. the change in vergence of  $F_1$  small folds from dextral to symmetrical and sinistral to dextral across the fold,
2. the change in sense of  $S_0/S_{1N}$  intersections from dextral to high angle or sinistral to dextral across the fold,
3. the parallelism between  $S_0/S_{1N}$  intersections and  $F_1$  small folds with the major anticlinal and synclinal axes,
4. the parallelism between  $S_{1N}$  and axial surfaces constructed through the major hinges, and

---

\* The fold pair on Mt Franks is even more open than shown on Map 3 because of a 150 m difference in height between the synclinal hinge near the shoulder of Mt Franks and the anticlinal hinge near the alluvial flat of Eldee Creek.



5. the fact that  $S_3$ , the only other crystallisation fabric in the area, overprints both  $S_0$  and  $S_{1N}$  on a sinistral southwesterly plunge and is thus incongruent to the fold.

Relations across the Mt Franks fold pair will now be described in two traverses from the east to the west limb. One traverse passes north of Waterfall Gully (Map 3); the other passes through the Cascade Creek area (Map 3).

#### *Traverse north of Waterfall Gully*

In the eastern, dextral limb east of Eldee Creek (subarea 3, Map 2),  $S_0$  strikes northeast and dips to the southeast.  $S_{1N}$  (NNW strike, steep SW dip) crosses  $S_0$  on a dextral southwest plunge whereas  $S_3$  (NE strike, sub-vertical dip) crosses  $S_0$  on a dextral south plunge (Fig. 6.12a).  $S_{1N}/S_3$  intersections are southwest plunging, parallel in part to  $L_3$  and close to  $S_0/S_{1N}$  in orientation (Fig. 6.12b).

In the shared limb, (Map 4) biotite laminations outline small sinistral southwest plunging folds, whereas larger scale psammite/pelite bedding is generally unfolded on a mesoscopic scale. Higher up the stratigraphic sequence  $F_1$  folds in more thinly bedded chistolite schist vary from symmetrical to sinistral southwest plunging. Bedding in the shared limb trends NW or W and dips at variable angle to the south.  $S_0$  crosses  $S_1$  (NW strike, SSW dips) at a high angle and observed and calculated  $S_0/S_{1N}$  intersections are SW plunging (Fig. 6.12c). In the northern ridge of Mt Franks, measured orientations of  $S_1$  are only meaningful in psammite because intense crenulation of  $S_{1N}$  in pelites ( $S_{1N}^{Pe}$ ) has resulted in the formation of  $S_3$  and  $S_3'$ . Plots of  $S_{1N}^{Ps}$  in this ridge lie parallel to values of  $S_{1N}^{Pe}$  in less crenulated rocks further south (also lying in the shared limb) and indicate the lack of refraction or differential  $F_3$  folding between  $S_{1N}^{Ps}$  and  $S_{1N}^{Pe}$  (Fig. 6.12d and Fig. 6.12e). Although  $S_{1N}$  is dominantly NW trending in this limb N/S and E/W orientations do occur. N/S oriented  $S_{1N}$  lies parallel to  $S_{1N}$  in chistolite schist just west of the Mt Franks Retrograde Schist Zone (east limb of fold)

and suggests that NW trending orientations of  $S_{1N}$  are due to  $F_3$  rotation. E/W oriented  $S_1$  lies in the short limbs of  $F_3$  parasitic folds.

The shared limb and synclinal hinge of the fold pair contain roughly N/S trending terraces which cut across bedding and locally offset bedding in the right sense for the fold (Fig. 6.13e). These terraces are zones of strong  $S_{1N}$  development and  $S_{1N}$  within them lies parallel to  $S_{1N}$  in the adjacent "country rock." The presence of pegmatites with some of these terraces suggests late stage dilation.

In the shared limb, south dipping  $S_0$  crosses  $S_3$  (NE strike, steep E dip) dextrally on a southwest plunge; the  $S_0/S_3$  intersection lies parallel to  $F_3$  folds in  $S_{1N}$  and parallel to  $S_0/S_{1N}$  intersection (Fig. 6.12f). The change in orientation of the  $S_0/S_3$  intersection between eastern and shared limbs reflects the  $F_1$  folding of  $S_0$ . In the northern ridge of Mt Franks,  $S_3'$  is developed as a long limb schistosity. It is locally not parallel to  $S_3$ , and there is a general tendency for the angle between  $S_3'$  and  $S_3$  to decrease towards the east as  $S_3'$  rotates into  $S_3$ .  $S_0/S_3'$  is a prominent south plunging lineation in this area (Fig. 2.8).

In the western limb of the parasitic fold, bedding in the Robe Beds strikes NNE and dips steeply SE except in the south near Waterfall Gully where bedding is overturned on  $S_{1N}$  and dips to the west. In these rocks, east dipping  $S_0$  crosses  $S_{1N}$  (NW strike, SW dip) with a dextral southwest plunging intersection, whereas west dipping  $S_0$  crosses  $S_{1N}$  with a dextral northwest plunging intersection (Fig. 6.12g). In the overlying Apollyon Beds,  $S_0$  and  $S_{1N}$  have more northerly orientation;  $S_{1N}$  in particular strikes east of north with steep westerly dips and is partially redistributed about an  $F_3$  axis and shows two maxima corresponding to unrotated and partially rotated orientations (Fig. 6.12h).  $F_1$  folds in this limb are southwest plunging dextral and lie parallel to  $S_0/S_{1N}$  intersections, and  $F_3$  folds in  $S_{1N}$  in this limb are southwest plunging sinistral and  $S_0/S_3$  intersections are sinistral and display a spread within the  $S_3$  plane depending on the dip of  $S_0$ .

The calculated orientation of the anticlinal axis in the Robe Beds ( $40^\circ$  to  $197^\circ$ ) lies parallel to the synclinal axis in the same rocks ( $40^\circ$  to  $193^\circ$ ). (Figs. 6.12 i,j). The  $F_1$  axis lies parallel to  $F_3$  axis and to  $S_{1N}/S_3$ ; intersections (Fig. 6.12k) indicating the co-axiality of the first and third generation folds in this area. In the Apollyon Beds, the calculated orientation of anticlinal and synclinal axis is  $30^\circ$  to  $209^\circ$  (Fig. 6.12 l), indicating that there is a shallowing of plunge to the south.

#### *Traverse in the Cascade Creek Area*

Because of poor outcrop, relations across this fold are best seen along Cascade Creek itself (Map 3, Fig. 6.14). At the creek outlet,  $S_0$  strikes north-east, dips to the southeast and is crossed by  $S_{1N}$  (NNE strike, steep W dip) on a dextral, southerly plunge.  $S_{1N}$  maintains this orientation across the fold since  $F_3$  effects in this area are limited to crenulation of  $S_{1N}$  and formation of  $S_3$ . The shared limb of the fold consists of two sinistral folds which are marked by gently south dipping short limbs and steeply west dipping (i.e. overturned) long limbs in which  $S_0$  dips more steeply west than  $S_{1N}$  (Fig. 6.14). In the western dextral limb,  $S_0$ , striking NNE and dipping to the west, is generally crossed by  $S_{1N}$  on a dextral, northwesterly or southwesterly intersection (Map 3). These relations are best seen in equal area plots of Fig. 6.14a-d.

In the Apollyon andalusite schist and the underlying Apollyon chiasolite schist,  $S_1$  trends north south and dips to the west (Figs. 6.14a,b). Note that although  $S_1$  in Fig. 6.14b shows the effects of  $F_3$  redistribution, it lies at a more gentle angle than  $S_1$  in Fig. 6.14a. Poles to  $S_0$  in the Apollyon andalusite schist along Cascade Creek define a south plunging axis of  $F_1$  folding which lies in the field of  $S_0/S_1$  intersections and  $F_1$  small folds (Fig. 6.14c). Parasitic  $F_1$  folds in Apollyon chiasolite schist in the western limb of this fold are dextral south plunging and consist of eastern anticlines and western synclines. A cross section of folding in this area is shown in Fig. 6.15 and poles to  $S_0$  in this area indicate a gentle southerly plunge (Fig. 6.14d).

*F<sub>1</sub> folds in the dextral limb of the F<sub>3</sub> synform and relation to  
the Mt Franks Fold Pair (Map 3, Map 4)*

The Mt Franks fold pair cannot be traced across the F<sub>3</sub> synformal axis (Map 3, Map 4). The eastern anticlinal hinge becomes more open up plunge and dies out still within the eastern limb of the F<sub>3</sub> synform; it can no longer be identified by folds in bedding or by change in sense of S<sub>0</sub>/S<sub>1N</sub> intersections and minor F<sub>1</sub> folds. The western synclinal hinge, on the other hand, persists almost up to the F<sub>3</sub> hinge zone where it can still be identified by folds in S<sub>0</sub>. The F<sub>3</sub> synform in this area is outlined by rotation of S<sub>1N</sub>Ps across planar S<sub>0</sub>, and S<sub>0</sub> is unfolded immediately across the F<sub>3</sub> hinge in the western limb of the F<sub>3</sub> synform.

The western limb of the F<sub>3</sub> synform is characterised, however, by the presence of a sinistral steeply east plunging F<sub>1</sub> fold pair which lies along strike from the synclinal hinge of the Mt Franks fold pair. This sinistral fold pair has an open style in the east, closest to the F<sub>3</sub> axis, and become tighter up plunge to the west. Despite poor outcrop in the vicinity of the F<sub>3</sub> synformal hinge, it is apparent that no other major F<sub>1</sub> folds occur in this area. Detailed relations across this fold pair in one area will be discussed on page 203.

*Discussion of Macroscopic Geometry in the Mt Franks Area*

The dextral south plunging F<sub>1</sub> folds in the east limb of the F<sub>3</sub> synform are congruent to F<sub>1</sub> folds east of the Mt Franks Retrograde Schist Zone, and both are parasitic on a major syncline lying further to the east. Consistency of structural facing in the Mt Franks area (Fig. 6.13) demonstrates the absence of any small scale pre-F<sub>1</sub> inversions in this area, confirming that F<sub>1</sub> is the earliest generation folding episode at this scale. The southward shallowing of F<sub>1</sub> plunge of the Mt Franks fold pair is regarded as a primary feature of the D<sub>1</sub> event, since similar reversals occur further south (see below) and also east of the Mt Franks Retrograde Schist Zone (Section 6.2.2).

The open nature of the Mt Franks Fold pair can be explained in terms of:

- (1) the non isoclinal nature of the fold
- (2)  $F_3$  refolding.

This refolding has resulted in the curved axial traces of the Mt Franks fold pair, and as a consequence, a northward increase in the perpendicular distance between the axial traces. This in turn has led to an increase in the interlimb angles of the fold - that is an opening-up of the fold.

The relation of the sinistral  $F_1$  fold pair in the western limb of the  $F_3$  synform to the dextral  $F_1$  Mt Franks fold pair in the eastern limb is complex. However,  $S_0/S_{1N}$  relations change from dextral to sinistral across the  $F_3$  axis, because of non folding of  $S_0$ , and it might be expected that before "rotation" this fold pair was dextral and parasitic on the Mt Franks fold pair. "Refolding" of this dextral fold pair is constrained by non folding of  $S_0$  where it lies parallel to the future  $S_3$ . In reality, this means that the long limbs of this fold pair have not been rotated although the short limb and hinge areas which lie at an angle to  $S_3$  have undergone rotation. Bearing in mind that the Mt Franks fold pair has been opened up by  $F_3$  folding, one possible folding model predicts that a dextral fold pair has been opened up by  $F_3$  folding and then suffered further contraction because of its position in the western limb of the  $F_3$  fold. This contraction has resulted in the formation of a sinistral fold pair without rotation of long limbs. The main constraint on refolding is that because the long limbs lie parallel to  $S_3$ , there cannot have been any bulk rotation of an originally formed fold system.

#### MACROSCOPIC STRUCTURES IN AREA 4 - OTHER AREAS

This discussion so far of Area 4 has concentrated on the Mt Franks Area. North of this area (subarea 3f)  $S_0/S_{1N}$  relations are consistently dextral on a southerly plunge. South of the Mt Franks Area, three features are noted:

- 1) Just west of the boundary between the Apollyon Beds and Robe Beds,  $S_0$  is overturned through the vertical to dip to the west in the western part

of Area 4. This overturn is shown in Fig. 6.16. Equal area plots confirm that  $S_0$  changes orientation about a constant  $S_{1N}$  (Fig. 6.16 a and b) and thus this overturn is either pre- or syn- $S_{1N}$  in age. Comparison with the southern part of the Mt Franks Area, in which  $S_0$  becomes overturned in the long limb of the Mt Franks fold pair, suggests that the overturn may be an  $F_1$  feature.

2) Where  $S_0$  dips and youngs to the east, there is a north to south change in the plunge of small  $F_1$  folds and  $S_0/S_1$  intersections from gentle southerly through the horizontal to steep northerly in subarea 12. Because of the small  $S_0/S_{1N}$  angle in the overturned domain,  $S_0/S_{1N}$  plunges may be quite variable.  $S_0/S_{1N}$  is commonly dextral northwest plunging but  $S_0$  may lie parallel to  $S_{1N}$  in strike.

3) Rotation of  $S_0$ ,  $S_1$  and  $S_3$  about a gentle  $F_4$  warp in subareas 10 and 11.

Macroscopic  $F_1$  relations in subarea 12 will be treated in a separate section (Section 6.2.3.6) together with data from subarea 24 and the central block.

#### 6.2.3.5 Correlation Between $S_{1N}$ and $S_{1P}$ - Relationship Between Areas 2, 3 and 4 in the Western Block

Mesoscopic and microscopic data of Sections 3.5.2.3 and 4.3.6 respectively have suggested that  $S_{1N}$  is equivalent to  $S_{1P}$  ( $=S_1$ ). This section attempts to extend this correlation to the macroscopic scale by examining the relationship between  $S_{1N}$  and  $S_{1P}$  in a transect from area 4 into area 2 south of Mt Franks (Fig. 6.16) and in the Mt Franks area itself.

#### *$S_{1N}/S_{1P}$ Relations in a Transect South of Mt Franks*

(Fig. 6.16)

The overturn in bedding in this figure has already been discussed in the last section. In the overturned domain,  $S_0$  dips west more steeply than  $S_{1N}$ , and  $S_0/S_{1N}$  relations are either parallel in strike or are dextral northwest plunging.

Passing further west, the angle between  $S_0$  and  $S_{1N}$  decreases. Further

west again, in the most westerly part of the andalusite schist and in the sillimanite schist,  $S_{1P}$  relations prevail. This is now the eastern part of Area 3.

Selected thin section data, shown on Fig. 6.16 confirm, in this traverse, the general microscopic finding (Section 4.3.6) that  $S_{1N}$  is equivalent to  $S_{1P}$ .  $S_{1N}$  overprints biotite and andalusite porphyroblasts as well as an early biotite preferred orientation (Fig. 6.16(i)).  $S_{1P}$  rocks similarly overprint biotite inclusion trails within pre- $S_{1P}$  andalusites (Fig. 6.16(ii)).

Although the macroscopic data in Fig. 6.16, when taken by itself is consistent either with  $S_{1N}$  overprinting  $S_{1P}$  or with  $S_{1N}$  equivalent to  $S_{1P}$ , the first possibility is inconsistent with the microfabric evidence in this transect.

#### *$S_{1N}/S_{1P}$ Relations in the Mt Franks Area (Map 3, Map 4)*

In the western, dextral limb of the  $F_3$  synform in this area (see last section)  $S_{1N}$  dips to the southeast more gently than  $S_0$ . This rotated orientation of  $S_{1N}$  lies close to the orientation of  $S_{1P}$  in Area 3, and direct relations between  $S_{1N}$  and  $S_{1P}$  can be examined in three small critical areas - Figs. 6.11, 6.17, 6.18 which are located on Map 3 and Map 4. (A clear relationship between  $S_{1N}$  and  $S_{1P}$  cannot be deduced from Fig. 6.10 discussed in Section 6.2.3.4 because of intervening alluvial cover).

#### Figure 6.11

There is no outcrop gap between  $S_{1N}$  and  $S_{1P}$  relations in Fig. 6.11. Macroscopic relations show that southeast dipping  $S_{1N}$  in the dextral limb of the  $F_3$  fold has a similar orientation to  $S_{1P}$  further west. The boundary between Areas 3 and 4 is thus crossed in this figure.

The macroscopic relations in Fig. 6.11 suggest two possible correlations between  $S_{1N}$  and  $S_{1P}$ :

- 1)  $S_{1N}$  is equivalent to  $S_{1P}$ , or
- 2)  $S_{1N}$  actually overprints  $S_{1P}$ .

Microscopic data from this area (see Fig. 6.11) demonstrates two critical

points. Firstly, thin sections taken from  $S_{1N}$  rocks show variable  $S_0/S_{1N}$  relations. Even within a thin section (Figs. 6.11 (i) and (ii) )  $S_0$  lies both parallel and at an angle to  $S_{1N}$  - this means that microscopic  $S_{1P}$  relations can be found within a macroscopic  $S_{1N}$  domain (it was shown in Section that even mesoscopic  $S_{1P}$  relations occur in this domain). Secondly, both  $S_{1N}$  rocks (Fig. 6.11 (i) ) and  $S_{1P}$  rocks (Fig. 6.11 (ii), (iii) ) overprint andalusite containing oriented and random inclusions of biotite and ?ilmenite, and both  $S_{1N}$  (Fig. 6.11 (ii), (iii) ) and  $S_{1P}$  (Fig. 6.11 (iv) ) overprint early biotite and a crenulated schistosity outlined by biotite laths in quartz rich layers (see also Section 4.3.6). Thus, microfabric relations in this Figure indicate that  $S_{1N}$  does not overprint any fabric which is not present in  $S_{1P}$  rocks. That is, microfabric evidence here suggests that  $S_{1N}$  and  $S_{1P}$  are equivalent. This is only consistent with the first of the possible macroscopic correlations - that  $S_{1N} = S_{1P} = S_1$ .

#### Figure 6.17

Figure 6.17 represents a traverse across  $F_1$  folds and  $S_{1N}$  lying in the dextral limb of the  $F_3$  synform discussed in the last section. The boundary between Area 3 ( $S_{1P}$ ) and Area 4 ( $S_{1N}$ ) lies across this figure. In the  $S_{1N}$  rocks, a parasitic  $F_1$  fold in bedding is overprinted by  $F_3$  folds which fold  $S_{1N}$ . The axial surface traces of the  $F_1$  folds are constructed through mapped hinge zones in bedding;  $S_{1N}$  trend lines on the other hand are only approximately shown and while they are no doubt parallel to  $F_1$  axial surface traces, individual measured values reflect the effect of small scale  $F_3$  folding.

$F_1$  structures in this area form a steeply east plunging, sinistral fold pair.  $S_{1N}$  relations occur in all limbs, and  $S_0/S_{1N}$  (psammite) relations change sense from sinistral to dextral to sinistral across folds. Both sinistral limbs are marked by  $S_{1N}$  (psammite) dipping more gently to the south-east than  $S_0$ .

The northern sinistral  $F_1$  limb is marked not only by  $S_{1N}$  relations, but also by  $S_{1P}$  relations, and Fig. 6.13 suggests that  $S_0/S_{1N}$  angles



decrease to the north as  $S_{1P}$  relations are reached.

As in the Figure just discussed, both  $S_{1N}$  and  $S_{1P}$  in this area overprint early biotite and andalusite growth, and early mineral preferred growth (Figs. 6.17 (i) and (ii) ). Since both  $S_{1N}$  and  $S_{1P}$  overprint the same phases they only allow one interpretation of the macroscopic relations in this area, that of  $S_{1N}$  and  $S_{1P}$  equivalence.

#### Figure 6.18

$S_{1P}$  relations occur in the northern part of this figure (Area 3) and also in two narrow, parallel, northwest trending zones which are flanked by  $S_{1N}$  relations. The 'country rock' around these  $S_{1P}$  zones is characterised by  $S_0$  trending northeasterly across a northwest trending, southwest dipping  $S_{1N}$ .  $S_{1N}$  in the 'country rock' lies parallel to  $S_{1P}$  in the northwest trending  $S_{1P}$  zones and a simple explanation of this relationship is that  $S_0$  has been rotated into parallelism with  $S_{1P}$ . However, it would be difficult to argue against a hypothesis involving  $S_{1N}$  overprinting  $S_{1P}$  in these zones and no microfabric data is available on these relations.

In the northeastern part of Fig. 6.18  $S_{1N}$  is folded around an  $F_3$ , southwest plunging synform and becomes northeast trending, southeast dipping in the dextral limb of this fold.

Because  $S_0$  lies parallel to  $S_3$ , it is not folded by  $F_3$  (see herringbone structures, Section 3.5.2.2) and  $S_0/S_{1N}$  relations thus change from dextral to sinistral across the fold. In the dextral limb of the  $F_3$  fold,  $S_{1N}$  approaches  $S_{1P}$  in orientation.

Thin sections from Figure 6.18 show the following features:

- 1)  $S_{1N}$  overprints andalusites containing oriented biotites and ?ilmenites and also overprints an early biotite preferred orientation (Figs. 6.18 (i), (ii) ).
- 2)  $S_{1P}$  overprints andalusite with inclusion trails of biotite, and also overprints an early biotite preferred orientation (Fig. 6.18 (iii) ).

Thus whilst the macroscopic evidence is consistent either with  $S_{1N}/S_{1P}$

equivalence or  $S_{1N}$  overprinting  $S_{1P}$ , the microfabric data suggests the former.

These microfabric suggestions of  $S_{1N}/S_{1P}$  equivalence can only be extrapolated to the regional scale if it can be shown that  $S_{1N} = S_{1P}$  is a continuous schistosity, traceable through the Area 4 (and especially the Mt Franks Area) from south to north. If  $S_{1N}$  cannot be traced into  $S_{1P}$  in this way, then it must be a localised overprinting fabric. For  $S_{1N} = S_{1P} = S_1$ , it is necessary to show that there is a complimentary  $F_3$  antiform to the  $F_3$  synform in  $S_{1N}$  so that  $S_1$  is rotated around a parasitic fold and can be traced to the north. From the data available, it is suggested that this  $F_3$  antiform is shown in the trend map of Fig. 6.1, and relations between  $S_{1N}$ ,  $S_{1P}$  and the two  $F_3$  folds are best seen in Fig. 6.18 where the western limb of the  $F_3$  synform in  $S_{1N}$  corresponds to the shared limb of the fold pair.

This macroscopic  $F_3$  antiform occurs in Area 3 discussed above (subareas 19, 20, 21 and 22) and changes plunge through the horizontal from southwest in the south to northeast in the north where it degenerates into an antiform/synform pair. Two points need emphasis here:

- 1) the synformal fold in  $S_{1N}$  does not fold bedding whereas the antiformal fold is outlined by bedding and bedding-parallel  $S_1$ .
- 2) because of plunge variations of the antiform without corresponding plunge variations of the synform, continuity of  $S_1$  between both structures only occurs where both are southwest plunging. There is no visible continuity of  $S_1$  on the map where these folds are oppositely plunging.

#### *Synthesis and Implications of $S_{1N}/S_{1P} = S_1$ Correlation*

The extension of the macroscopic  $S_{1N}/S_{1P}$  relations described above to the regional scale is crucial to a reconstruction of the regional fold discussed in Section 6.3. If  $S_{1N}$  is equivalent to  $S_{1P} = S_1$ , then early folds in the Apollyon Beds and in the Robe Beds are  $F_1$  in age, and there is a progressive change in fold style from open and upright in the Apollyon

Beds to isoclinal and overturned in the underlying Robe Beds. Alternatively, if  $S_{1N}$  overprints  $S_{1P}$ , then the early folds referred to are second generation and fold not only  $S_0$  but also  $S_1$  parallel to  $S_0$ .

The macroscopic data of the last section are consistent with microscopic data which suggests that  $S_{1N}$  is equivalent to  $S_{1P}$ .

#### 6.2.3.6 Correlation of $S_{1N}$ in the Western Block and $S_1$ in the Central Block

It is suggested that there is a direct correlation between  $S_{1N}$  in the Western Block and  $S_1$  in the Central Block.  $S_{1N}/S_0$  relations are congruent to  $S_1/S_0$  relations and there is a good correlation between  $S_{1N}$  and  $S_1$  on orientation data and on morphology (Sections 4.2.1, 4.2.2.).

#### 6.2.3.7 Possibility of Mesoscopic Transposition During $D_1$

Anderson (1966) suggested that his  $D_1$  event, which is correlated with the  $D_1$  event of this study, was marked by pervasive mesoscopic transposition. However, evidence from this study suggests that widespread transposition has not taken place in  $S_{1P}$  rocks because:

- 1) layering can be defined as bedding by the presence of sedimentary structures,
- 2) bedding is not lenticular but is continuous within whole outcrops,
- 3) bedding lies parallel to large scale marker units, and
- 4) sedimentary younging directions can be related to visible macroscopic structures.

Further, if  $S_{1N}$  is correlable with  $S_{1P}$ , as is suggested in Section 6.2.3.5, then the presence of  $S_1$  at high angles to bedding over large areas also invalidates the suggestion of widespread transposition.

#### 6.2.4 Macroscopic Structure in the Southern Area Spanning the Central and Western Blocks (subareas 12, 24, Map 2)

This area spans the central and western blocks and contains the southern termination of the medium and low grade rocks.

Macroscopic folds west of the Mt Franks Retrograde Schist Zone are outlined by the boundary between the Robe and Apollyon Beds and by bedding trends in both lithologies. Although the andalusite/sillimanite isograd in this area cannot be mapped in the field, extensive thin section examination in an area of  $F_1$  folding suggests that in part it cuts across  $S_1$  at high angles, and lies close to or parallel to  $S_0$ , and in part cuts across bedding parallel or at low angles to  $S_1$ . Coupled with microfabric data which suggests that andalusite and some sillimanite is pre- $S_1$  in age, this suggests that the isograd is in part folded around  $S_1$ .

The dominant schistosity in this area has subvertical dips and trends  $050^\circ$ - $060^\circ$ . Recognition of  $S_1$  is complicated by strong retrogression, mimetic mineral growth and new penetrative schistosity formation which accompanies  $D_3$  events in this area. Nonetheless,  $S_1$  here is correlated with the schistosity parallel to the axial surfaces of folds in the Mt Franks area; the change in orientation between these two areas is due to  $F_4$  warping.

$F_1$  folds in this area span the overturn of bedding discussed further north. Fold axes and  $S_0/S_1$  intersections which are therefore northeast plunging where bedding dips southeast are southwest plunging where bedding is overturned.

In the chiastolite schist (Fig. 6.19), bedding outlines an open  $F_1$  fold pair with axes plunging very steeply to the northeast. This unit thins rapidly in the southeast limb of the fold which, except for a minor parasitic fold near the sillimanite incoming line, is unfolded. In the underlying andalusite schist the equivalent short limb of this fold pair has degenerated into a series of parasitic folds.  $S_1$  has a sinistral relation to  $S_0$  in long limbs (which trend northeasterly) and a high angle relationship in the northerly trending short limbs.

Poor outcrop limits the ability to trace individual axial surfaces across the andalusite/sillimanite isograd into the sillimanite schist. However, in the high grade rocks,  $F_1$  folds are characterised by a smaller interlimb angle,

and as a consequence dextral relations occur in the short limbs.

Equal area projections of data from the western part of Subarea 12 are shown in Fig. 6.19. Where bedding is right way up, it is folded about an axis plunging  $80^{\circ}$  to  $50^{\circ}$  (Fig. 6.19a), and  $S_1$  has an average orientation of  $050^{\circ} 88^{\circ}W$  (Fig. 6.19b).  $S_0/S_1$  intersections vary in the plane of  $S_1$  (Fig. 6.19c) and show two maxima - one at  $84^{\circ}$  to  $057^{\circ}$  and the other  $40^{\circ}$  to  $246^{\circ}$  for overturned bedding.

The sillimanite incoming line cuts across the Apollyon chiasmolite schist so that the southern part of this unit contains sillimanite <sup>†</sup>relict, retrogressed andalusite. The southern part of this unit is associated with a lightening of colour; it thus becomes indistinguishable from the surrounding rocks. This lightening of colour is due to removal of graphite as it buffers the oxygen fugacity of the system (Section 5.2.5.1).

A retrograde schist zone east of the Apollyon chiasmolite schist separates it from a highly retrogressed sillimanite schist which is dominated by a second schistosity which is probably  $S_3$ . In the south of this unit, bedding and a cross-cutting schistosity, thought to be  $S_3$ , are folded around a sinistral east plunging fold pair which is probably  $F_4$  in age (Fig. 6.21<sup>19</sup>, Loc.A). East of this sillimanite schist, a fault bounded block (subarea 24) contains a carbonaceous schist unit which is presumably obscured by the Mt Franks Retrograde Zone further north. This unit is characterised by sillimanite and retrogressed andalusite in the north and by sillimanite in the south. A sinistral, east plunging fold pair in the south of this subarea (Fig. 6.21<sup>19</sup>, Loc.B) may be  $F_4$  in age.

East of the Mt Franks Retrograde Schist Zone, calc silicate units outline north plunging folds discussed in Section 6.2.2. The enclosing schists are highly retrogressed and there is some evidence of sillimanite. The northern extent of sillimanite needs to be refined by more thin section work, but definite sillimanite occurs north of an ENE trending granitoid sheet. South of this sheet, migmatites and sillimanite schists are present -

in contrast to the finer grained rocks north of the granitoids and these schists are dominated by a sillimanite schistosity (probably  $S_1$ ) which has been overprinted by late stage muscovite and sericite growth. The bending of  $S_1$  into and out of the granitoid sheets suggests that they may be localised along a post- $S_1$  shear zone. However, the presence of calc silicate units south of these granitoids suggest a limited amount of displacement, and further work should be carried out to refine relations in this area. Minor  $F_4$  folds in this area lie subparallel to the major folds, inferred to be  $F_4$ , further to the southwest. However, the significant fact is that the sillimanite -in line appears to cut across both  $S_0$  and  $S_1$ .

### 6.3 SYNTHESIS OF MACROSCOPIC STRUCTURES IN THE MT FRANKS - MUNDI MUNDI AREA.

The spatial relations between the macroscopic structures described in the Sections 6.2.3, 6.2.4 can best be summarised and analysed by reference to serial cross sections (Fig. 6.20) and to a three dimensional sketch (Fig. 6.21). The eastern block (east of the Apollyon Valley R.S.Z.) is dominated by  $S_0//S_1$  which is folded around  $F_3$  fold pairs which are parasitic on a synform to the east. In the central block (between the Apollyon Valley and Mt Franks R.S.Z.'s),  $S_1$  lies at an angle to bedding and  $F_1$  folds vary in plunge in this block from southerly to northerly (from north to south) and are parasitic on an  $F_1$  syncline to the east. Since  $F_3$  folds are parasitic on a synform to the east, there is no major  $F_3$  structure obscured by the Apollyon Valley Retrograde Schist Zone.

$F_1$  folds in the western block also vary in plunge from southerly to northerly (from the Mt Franks area to the south) and are parasitic on a major syncline to the east (Fig. 6.20, Section AA' and DD'). West of this hinge,  $S_0/S_1$  angles decrease westward until  $S_{1P}$  relations are reached, and the amplitude and number of  $F_1$  folds also decreases to the west.

It is suggested that all these  $F_1$  folds are parasitic on a regional

hinge which has been removed by movement on the Apollyon Valley Retrograde Schist Zone. This disruption accounts for lack of lithological repetition, and accounts for the juxtaposition of the  $S_{1P}$  Parnell Beds (characteristic of a limb position - cf.  $S_{1P}$  Robe Beds) against the  $S_{1N}$  Apollyon Beds. Although this hinge cannot be located in this area, regional correlations in the next chapter suggest that it occurs north of the Mt Robe in the Kantappa - Brewery Well area. The Apollyon and Robe Beds are thus interpreted as lying in the western limb of this regional syncline.

According to the model in which  $S_{1N}$  is equivalent to  $S_{1P}$ , this regional syncline is  $F_1$  in age and is characterised by a change in  $S_0/S_1$  relations from high angle in the core of the fold to parallel in the western limb. If  $S_{1N}$  overprints  $S_{1P}$ , on the other hand, this syncline is in reality a second generation structure overprinting  $S_0/S_1$ . Before discussing the variation in  $S_1$  orientation which is a necessary feature of this regional fold in either model, the extent of the western limb will first be considered.

The extent of this limb to the west depends on consistent "syncline to the east" relations in the  $S_{1N}$  domain, and on consistent eastward youngings in the  $S_{1P}$  domain when  $F_2$  and  $F_3$  effects have been removed. The extension of the west limb of this syncline to the Mundi Mundi plain relies heavily on the downward facing  $F_3$  folds in the hinge of the Mt Robe Synform in the Mundi Mundi facies. There is, however, a gap in sedimentary younging directions in subarea 15, and it is possible that the downward facings in the Mundi Mundi facies could result from crossing two pre- $D_3$  fold hinges in this area.

Three further points need to be made in this regard.

(1)  $F_3$  folding of  $S_1$  across  $S_0$  on Mt Franks results in a change in  $S_0/S_1$  relations which then cannot be used to determine the position of major  $F_1$  axes (see herringbone structures, Section 3.5.2.2),

(2)  $S_0/S_1$  relations in subarea 18 are sinistral, southwest - plunging

but are believed to belong to a "short limb" situation, rather than to crossing an  $F_1$  axis since sedimentary structures are still eastward younging,

(3) during the early stages of mapping the possibility was considered that the Apollyon chistolite schist is continuous with the Mundi Mundi facies. If these units are to be equated stratigraphically, they must cross a major anticlinal axis - with attendant change in younging. Because of the different orientations of these two units, such a fold cannot be isoclinal. Since extensions of the Mundi Mundi facies to the southwest were not mapped, this possibility could not be determined on lithological grounds. However, in the area mapped no change in  $S_0/S_1$  relations or in younging directions was found to indicate the presence of an anticlinal axis which must lie west of eastward younging rocks in subarea 18.

#### 6.3.1 Variation in the Orientation of the Western Limb of the Regional Syncline

In the Robe Beds, Sections AA', BB', CC' and DD' (Fig. 6.20) show that  $S_0$  changes dip through the vertical from easterly to westerly southwest of Mt Franks, whereas Sections EE', GG', HH' indicate that north of Mt Franks,  $S_0$  is southeasterly dipping. This change of dip occurs just west of the Apollyon/Robe Beds boundary which is east or southeasterly dipping throughout the area. If a bedding surface near the andalusite/sillimanite isograd is used as a form surface, it changes dip from westerly southwest of Mt Franks (Section AA', BB', CC', DD') to southwesterly northwest of Mt Franks (Sections EE', GG', HH') and then becomes southwesterly dipping again northwest of Black Prince Mine (Map 1).

The trace of the overturn in bedding can thus be defined as running north/south just west of the Apollyon Beds south of Mt Franks, and then swinging northwest near Waterfall Gully (Map 1). North of this overturn,  $S_0$  dips to the southeast; south of it  $S_0$  dips to the west. Along the boundary between Areas 2 and 3, as discussed in the summary to Area 3 (Section 6.2.3.3), the trace of this overturn is folded around the antiform and is



faulted off by a northwest trending fault.

Southeast dipping, southeast younging beds north of this overturn become overturned themselves further north in the Black Prince Fold Pair (Section 6.2.3.3) so that the Mt Robe Synform to the north is also overturned. There is thus an area northwest of Mt Franks in which bedding is rightway up. The rest of the western block, with the exception of a thin strip of Robe andalusite schists and the Apollyon schists is overturned.

South of Mt Franks, west dipping bedding occurs either by overturning across a constantly oriented  $S_1$  (Sections AA', BB', CC') or in the western limb of the Mt Franks fold pair (Fig. 6.19, and Fig. 6.20, Section DD'). This change in bedding dip is probably  $D_1$  in age although  $S_1$  overprinting on an earlier overturn cannot be totally ruled out in Sections AA', BB' and CC'. Further north, the change from rightway up  $S_0$  to overturned  $S_0$  in Area 3 is pre- $D_3$  in age.  $D_2$  effects are discounted because of their limited occurrence and it is suggested that this overturning is a late stage effect of the  $D_1$  event.

### 6.3.2 Variation in the Orientation of $S_1$

Changes in the orientation of  $S_1$  throughout the area can be analysed in two parts.

Firstly,  $S_{1N}$  fans about the vertical in the Apollyon Beds south of Mt Franks - from steeply east dipping in the east to steeply west dipping in the west. These dips of  $S_{1N}$  shallow to the west and  $S_{1N}$  merges into west dipping  $S_{1P}$ . This shallowing is independent of  $F_3$  folding because:

- 1) There is no significant change in strike of  $S_1$ , indicating that  $S_1$  is fanning about a subhorizontal axis, not an axis parallel to  $F_3$ .
- 2) There is no simultaneous change in orientation of  $S_0$ . Thus in sections BB' and CC',  $S_0$  shows little, or irregular, dip variation.
- 3) There is a change in the orientation of  $S_1/S_3$  intersections which indicates that  $S_1$  was curvilinear before  $D_3$  time. Thus in subareas 6, 10 and 13,  $S_1/S_3$  intersections become shallower to the east (Fig. 6.23) and

this trend is continued across the Mt Franks Retrograde Schist Zone into the central block to the east.

North of Mt Franks,  $S_{1N}$  remains westerly dipping just west of the boundary between the Robe Beds and the Apollyon Beds and is then folded around  $F_3$  folds to dip to the southeast in the dextral limb of an  $F_3$  synform.

Secondly,  $S_{1P}$  changes orientation from (south)west dipping southwest of Mt Franks (Area 2) to southeast dipping northwest of Mt Franks (pre- $F_3$  orientation) and then back to southwest dipping west and northwest of the Black Prince Area.

Little change is needed in the orientation of  $S_{1N}$  to bring it into parallelism with  $S_{1P}$  southwest of Mt Franks. However, north of Mt Franks,  $S_{1N}$  dips to the southeast more gently than  $S_0$  in the dextral limb of the  $F_3$  synform, and if  $S_{1N}$  is equivalent to  $S_{1P}$ , it must undergo a clockwise rotation to steepen its dip. If  $S_{1N}$  is equivalent to  $S_{1P}$ , this amounts to a pre- $D_3$  rotation of  $S_{1N}$  through the vertical. Steepening of  $S_1$  through the vertical does occur south of Mt Franks (from east to west dip) and can be seen north of Mt Franks in Section HH' (Fig. 6.20).

These changes in  $S_1$  orientation are pre- $D_3$  in age.\*  $D_2$  effects are discounted because of their limited occurrence and they are thus regarded as late stage  $D_1$  features, occurring after  $S_1$  formation.

These changes in  $S_1$  orientation must be mirrored by changes in the orientation of the axial surface of the regional synform. This surface is then curved: in the core of the major fold it is subvertical; further west it becomes inclined to the west both south of Mt Franks and west of the Black Prince Fold Pair. Between these areas,  $S_1$  dips to the southeast.

---

\* With the exception of the change in  $S_1$  discussed in the last paragraph, all these changes in  $S_1$  orientation occur if  $S_{1N}$  is or is not equivalent to  $S_{1P}$ .

### 6.3.3 Shape of the Reconstructed Regional Syncline

This reconstruction only discusses the shape of the western limb of the  $F_1$  Syncline. The shape of the eastern limb is not known; it has been removed by the Apollyon Valley Retrograde Schist Zone - an  $F_3$  zone (Section 6.4 which may possibly have originated as a slide during  $F_1$  folding. This reconstruction is based on the variation in  $S_0$  and  $S_1$  discussed in the last two sections. Figure 6.23 illustrates three possible profile sections of this syncline south and north of Mt Franks. Fig. 6.23b is untenable since it is incompatible with refolding by a downward facing synform in the west. Between sections Fig. 6.23a and c,  $S_0$  and  $S_1$  pass through the vertical (see last two sections). These sections indicate that the western limb of this syncline is marked by progressive overturning with depth.

Although the plunge of small scale structures indicates that there is a change in regional plunge from south on Mt Franks to north in the south of the area, the regional plunge is not known. Consideration of evidence further north (Section 7.2.1), which suggests that younger rocks are progressively exposed in the core of the synform to the north, indicates that there may be an overall northerly plunge. This then suggests that more bedding will be right way up to the north.

The  $F_1$  syncline shown in Fig. 6.23 is not recumbent. It is subvertical in low grade rocks and is progressively overturned with depth. This variation in attitude could be:

- 1) caused by  $F_3$  folding of a planar syncline,
- 2) caused by pre- $F_3$  folding of a planar syncline, or
- 3) the original orientation of the syncline at the end of a complex  $D_1$

deformation. The effect of hypothetical pre- $F_1$  folding here cannot be discount

Point 1) is militated against by the arguments in Section 6.3.2, i.e. that  $S_1$  is curved before the  $D_3$  event. Point 2) is militated against in the preferred model of  $S_{1N}/S_{1P}$  equivalence because  $D_2$  effects are only minor, and folding around a  $D_2$  axis cannot result in the re-orientation of

$L_1$  from steeply south plunging in the core of the syncline to southwest plunging in the limb. However if  $S_{1N}$  overprints  $S_{1P}$ , this is a possibility. In the preferred model of  $S_{1N} = S_{1P} = S_1$ , it is considered that variation in the syncline shape is a result of  $D_1$  folding and final  $D_1$  modifications after  $S_1$  formation.

If  $S_{1N}$  is equivalent to  $S_{1P}$ , the variation in orientation of  $L_1$  indicates a change from sub vertical extension in the core of the syncline (the "steep belt") to a moderately plunging direction of extension in the more fluid, higher grade rocks (the "flat belt"). This is plausibly associated with a change in direction of mass transfer from sub vertical towards sub horizontal - i.e. a spreading out effect.

These features can be explained by the following speculations. The syncline was formed as a tight, upright fold, the orientation of which is preserved in the "steep belt," and movement in this belt was subvertical. In the higher grade rocks, the syncline became overturned, or was formed with a dipping axial surface. Later movement, perhaps due to gravitational collapse, led to a modification of this fold in the high grade rocks, and to an overturning which is recorded by the changes in orientation of  $S_0$  and  $S_1$ .

Similar variably oriented large scale first generation folds have been described from the Dalradian of Scotland by Roberts (1974) - the Tay Nappe - and from the Appalachian Piedmont by Tobisch and Glover (1971) who studied relations across the Carolina Slate Belt - Charlotte Belt Boundary. In both these papers, the variation in orientation of  $S_1$  is regarded as an integral part of the main deformation.

#### 6.3.4 Relations Between the Regional Syncline and Metamorphic Zones

If the metamorphic zones are pre- $D_1$  in age (Section 5.2.1) they must be folded around the  $F_1$  hinge now occupied by the Apollyon Valley Retrograde Schist Zone. Low grade rocks between the Apollyon Valley Retrograde Schist Zone and Mt Franks Retrograde Schist Zone pass westwards into medium grade rocks and then into high grade rocks. To the east, low grade rocks

pass across the Apollyon Valley Retrograde Schist Zone into high grade rocks and very high grade rocks (K feldspar, + sillimanite). The boundaries between the low/medium and medium/high grade zones are defined by pre- $S_1$  minerals and are thus pre- $D_1$  in age.

The distribution of these metamorphic zones is in accord with the concept of a regional  $F_1$  syncline which folds the low/medium and medium/high grade boundaries, and with the hinge zone and part of the eastern limb removed by movement on the Apollyon Valley Retrograde Schist Zone.

#### 6.3.4.1 Structural Relations between Low and Medium Grade Zones

The boundary between these two zones is localised along the Mt Franks Retrograde Schist Zone in this area, but lies parallel to bedding further north (Section 7.2.3.2). The medium grade rocks thus underlie the low grade rocks, both structurally and stratigraphically.

#### 6.3.4.2 Structural Relations between Medium and High Grade Zones

The boundary between these two zones is in general parallel to bedding and lies in the western limb of the regional syncline. Between Mt Franks and the Black Prince Mine, sillimanite schist underlies andalusite schist structurally and stratigraphically. North of Black Prince Mine, and south of Mt Franks, bedding is inverted (dips to the west) and sillimanite schist structurally overlies but stratigraphically underlies the andalusite schist. Just north of Lakes Nob, the andalusite/sillimanite isograd outlines steeply north plunging  $F_1$  folds, and cross cuts bedding parallel to  $S_1$  in places. Sillimanite schist in this area underlies andalusite schist, and the belt of andalusite grade rocks terminates in steeply north plunging folds. This boundary is regarded as a gradational boundary, not a tectonic boundary because:

- 1) there is no evidence of a bedding-parallel fault or slide,

2) zones of mixed andalusite + sillimanite co-exist for distances up to 150 m about the 'isograd,'

3) andalusite occurs as scattered relicts throughout the sillimanite grade rocks, and

4) microscopically visible sillimanite occurs in andalusite schists just below the first appearance of sillimanite defined in the field.

The inversion of the andalusite/sillimanite isograd in the western limb of the Kantappa - Lakes Nob Syncline is attributed to late stage  $D_1$  folding (see below). However, south of Mt Franks, bedding and the isograd were inverted during the  $D_1$  event, and not by late stage tilting or folding. Evidence against late stage tilting is provided by similarity of  $S_3$  orientation throughout the area, and also with other parts of the Broken Hill area (Laing, 1977).

Although the three metamorphic zones are folded around the regional  $F_1$  syncline, their folded distribution controls aspects of the  $D_1$ ,  $M_1$  event. Thus in  $D_1$  time:

1) the low grade zone is characterised by a subvertical, dominantly homogeneous, muscovite  $\pm$  biotite  $S_1$ , upright, tight folds and  $S_{1N}$  relations.

2) the medium grade zone is characterised by an inclined, homogeneous to layered muscovite  $S_1$ , overturned, tight to rarely isoclinal  $F_1$  folds and  $S_{1N}$  as well as  $S_{1P}$  relations.

3) the high grade zone is characterised by an inclined, layered biotite + muscovite  $\pm$  sillimanite  $S_1$ , overturned tight to isoclinal folds,  $S_{1P}$  relations and migmatite formation.

The folded distribution of metamorphic zones also controlled aspects of the  $M_1$  metamorphism. Thus migmatites occur only in the folded sillimanite zone and are  $S_1$  in age, and  $S_1$  sillimanite growth also occurs only in the folded sillimanite zone.

Syn- $S_1$  sillimanite growth in sillimanite schists which structurally overlie andalusite schists causes no problems if the overturning is post  $S_1$

in age. However, the overturning of bedding both northwest and south of Mt Franks are regarded as  $D_1$  in age (Section 6.3.1), and this demands a heat source "up in the air."

This paradox, however, can be explained in terms of three factors:

- 1) Rapid  $F_1$  folding,
- 2) non recumbent  $F_1$  folding, and
- 3) greater heat capacity of low grade rocks.

Consider the formation of flat lying isograds in pre- $S_1$  time (Fig.6.25a) (Strictly speaking these isograds were not everywhere flat lying). As a result of  $F_1$  non recumbent folding, the low grade zone is depressed into the region where P,T conditions gave rise to minerals characterising the medium grade zones. Similarly the medium grade zone was infolded into the old high grade zone. This leads to a pattern of isotherm distribution as shown in Fig. 7.25b. The infolded low grade rocks are at a lower temperature than the medium grade rocks which formed in the zone they now occupy. If folding is relatively rapid, these low grade rocks can absorb a large amount of heat, i.e. they have a large heat capacity, before the rocks reach the critical temperature for new mineral growth. The amount of heat now trapped in this zone is used by reactions producing muscovite + quartz in  $S_1$  time. If all the available heat is used up by these reactions, there is no further advance of the metamorphic front. A similar situation is envisaged with medium grade rocks infolded into the old high grade field. The cold nature of these rocks is able to absorb all the available heat by the (re)crystallisation of muscovite and quartz, without reaching the field of sillimanite growth. The sillimanite grade rocks, however, are already at sillimanite-forming conditions. During inversion of the andalusite/sillimanite boundary, sufficient heat is trapped in the core of the adjacent anticline to enable new sillimanite recrystallisation to occur.

### 6.3.5 Metamorphic Zones and Tectonic Levels

The general formation of metamorphic zones parallel to bedding before large scale  $D_1$  folding suggests a rise in the regional geothermal gradient before the onset of the main deformation. However, the presence of pre- $S_1$

oriented growth predates the formation of static andalusite and sillimanite and indicates that there is a general association of metamorphism and deformation. Unless the pre-S<sub>1</sub> deformation is associated with the production of isoclinal folds of large extent, the increase in metamorphic grade with depth may be related to the concept of 'tectonic levels.'

From studies in the Greenland Caledonides, Wegmann (1935) was able to recognise the broadly contemporaneous development of different structural styles at different depths. This enabled him to recognise a number of tectonic levels. "Tectonic levels (Stockwerke) of the same movement cycle are here designated 'superstructure' ('Oberbau') and infrastructure ('Unterbau'). They should not be confused with the relationship between cover and basement; these belong to different movement cycles and are separated by an unconformity..." (Wegmann, 1935, p.332, my own translation). This concept was amplified by Haller (1967) who recognised:

- a) an upper superstructure characterised by open, more upright folds in low-grade or non-metamorphosed sediments,
- b) an underlying zone of disharmonic detachment, and
- c) a granitic and magmatic infrastructure characterised by flat-lying folds.

In the Pyrenees, de Sitter (1960), de Sitter and Zwart (1960), and Oele (1966) recognised:

- a) a weakly metamorphosed superstructure characterised by vertical cleavage,
- b) a transition zone with subvertical to subhorizontal cleavage,
- c) a highly metamorphosed infrastructure characterised by horizontal cleavage,

and Oele (1966) showed that there is a continuous gradation between vertical



and flat-lying schistosity in the Vall Ferrera Area.

Iwamatsu (1975) has applied this concept to Japan, but he regarded the change in orientation of schistosity from flat lying at depth to sub-vertical at higher levels as a result of different deformations. Tobisch and Glover (1971), on the other hand, have interpreted Carolina Slate Belt - Charlotte Belt relations in the Appalachians as analogous to relations found in superstructure and infrastructure.

Application of the 'tectonic levels' concept to the Mt Franks - Mundi Mundi Area differs from all the above applications in that tectonic zones are disrupted and folded about the earliest recognisable folds. Despite this, their folded distribution still influences the style and orientation of  $D_1$  structures (Section 6.3.4).

#### 6.4 THE RETROGRADE SCHIST ZONES.

##### 6.4.1 Mt Franks Retrograde Schist Zone

Background.

The Mt Franks Retrograde Schist Zone was first mapped by Andrews (1922) who regarded it as a crush zone extending from north of Lakes Nob to the Terrible Dick Mine and containing a steeply ( $80^\circ$ ) southeast dipping schistosity. King and Thomson (1953) renamed this structure the "Mt Franks Fault," and extended it further along strike to the northeast, underneath the Gum Creek Alluvial flat, along the western side of the Kantappa 'Trough.' These authors suggested that the Mt Franks Fault was part of the Mundi Mundi Fault set which were characterised by northeast trends, steep dips, and unknown offsets.

Binns (1963, Fig. 3) suggested that the formation of the Mt Franks fault was associated with his  $M_3$  event, which was characterised by the formation of andalusite after sillimanite. He suggested that the northeast extension of the fault did not mark the western edge of the Kantappa 'Trough,' but rather continued right up to the Adelaidean Unconformity east of Brewery Well.

However, in his mapping of the Mt Robe District, Anderson (1966) found

no evidence to substantiate the existence of the fault. He considered that the fine grained, grey schist previously described as the schist zone was really a primary lithological unit. His main evidence against the presence of the fault was that the fault trace delineated by King and Thomson (1953) crossed his mapped lithological units without disrupting them. In addition, Anderson (1966) refuted Binns' suggestion that andalusite was retrograde after sillimanite; he considered them to be co-eval and part of his  $M_1$  event. Present Study.

The Mt Franks Retrograde Schist Zone is a remarkably straight northeast trending valley containing poor outcrop. Within this zone, grey coloured phyllites occur on the western margin of the zone where they grade into carbonaceous schist, and buff, khaki coloured phyllites occur in the eastern part of the zone where they grade into quartz mica schists. Also present within this zone are a carbonaceous schist unit, local calc silicate pods, and pegmatites. As defined in Map 1 the Mt Franks Retrograde Zone can be traced from the Gum Creek Alluvial Flat, southeast past Mt Franks, into a zone of poor outcrop north of Lakes Nob where it terminates in a number of splay faults. Although the retrograde zone is locally concordant to bedding in country rock it does cut off a number of units on its eastern and western boundaries (Map 1).

Within the Retrograde Zone a vertical quartz-muscovite retrograde schistosity ( $S_R$ ) generally strikes parallel to the trend of the zone boundaries.  $S_R$  generally obliterates all previous fabrics, although in local less strongly deformed domains, an early schistosity and bedding can be seen, both having a sinistral relation with  $S_R$ . On the western margin of the zone  $S_R$  is axial plane to small, less than 10 cm amplitude, tight folds. Axes and  $S_R/S_0$  intersections generally plunge to the southwest but shallow passing to the north. Towards the centre of the zone, only very scarce isoclinal  $F_R$  folds can be recognised and it is thus suggested that the retrograde zone forms as a planar zone of mesoscopic transposition in " $F_R$ " time.

An equal area plot of poles to  $S_R$  indicates the constant orientation of this schistosity ( $039^\circ$   $90^\circ$ , Fig. 6.26a). Within  $S_R$ , a down dip mineral lineation ( $L_M$ ) plunges  $70^\circ$  to  $211^\circ$  (Fig. 2.26b).

Small  $F_{R+1}$  folds and crenulations in  $S_R$  are common. These plunge both to the east ( $65^\circ$  to  $106^\circ$ , main maxima, Fig. 6.26c) and also to the southwest ( $82^\circ$  to  $248^\circ$ ). The southwest plunging maxima is parallel to the orientation of the mineral lineation within  $S_R$ , and may be controlled by it. The axial surfaces of these folds are rarely marked by a new schistosity, but may contain fractures.

Relation between  $S_R$  and  $S_3$ .

$S_R$  in the Mt Franks Retrograde Schist Zone is parallel in strike to  $S_3$  in the surrounding rocks, and evidence for a direct age relationship between  $S_R$  and  $S_3$  is supported by several other important features:

1) In the Robe andalusite schist of the  $S_{1N}$  domain,  $F_3$  crenulations occur on a regional scale and increase in intensity and frequency towards the Mt Franks Retrograde Schist Zone. This is best seen in a west-east traverse across the eastern dextral limb of the Mt Franks fold pair. Uncrenulated  $S_{1N}$  occurring on the western side of this limb becomes increasingly tightly crenulated until a new schistosity  $S_3$  or  $S_3'$  is dominant on the eastern margin of this unit and in the overlying Apollyon chiasmolite schist.

South of Mt Franks,  $S_3$ ,  $S_3'$  or tightly crenulated  $S_{1N}$  lying just west of the retrograde zone becomes less deformed passing to the west.

In the Apollyon quartz mica schists,  $S_3$  is mainly developed in the western part of the unit although  $S_1$  is not everywhere crenulated.

2) Thin section examination across the Apollyon chiasmolite schist/Mt Franks Retrograde Zone boundary shows that the  $S_R$  microstructure is morphologically and mineralogically similar to  $S_3$  (See Section 4.6).

3) The metamorphic grade of  $S_R$  and  $S_3$  are similar: muscovite + quartz + chlorite + opaques (after biotite breakdown) (see Section 4.6).

4) The orientation of small  $F_R$  folds observed in the western part of the Mt Franks Retrograde Schist Zone is parallel to  $F_3$  folds in the adjacent andalusite and chiastolite schists.

5) The orientation of  $L_M$  in the retrograde schist zone is parallel to the orientation of  $L_3$ , a mineral lineation within  $S_3$ , in the Robe Andalusite Schist. In both cases  $L_3$  and  $L_M$  are not necessarily parallel to  $F_3$  and  $F_R$ . The  $L_3$  lineation is only visible close to the western margin of the schist zone.

6) The trend of  $S_4$  axial surfaces in the surrounding rocks is similar to  $S_{R+1}$  in the retrograde zone ( $110^\circ - 130^\circ$ ) and the plunge of  $F_4$  folds in the surrounding rocks is parallel to easterly plunging  $F_{R+1}$  folds within the Retrograde Zone.

#### 6.4.2 The Apollyon Valley Retrograde Schist Zone

##### Background.

This zone was first recognised by Andrews (1923) who suggested that Apollyon Valley marked a fault separating low grade rocks on the western side from sillimanite grade rocks on the eastern side. Later mapping by King and Thomson (1953) did not recognise a fault of this magnitude in the area, but did note the presence of shear zones near the Apollyon Mine. They also showed that Thackaringa type mineral deposits were located on these zones. Binns (1963) on the other hand, favoured the existence of a major fault extending from the Adelaidean Unconformity along Apollyon Valley and separating rocks of the Willyama Complex on the west from Adelaidean sediments on the east.

##### Present Study.

The present study has confirmed the existence of a major structural break, the Apollyon Valley Retrograde Schist Zone, within the Apollyon Valley. This retrograde zone can be traced from the Apollyon Mine in the south of the area on a north northeasterly trend through the Terrible Dick Mine, to the Gum Creek Alluvial flat. Further extensions along strike are

discussed in Section 7.2.1. The Apollyon Valley Retrograde Schist Zone separates retrogressed sillimanite schist (high grade rocks) on the east from retrogressed biotite schist (low grade rocks) on the west.

Although field mapping shows that the retrograde zone trends north - northeast, parallel to the Mt Franks Retrograde Schist Zone, there is no information on the dip of this zone. The western margin of the zone is partially obscured by alluvium, but is well defined, and cuts across the boundaries of a carbonaceous schist unit and also a calc silicate band north of Lady Dorothy Mine. The eastern boundary, on the other hand, is marked by splay faults which trend east northeast into the Parnell Beds.

The Apollyon Valley Retrograde Schist Zone itself is characterised by poorly outcropping grey and buff coloured phyllites which contain a penetrative north to north northeast trending, vertical schistosity. This schistosity is characterised by a steep southwest plunging mica lineation. Later folds and crenulations within this schistosity plunge steeply east and west.

Relations between  $S_R$  and  $S_3$ .

The Apollyon Valley Retrograde Schist Zone is surrounded by an envelope of strongly retrogressed country rocks which are dominated by a new crenulation schistosity ( $S_3$ ) defined by muscovite and quartz. This  $S_3$  schistosity is parallel to the orientation of the retrograde schistosity ( $S_R$ ) within the schist zone, and suggests a relationship between the age of the two fabrics. Evidence for a  $D_3$  age of the formation of the retrograde schist zone is also provided by the parallelism between  $S_R$ , and axial surface to  $F_3$  folds in the Parnell Beds.

#### 6.4.3 The Mundi Mundi Fault

Background.

Andrews (1922) suggested that the Mundi Mundi geomorphological scarp was fault controlled, and presented excellent evidence for Tertiary movement on it. B. Wasson (pers. comm., 1975) also concluded that the Mundi Mundi

scarp was generated by Tertiary movement, and suggested that more than one period of movement was involved, with the latest being pre-Upper Pleistocene. King and Thomson (1953) suggested that this Tertiary Movement represented only late stage reactivation of a fault which was initiated as part of a set (including the Mt Franks and Globe Vauxhall) in the main Willyama Deformation.

Present Study.

The present study did not define a Mundi Mundi fault trace since the scarp was only mapped over a small area. The only evidence of intense deformation in this area is a 30 m wide schist zone marked by muscovite and quartz after sillimanite biotite and K feldspar, and which contained local quartz augen. This retrograde schistosity is a crenulation fabric which trends  $025^{\circ}$  with subvertical dips and is tentatively regarded as a feature of the Mundi Mundi Retrograde Schist Zone. No information on the dip of this structure is available.

#### 6.4.4 Age of the Retrograde Schist Zones

The Apollyon Valley, Mt Franks Retrograde Schist Zones and the Mundi Mundi Fault are believed to define a major set of retrograde schist zones, and Laing (1977) includes the Globe Vauxhall Shear Zone at Broken Hill as part of this set. These structures all have NNE to ENE trends and are marked by a steeply dipping retrograde schistosity.

The strong relation between  $S_R$  in the schist zones and the regional  $S_3$ , suggests that these schist zones were initiated in the waning phase of  $D_3$  deformation. Although it could be argued that these schist zones are late stage features, mimetically reinforcing  $D_3$  features, this view is militated against in the Mt Franks Retrograde Schist Zone not only by the parallelism of  $L_3$  with  $L_M$ , but by the parallelism of  $F_3$  with  $F_R$ , and by the parallelism of  $F_4$  and  $S_4$  with  $F_{R+1}$  and  $S_{R+1}$ .

Both the Mundi Mundi Fault and the Apollyon Valley Retrograde Schist Zone have suffered later reactivation. Emplacement of Thackaringa - type

deposits in the Apollyon Valley Retrograde Zone suggest re-activation at about 500 Ma (Kansewich, 1962) and both Thomson (1969) and Laing (1969) show that the continuation of this retrograde zone to the north localises an anticline in the overlying Adelaidean sediments. Glen et al (1977, Appendix I) relate this to the Delamerian Orogeny (c.500 Ma).

#### 6.4.5 Displacement Across the Retrograde Schist Zones

Recent movement on the Mundi Mundi fault is west-block down with a displacement of about 300 m (B. Wasson, pers. comm., 1975). Little movement is envisaged on the Mt Franks Retrograde Schist Zone in this area since it is localised within a phyllitic lithology of this unit (cf. Anderson, 1966).

The Apollyon Valley Retrograde Schist Zone, however, is a more significant feature. This retrograde zone is localised near the margin of an  $F_1$  "steep belt" and an  $F_1$  "flat belt" and may have originally formed as a slide due to strain heterogeneities during  $D_1$ . The retrograde schist zone as now seen, however, is related to the  $D_3$  event. However, constancy of  $F_3$  vergence across this zone (Section 6.2.1) suggests it is not localised on a major  $D_3$  structure.

The absence of lower grade rocks east of the Apollyon Valley Retrograde Schist Zone may be accounted for either by east block-down or east block-up movement. Because of variation in the attitude of the western limb of the  $F_1$  regional syncline, correlation across the retrograde zone cannot be made using dip orientation. Correlation across the retrograde zone depends to a large extent on the significance placed on the poor younging directions found in the Parnell Beds. If these are eastward younging as suggested on Fig. 6.1, then none or two  $F_1$  hinges have been removed by the retrograde zone. If, however, this younging data is not correct, then correlation of metamorphism and structural styles across the retrograde zone would imply that the Parnell Beds represent the eastern limb of the  $F_1$  syncline. Until better younging directions are located, a decision between these two models cannot be made.

## 6.5 STRATIGRAPHY.

With the conditions of this reconstructed  $F_1$  syncline in mind, and from the serial sections of Fig. 6.20, it is possible to compile a stratigraphic sequence for the Mt Franks - Mundi Mundi area. The sequence, Fig. 6.27 is divided into two parts corresponding to different sides of the Apollyon Valley Retrograde Schist Zone. In the western limb of the  $F_1$  syncline, here called the Kantappa - Lakes Nob Syncline, approximately 4.2 km of conformable sediment are present. The sequence, as shown below, is based on the model that the western limb of the  $F_1$  syncline extends to the Mundi Mundi Plain. If the alternative model, that the Mundi Mundi facies correlates with carbonaceous schists further east, is correct (Section 6.3) the sequence is only about two thirds the thickness in this limb.

The base of the sequence, below the Mundi Mundi facies just south of the mapped area, consists of sillimanite grade metasediments with granitic material. Rocks of the Mundi Mundi carbonaceous facies are overlain by psammites, pelites and psammopelites of the Robe Beds. These rocks are associated with concordant amphibolites, sheets of granitoids and psammite rich units. Local calc silicates and gneisses are also present. Psammopelite rich rocks of the Mt Franks facies form the upper part of the Robe Beds; these are overlain by Apollyon Beds, the base of which consists of carbonaceous schist, and which is dominated by quartz mica schist with lenticular carbonaceous schist and calc silicate bands.

East of the Apollyon Valley Retrograde Schist Zone, the Parnell Beds consist of pelites, psammites and psammopelites with concordant sheets of amphibolites and granitoids. Their relation to the Robe Beds is unclear.



Fig. 6.1. Bedding trend map showing distribution of sedimentary  
younging directions.

DISTRIBUTION OF YOUNGING DIRECTIONS  
MT FRANKS - MUNDI MUNDI AREA

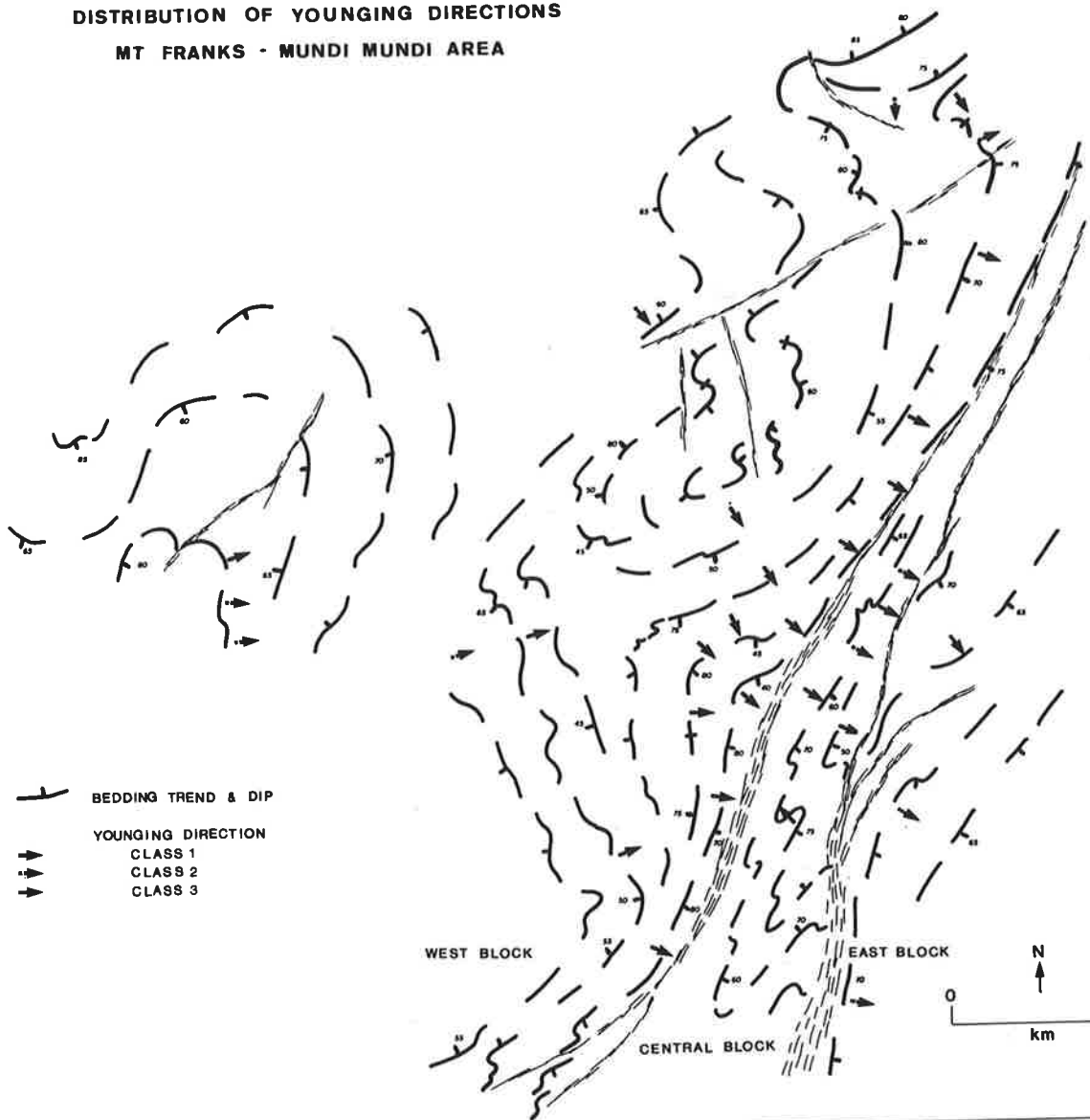


Fig. 6.2  $D_1$  interpretation map showing trend of bedding and  $S_1$ ,  $S_0/S_1$  relations and  $F_1$  major folds.

MT FRANKS MUNDI MUNDI AREA  
STRUCTURAL INTERPRETATION: D<sub>1</sub>

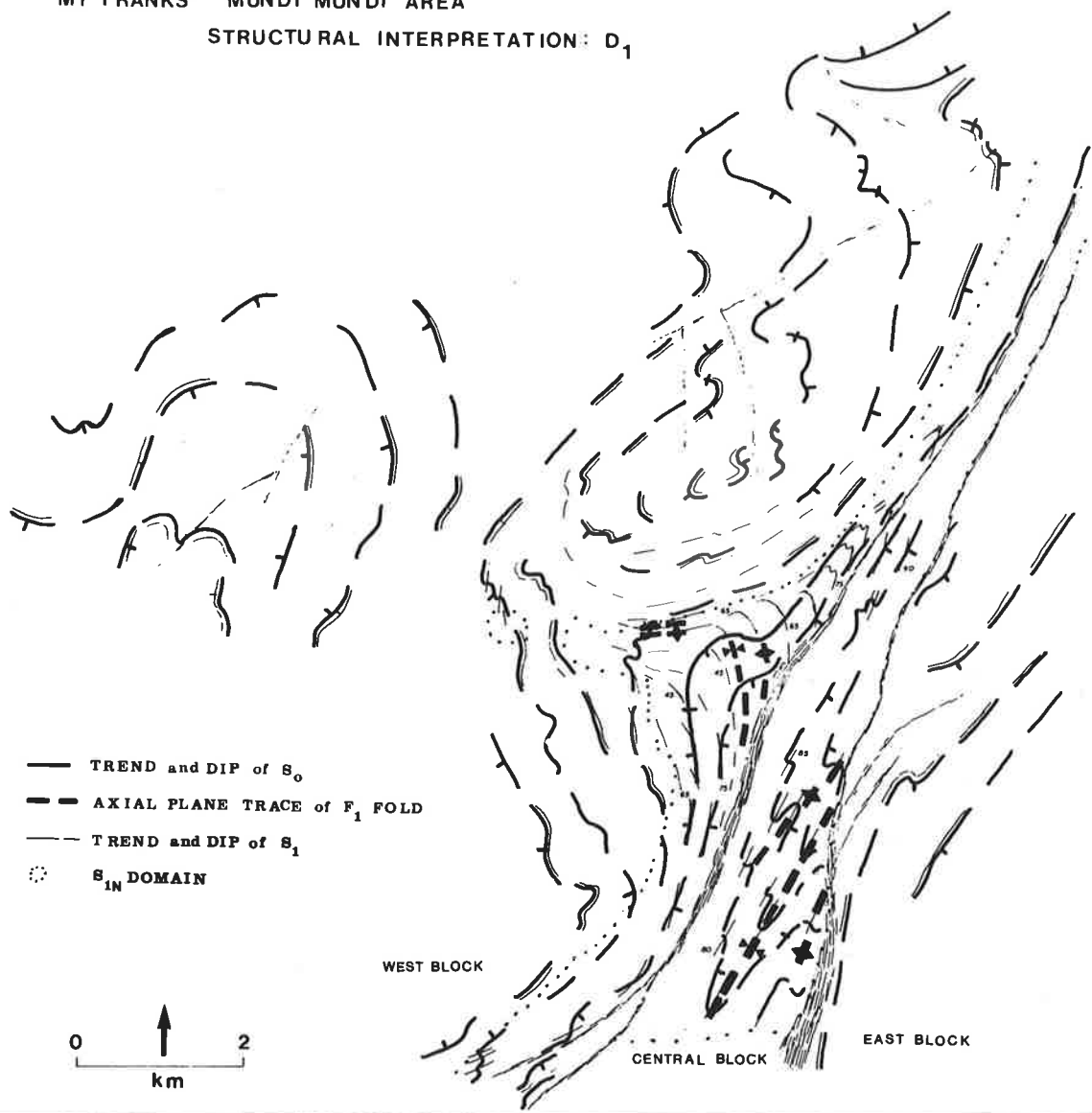


Fig. 6.3  $D_3$  interpretation may showing trend of bedding and  $S_3$ , and  $S_0/S_3$  relations. Note "conjugate" kink band development southeastern part of western block.

MT FRANKS MUNDI MUNDI AREA  
STRUCTURAL INTERPRETATION: D<sub>3</sub>

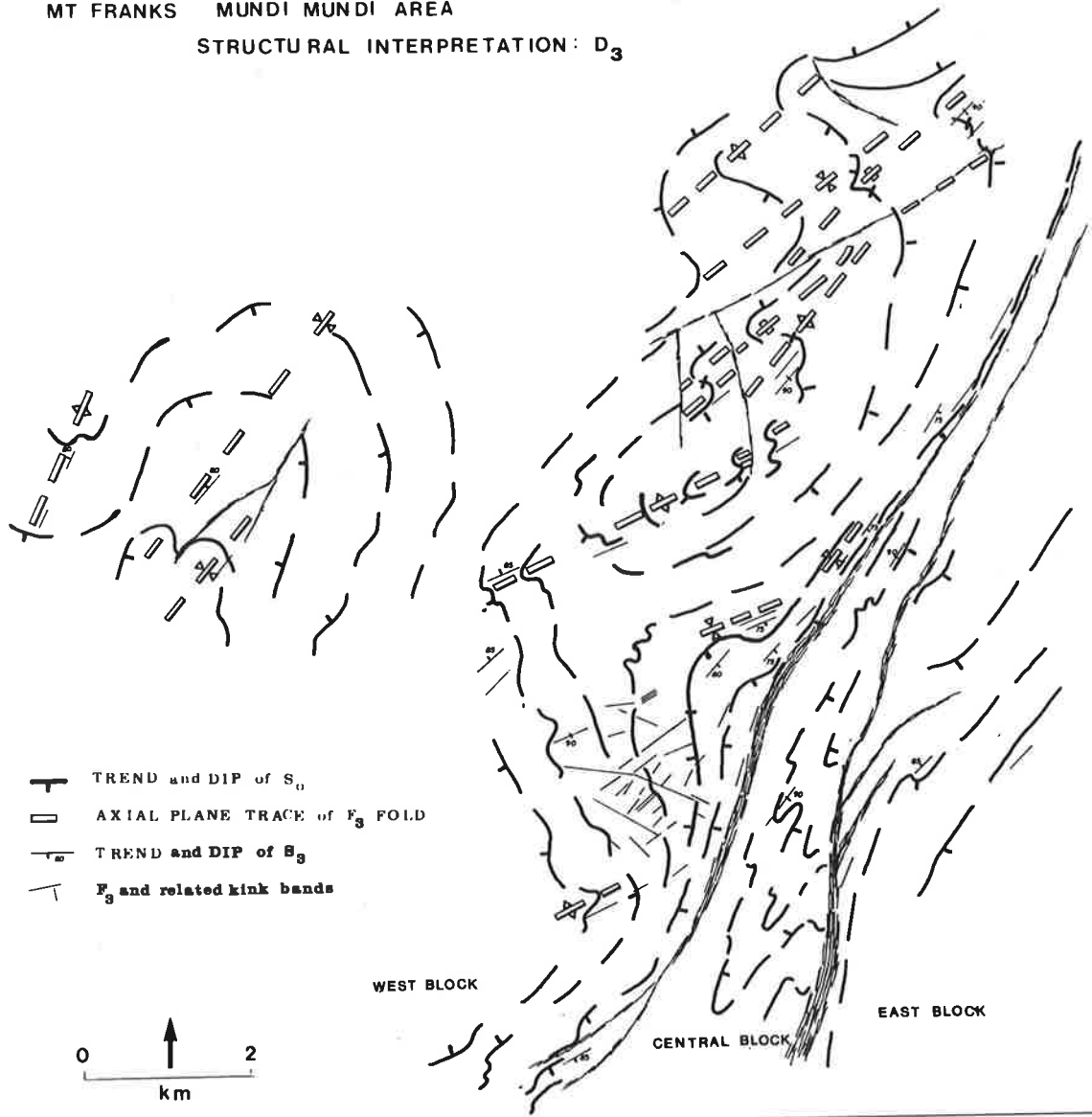


Fig. 6.4  $D_2$  and  $D_4$  interpretation maps.

MT FRANKS MUNDI MUNDI AREA  
STRUCTURAL INTERPRETATION: D<sub>2</sub> and D<sub>4</sub>

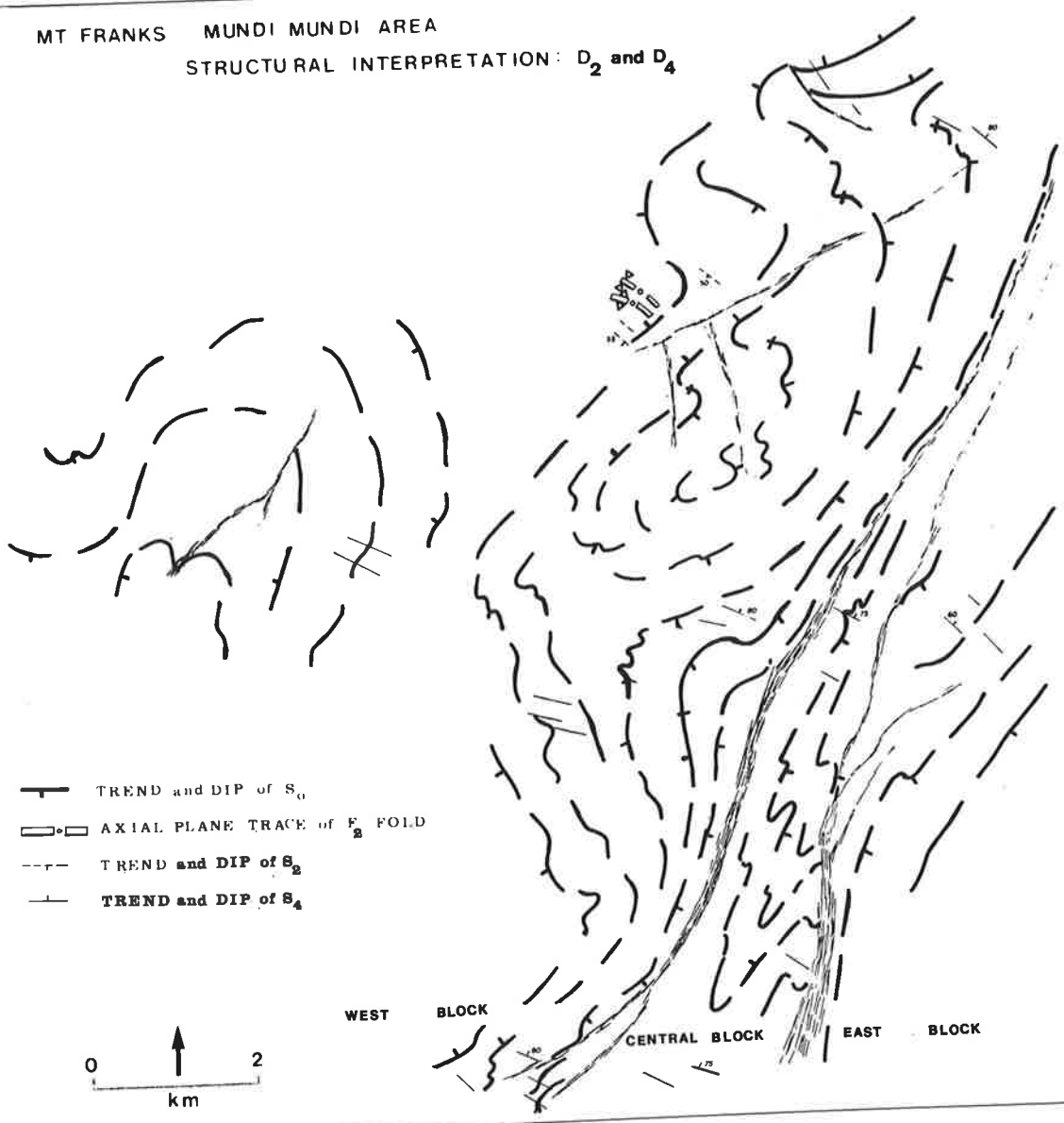




Fig. 6.5      Interpreted north plunging  $F_1$  folds in southern part  
of Apollyon Beds, central block.

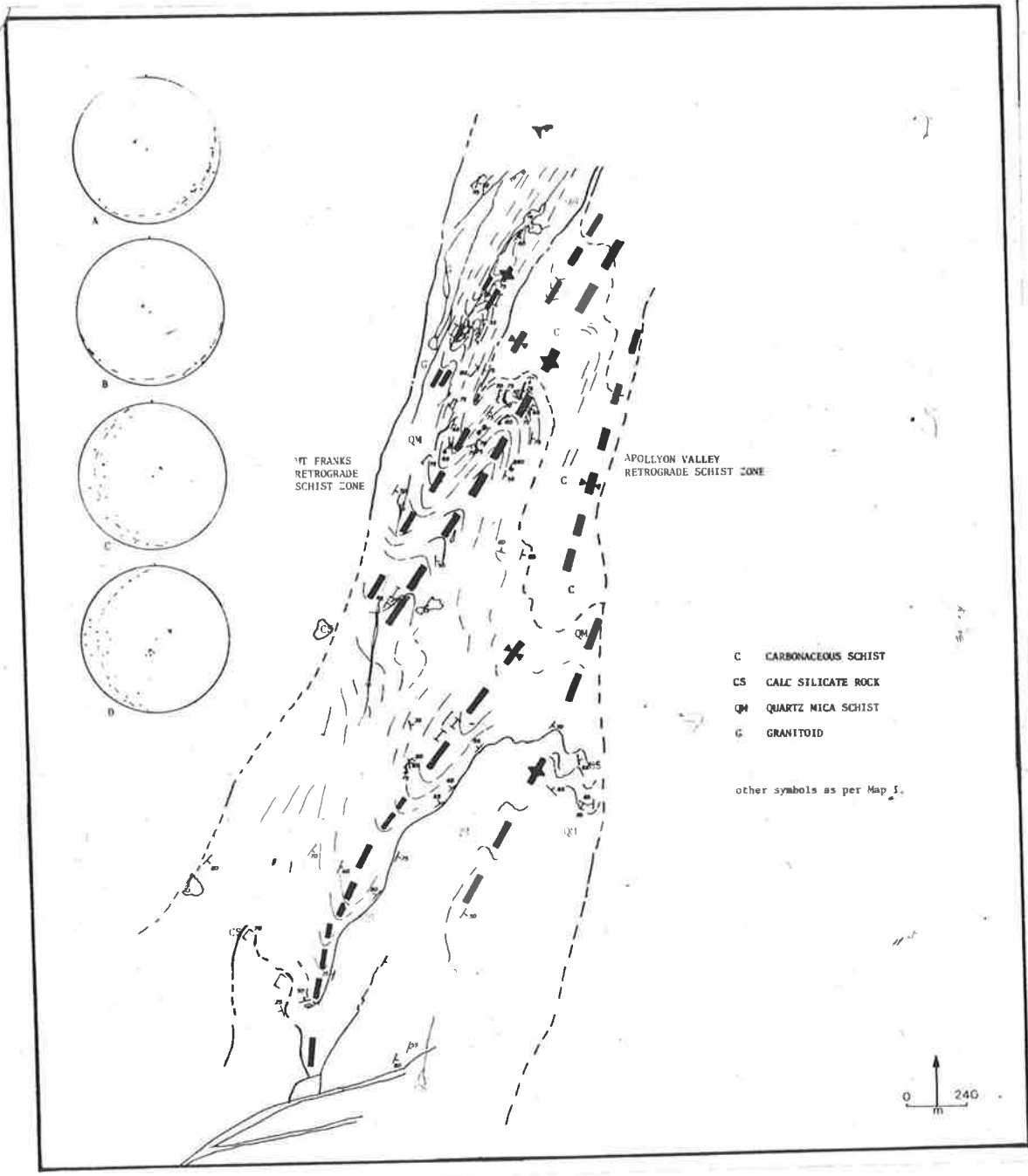
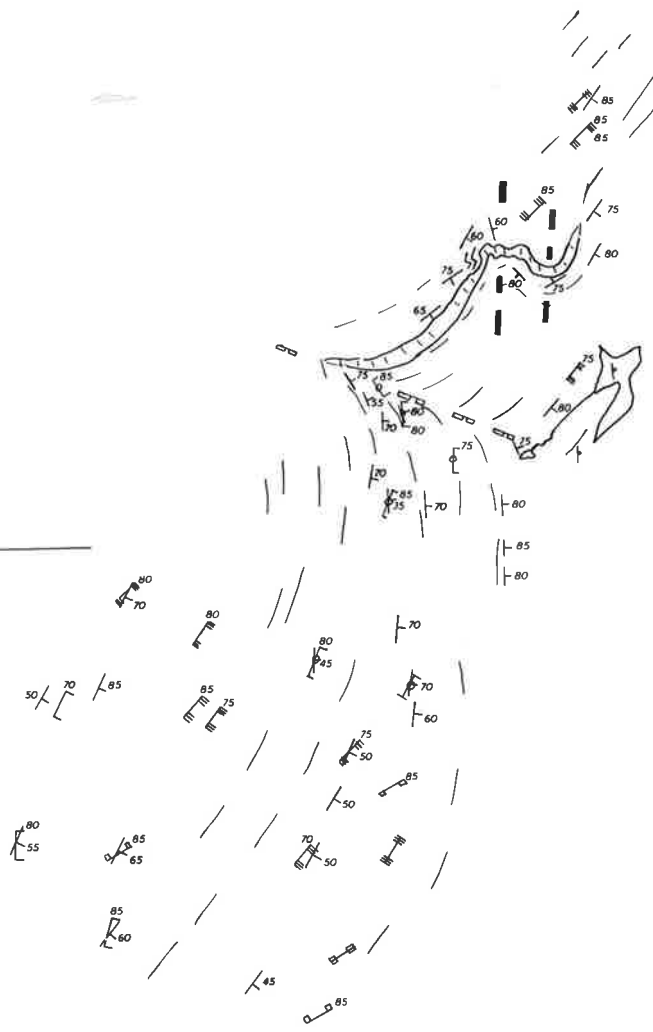


Fig. 6.6 South plunging  $F_1$  folds in the Apollyon Beds (central block) developed on the northern limb of an  $F_4$  cusp fold.

488



- S<sub>0</sub>
- S<sub>1</sub>
- S<sub>1-3</sub>
- S<sub>3</sub>
- S<sub>4</sub>
- F<sub>1</sub>
- F<sub>2</sub>
- Carbonaceous schist

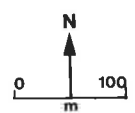


Fig. 6.7  $S_0/S_1$  relations in Robe sillimanite schist (subarea 18).

Equal area diagrams.

A Poles to  $S_0$ . 33 points; contours at 0.88, 1.75, 3.50,  
7.01, 14.02; maximum 15.15% per one % area.

B Poles to  $S_{IN}$ . 39 points; contours at 0.89, 1.78, 3.56, 7.12,  
14.23; maximum 15.38 % per one % area.

C  $S_0/S_{IN}$  intersections. 26 points; contours at 0.78, 1.56,  
3.11, 6.23, 12.45; maximum 13.46% per one % area.

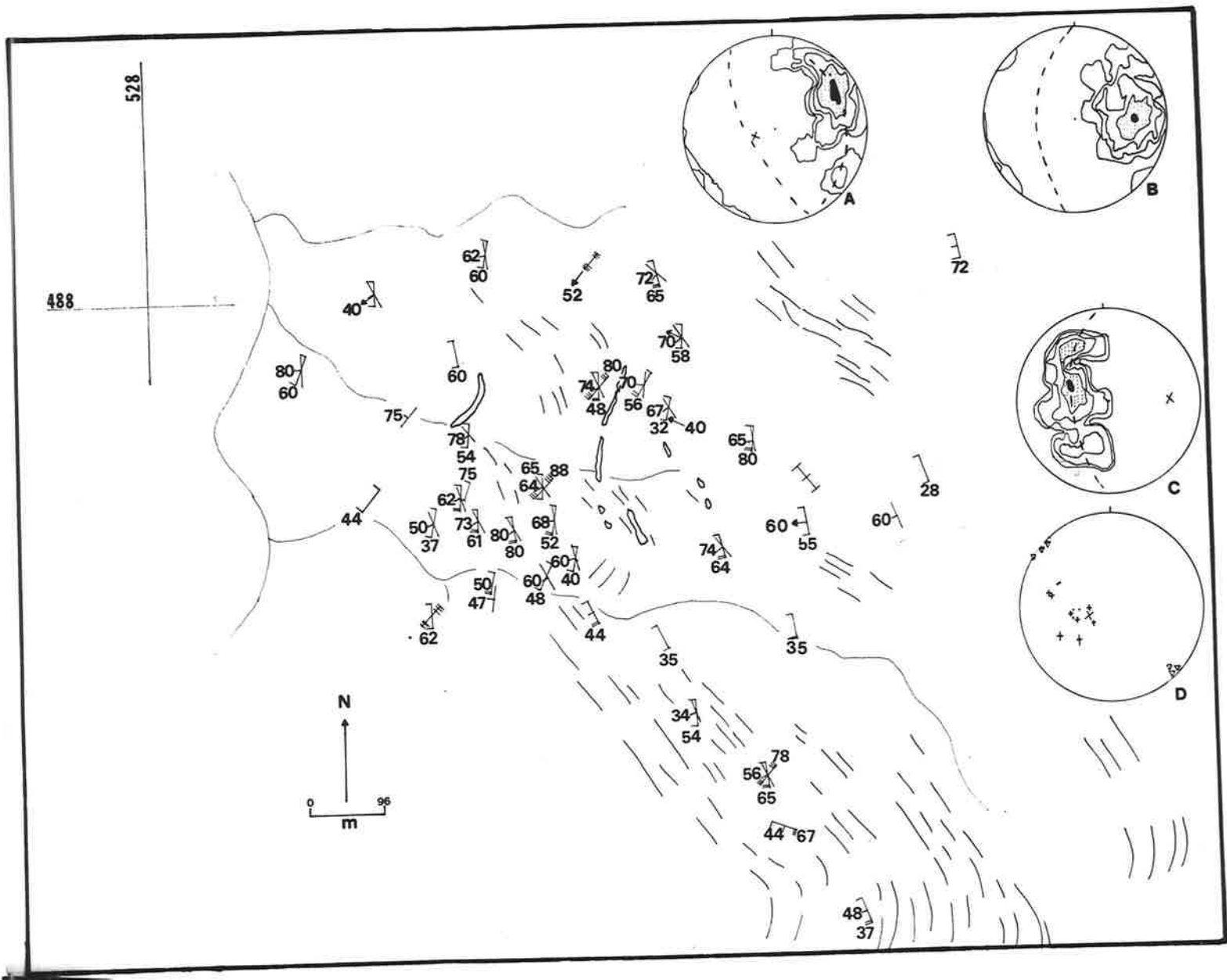


Fig. 6.8

Structural relations in the Black Prince - Eldee Creek Area.

Equal area diagrams

- A. Poles to  $S_0$  in northeast plunging  $F_3$  parasitic fold in subarea 23A.
- B. Poles to  $S_0 + S_1$  define the plunge of the Black Prince Antiform in subarea 23A.
- C. Poles to  $S_3$  (triangles) and small  $F_3$  folds (crosses), and  $S_1/S_3$  intersections (dots) in subarea 23A.
- D. Poles to  $S_0 + S_1$  in the Black Prince Antiform at Loc. 5338 64934.
- E. Poles to  $S_0 + S_1$  in the Black Prince Antiform near the limit of outcrop, southeast of Black Prince Mine. Poles to  $S_3$  shown as triangles. Note steepening of fold plunge from A,B,C to D and E.
- F. Poles  $S_0 + S_1$  around the hinge of the Black Prince Neutral Fold in subarea 23A and south of Eldee Creek.
- G. Poles to  $S_0 + S_1$  around the hinge of the Black Prince Neutral fold in subarea 23A and north of Eldee Creek.
- H. Poles to  $S_0 + S_1$  around the hinge of the Black Prince Neutral Fold near northern limit of outcrop in subarea 23B.
- I. Poles to  $S_0 + S_1$  define the axis of  $F_3$  synform at Loc. 5317 6493.
- J. Poles to  $S_0 + S_1$  define an axis of  $F_4$  warping just northwest of the Black Prince Mine. Small  $F_4$  folds shown by crosses.

Partly drawn by Judy Laing.

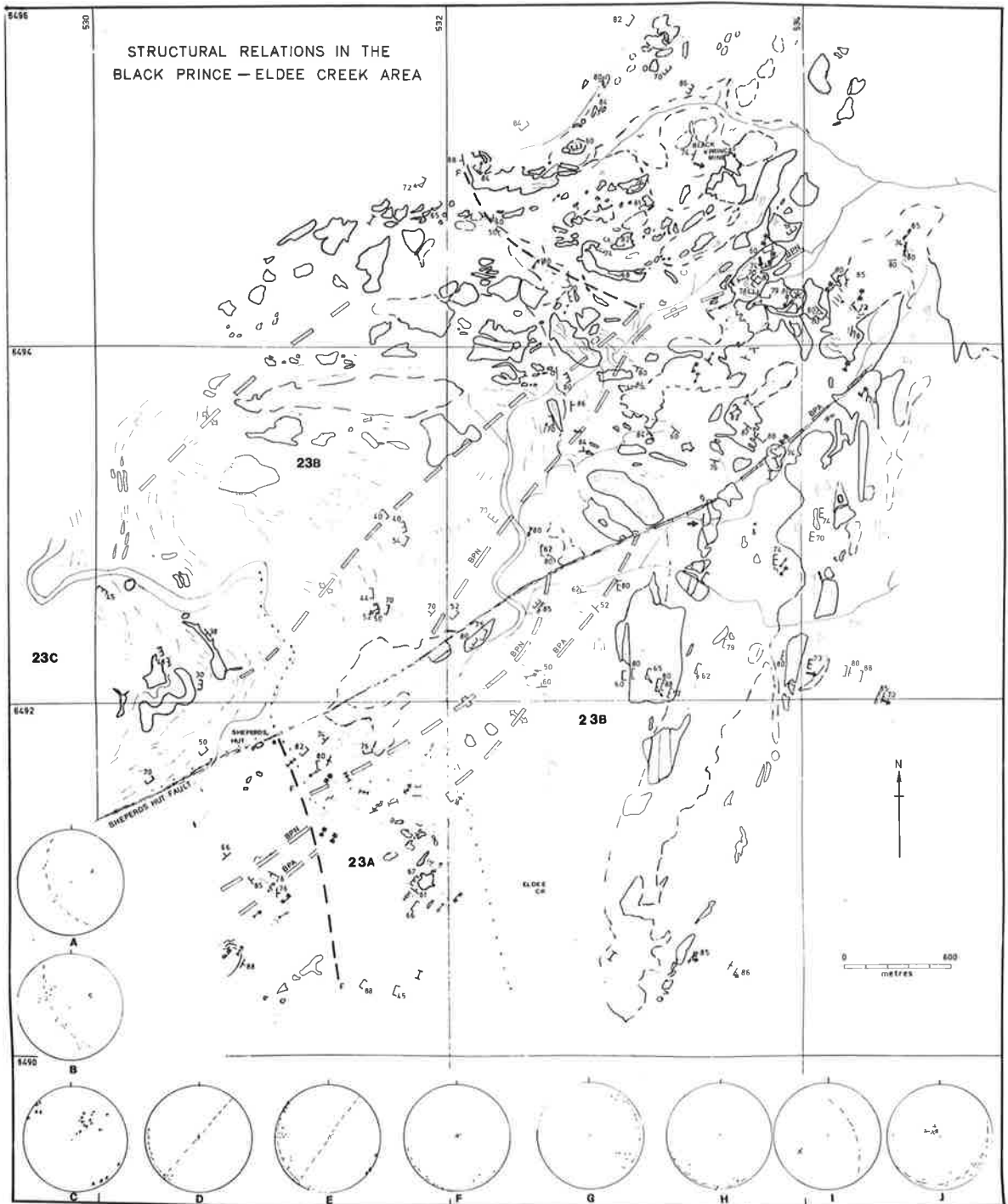




Fig. 6.9

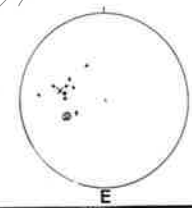
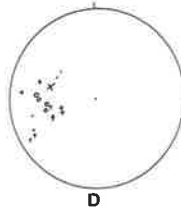
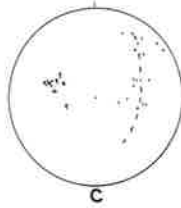
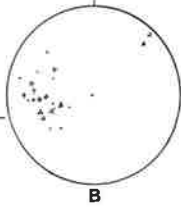
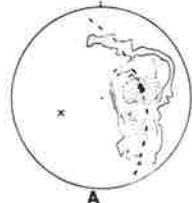
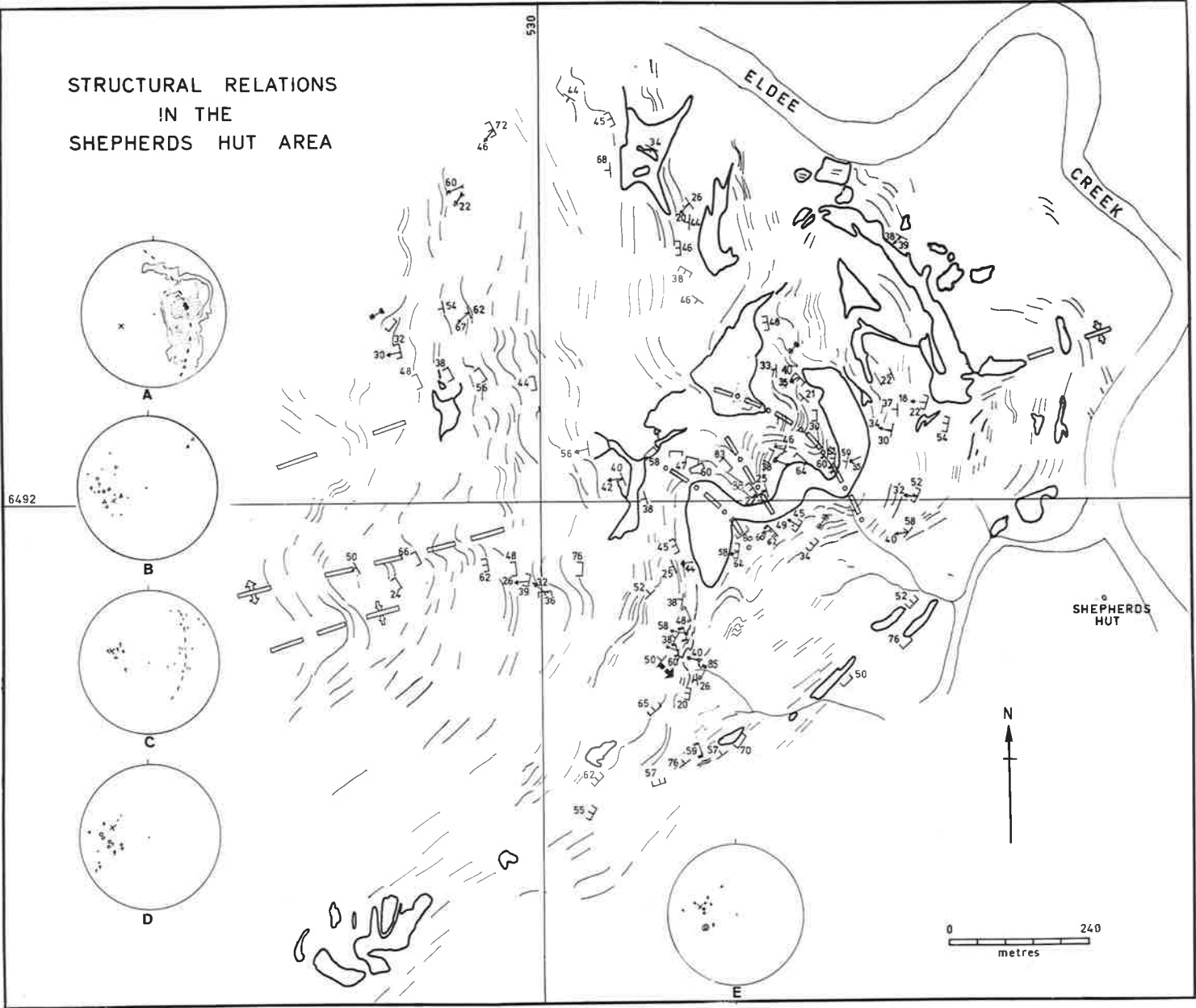
Structural relations in the Shepherds Hut Area  
(subarea 23C of previous figure).

Equal area diagrams

- A. Axis of  $F_3$  folding defined by poles to  $S_0 + S_1$ .  
44 points, contours at 0.59, 1.18, 2.37, 4.73,  
9.46; maximum 10.23%.
- B. Small  $F_3$  folds (triangles) and  $L_1$  sillimanite  
lineation (dots - short limb orientation, crosses  
- long limb, circles - hinge area). Diagonal  
cross marks axis of macroscopic folding.
- C. Poles to  $S_0 + S_1$  define an axis of  $F_2$  folding.  
Small  $F_2$  folds defined by crosses.
- D. Major axis of  $F_2$  folding and  $L_1$  sillimanite  
lineation around the  $F_2$  fold. (dots - short  
limb, crosses - long limb, circles - hinge  
area).
- E. Major axes of  $F_2$  (diagonal cross) and  $F_3$  (diagonal  
cross within circle). Small  $F_2$  folds (shown as  
crosses) indicate no obvious  $F_3$  folding.

Partly drawn by Judy Laing.

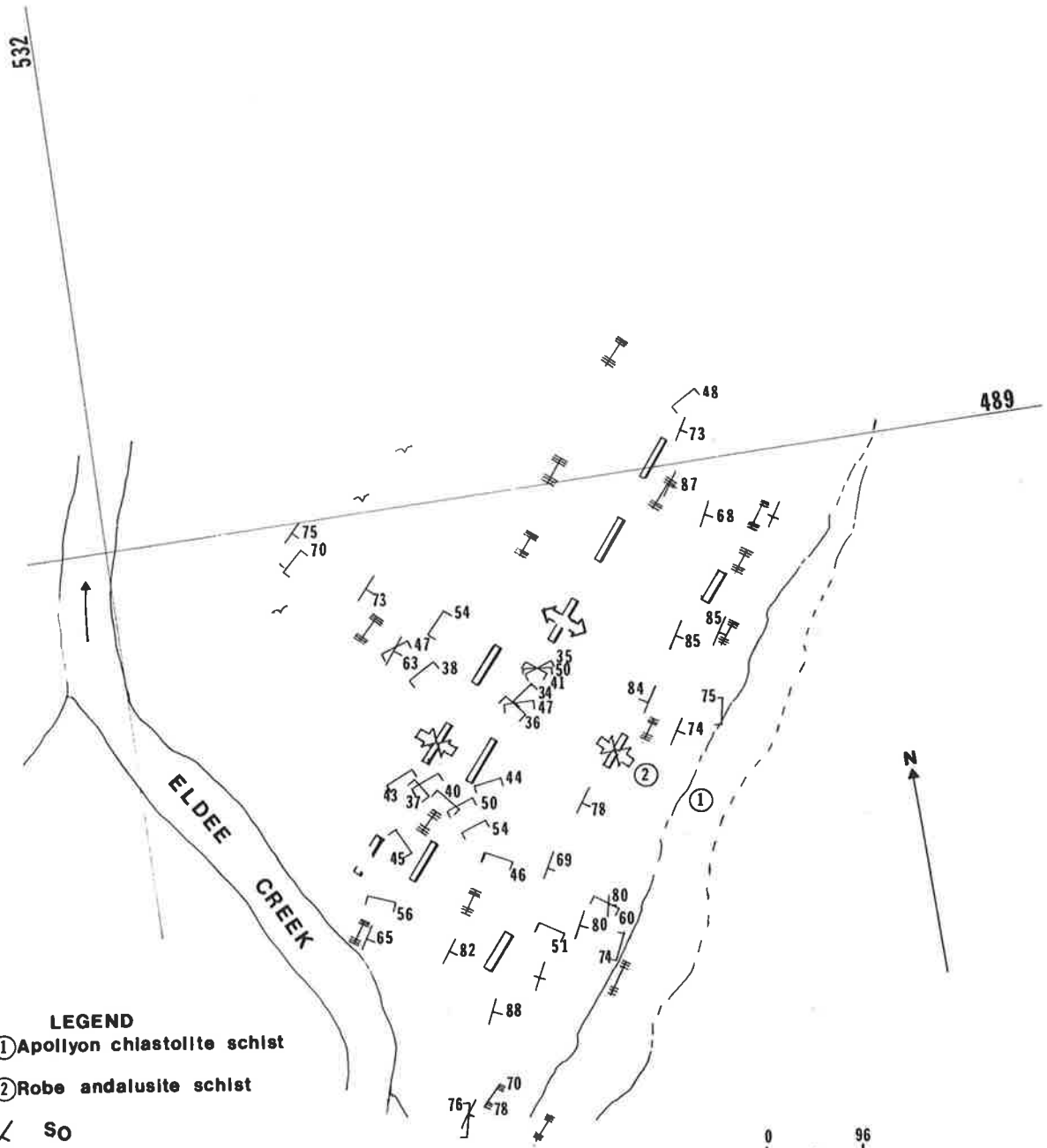
STRUCTURAL RELATIONS  
IN THE  
SHEPHERDS HUT AREA



0 240  
metres

N

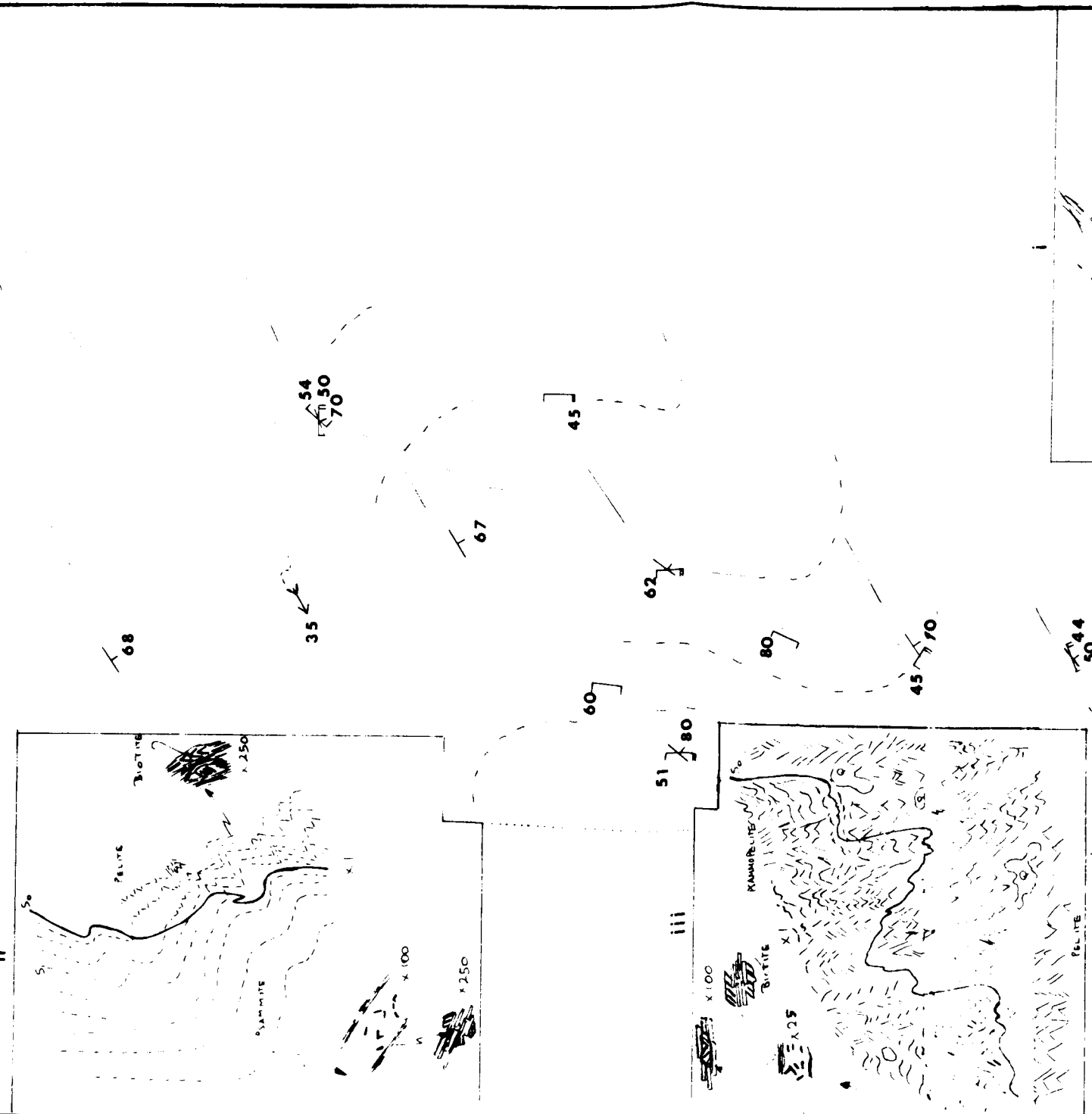
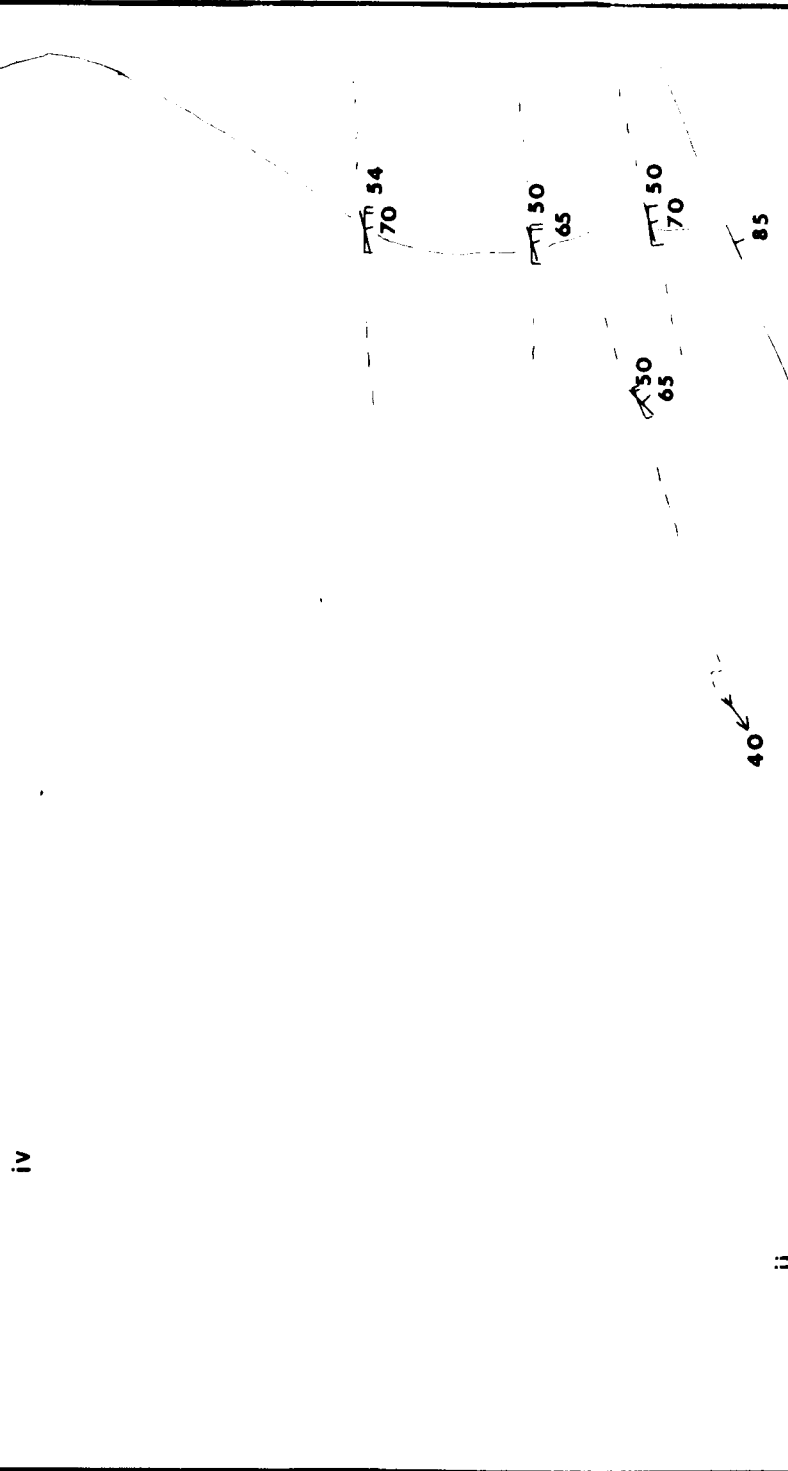
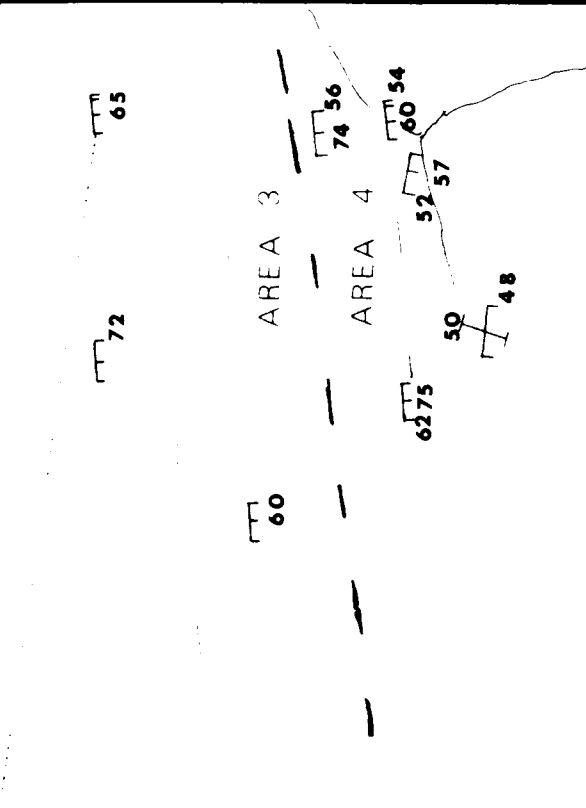
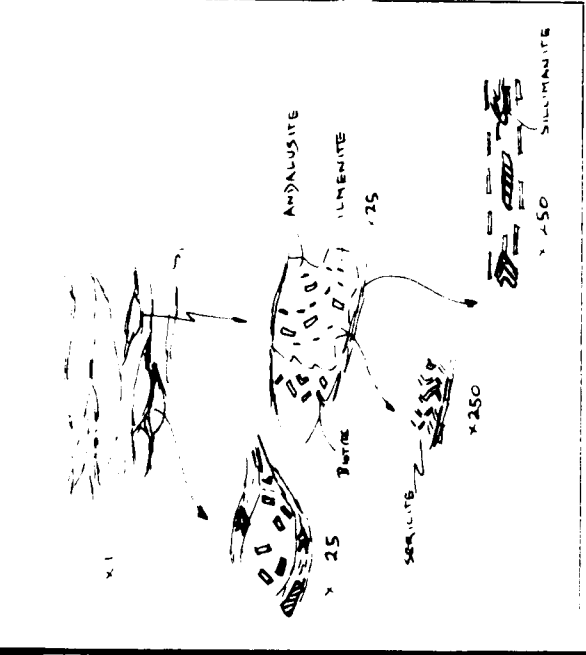
Fig. 6.10 Relations across hinge of  $F_3$  synform defined by change in orientation of  $S_1$ .  $S_0$  is unfolded. See Map 3 for location.



- LEGEND**
- ① Apollyon chlastolite schist
  - ② Robe andalusite schist
  - / S0
  - ∟ S1
  - ⊥ S3
  - ▭ Axial plane trace of F3 fold



Fig. 6.11 Relations across  $F_3$  synformal hinge defined by change in orientation of  $S_1$ , not by  $S_0$ . Note change from  $S_{1N}$  to  $S_{1P}$  relations in north of Figure.



Legend

$S_0$  & Trend

$S_1P_s$  & Trend

$S_1P_e$  & Trend

$S_3$

N

0 60 m

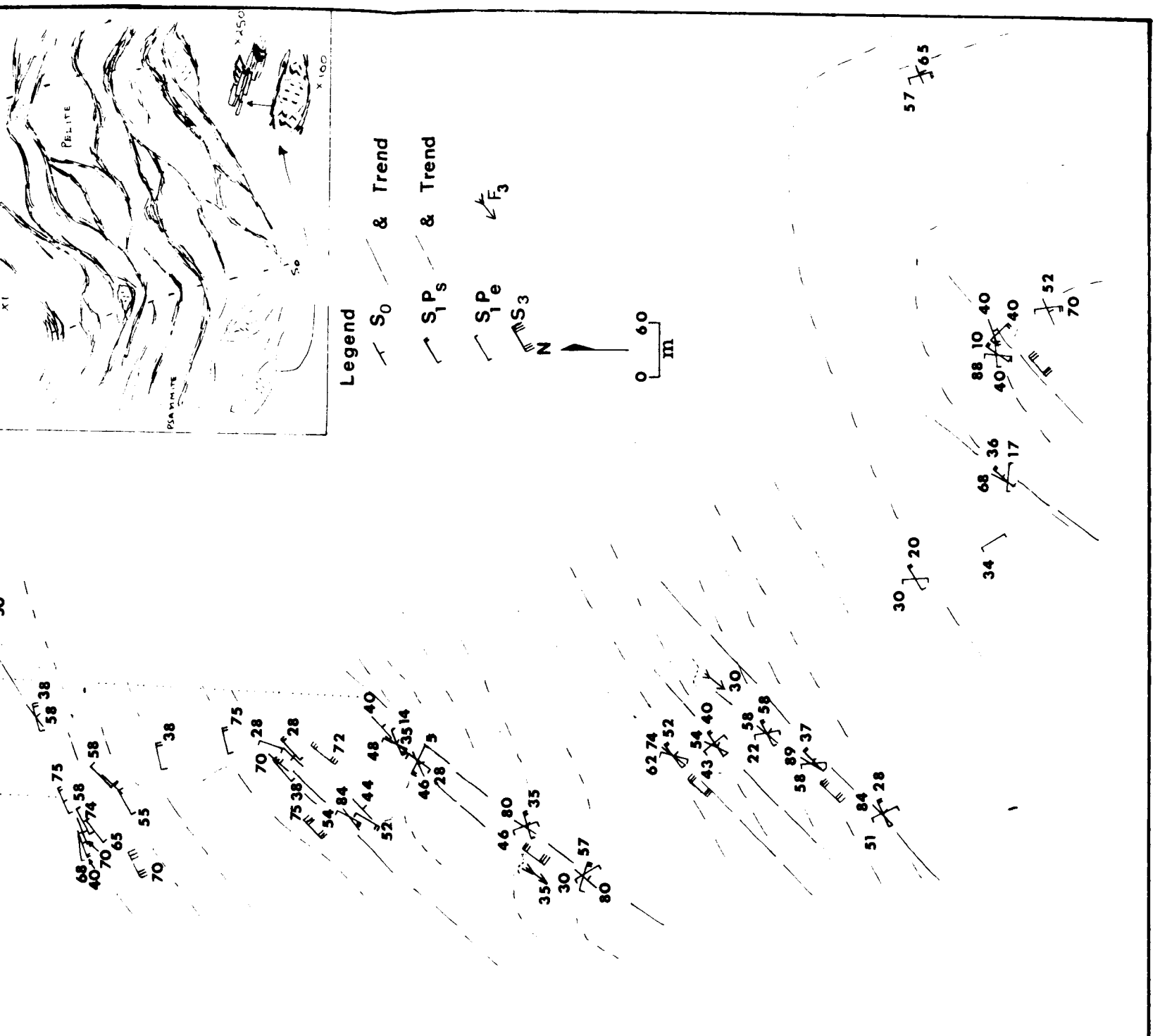


Fig. 6.12 Mt Franks fold pair.

Robe Beds.

- A. Eastern limb. Summary diagram  $S_0$ ,  $S_{1N}$ ,  $S_3$ .
- B. Eastern limb.  $L_3$  (crosses),  $S_0/S_{1N}$  intersections (dots) and  $S_{1N}/S_3$  intersections. ( 50 points, contours at 1.5, 3.01, 6.01, 12.02, 24.05; maximum 26.00%)
- C. Shared limb. Orientation of poles  $S_0$  (103 points, contours at 1.07, 2.13, 4.27, 8.53, 17.06; maximum 18.45%) pole to  $S_0$  girdle,  $S_{1N}$  orientation and  $S_0/S_{1N}$  intersections (70 points, contours at 1.24, 2.48, 4.96, 9.91, 19.82; maximum 21.43%).
- D. Shared limb. Orientation of  $S_{1N}$ Ps (64 points, contours at 1.45, 2.89, 5.78, 11.56, 23.12; maximum 25.00%).
- E. Shared limb. Orientation of  $S_{1N}$ Pe (141 points, contours at 1.38, 2.75, 5.51, 11.02, 22.04; maximum 28.83%).
- F. Shared limb. Orientation of  $S_3$  (99 points, contours 2.39, 4.79, 9.58, 19.15, 38.31; maximum 41.41%).  $S_0/S_3$  intersection (45 points, contours 1.86, 3.73, 7.45, 15.90, 29.81; maximum 32.22%), and  $S_0/S_{1N}$  intersection (outer two contours only shown; 70 points, contours 1.24, 2.48, 4.96, 9.91, 19.82; maximum 21.43%).
- G. Western limb. Orientation of  $S_{1N}$  (72 points, contours 0.48, 1.69, 3.37, 6.74, 13.49; maximum 14.58%), and intersection with easterly and westerly dipping  $S_0$ .

Apollyon Beds

- H. Whole fold,  $S_{1N}$  orientation which has been partly redistributed about an  $F_3$  axis (18 points, contours at 1.61, 3.21, 6.42, 12.85, 25.69; maximum 27.78%).

Fig. 6.12 (cont.)

Robe Beds

- I. Anticlinal axis and poles to  $S_0$  (274 points, contours 0.61, 1.22, 2.45, 4.90, 9.79; maximum 10.58%).
- J. Synclinal axis and poles to  $S_0$  (270 points, contours at 0.72, 1.32, 2.87, 5.74, 11.48; maximum 12.41%).
- K. Relationship between  $F_1$  axis (X),  $F_3$  folds (O) and  $S_{1N}/S_3$  intersections ( $\square$ ).

Apollyon Beds

- L. Averaged fold axis and poles to  $S_0$  (25 points, contours at 0.81, 1.62, 3.24, 6.47, 12.95; maximum 14.00%).
-



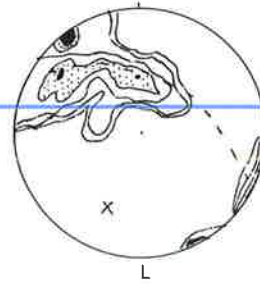
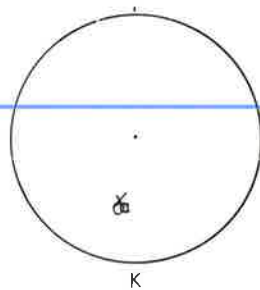
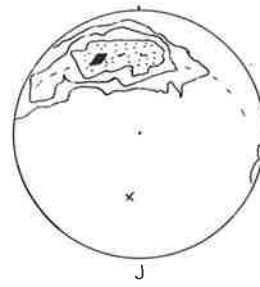
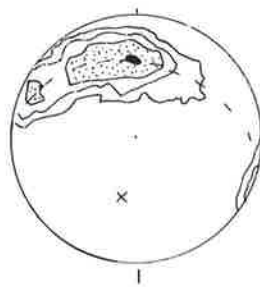
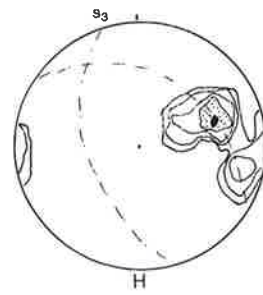
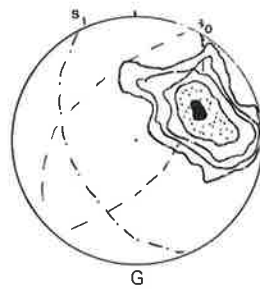
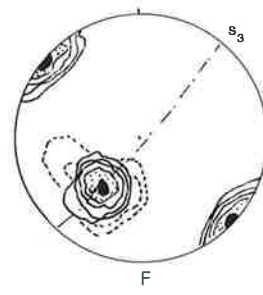
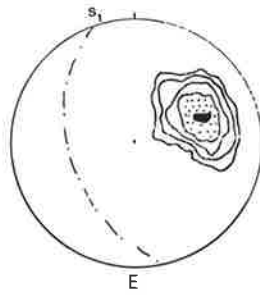
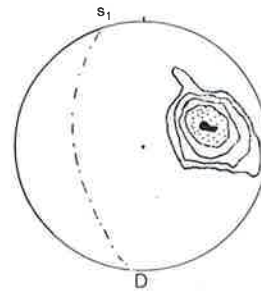
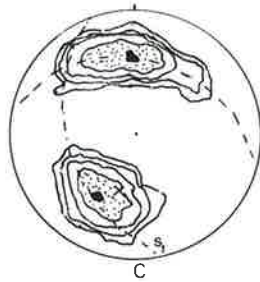
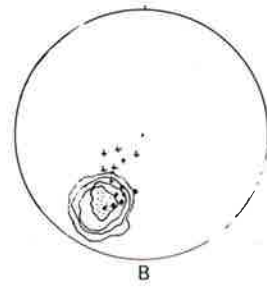
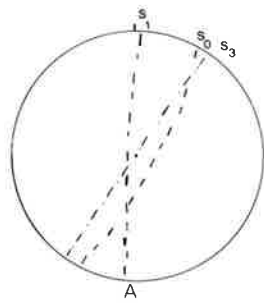


Fig. 6.13 Change in sedimentary younging direction around  
upward facing Mt Franks Fold Pair.  
Inset shows  $S_1$  terraces developed on the short limb.

---

DISTRIBUTION OF YOUNGING DIRECTIONS  
AROUND MT FRANKS FOLD PAIR

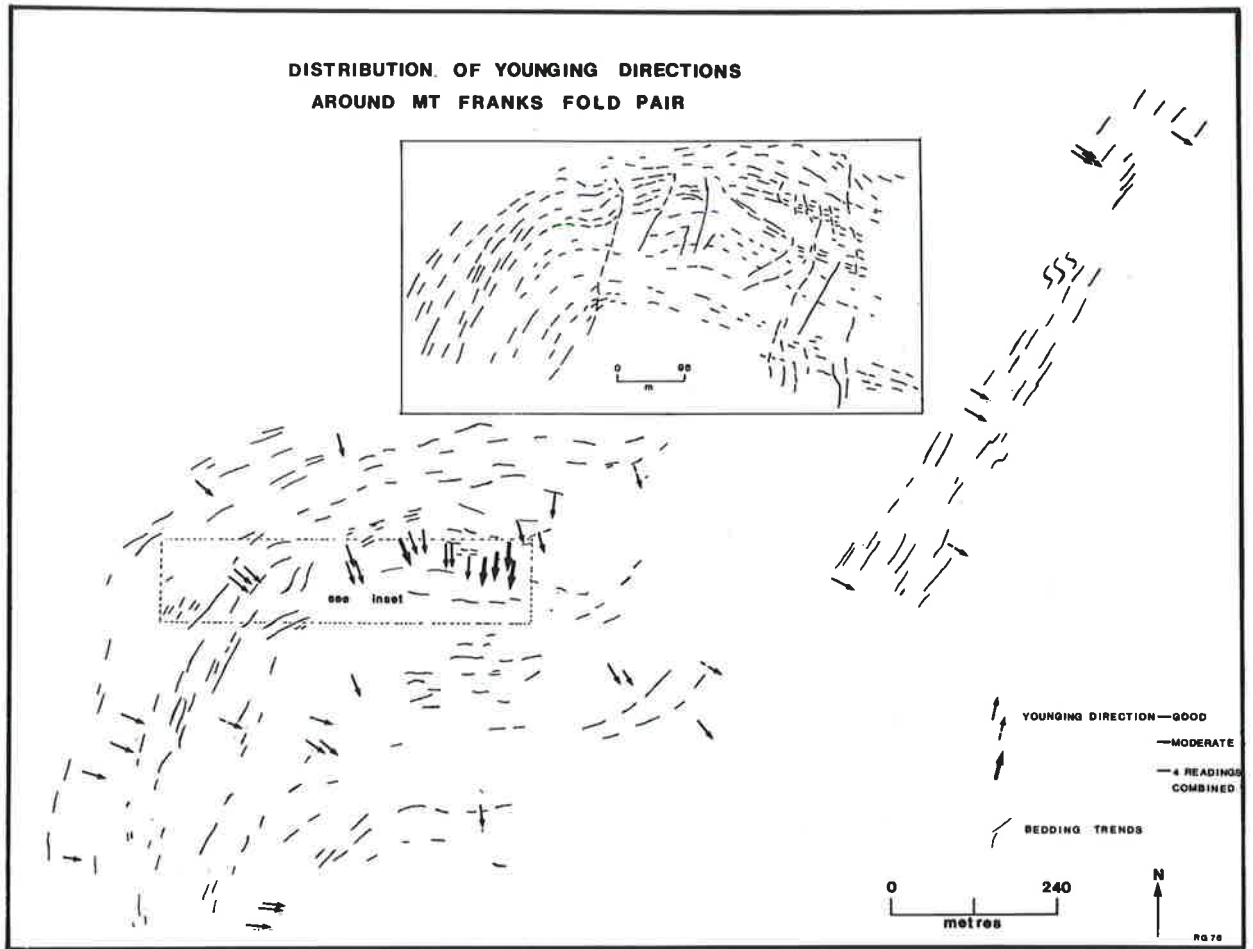


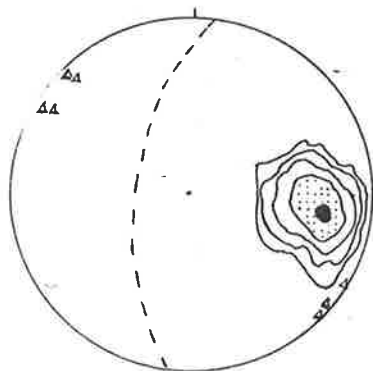
Fig. 6.14 Sketch of relations in Cascade Creek looking south.  
Base of sketch about 200 m long.

Equal area diagrams.

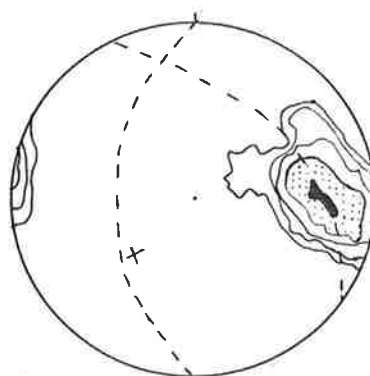
- A. Poles to  $S_1$  in Apollyon andalusite schist indicate an orientation of  $004^\circ 66^\circ W$ . 7 poles to  $S_3$  shown as triangles.  
48 points, contours at 1.57, 3.13, 6.26, 12.53, 25.05; maximum 27.08%.
- B. Poles to  $S_1$  in underlying Apollyon chiastolite schist indicate an orientation of  $001^\circ 53^\circ W$ , with a tendency to be refolded around an  $F_3$  axis plunging at  $40^\circ$  to  $225^\circ$ . Note that  $F_3$  axis almost lies in  $S_1$ , and that  $S_1$  here is more gently dipping than  $S_1$  above.  
57 points, contours at 0.91, 1.83, 3.65, 7.30, 14.61; maximum 15.79%.
- C. Poles to  $S_0$  in Apollyon andalusite schist (in area of major  $F_1$  folding) define an axis plunging south at gentle to moderate. Small  $F_1$  folds shown as crosses;  $S_0/S_1$  intersections shown as dots (observed) and circles (calculated).  
39 points, contours at 0.59, 1.19, 2.37, 4.74, 9.49; maximum 10.26%.
- D. Poles to  $S_0$  in underlying Apollyon chiastolite schist. Two strong maxima, corresponding to long and short limbs reflect  $F_1$  folds in parasitic fold.  $F_1$  axis plunges gently south.  
37 points, contours at 0.70, 1.74, 2.81, 5.63, 11.25; maximum 12.16%.
-



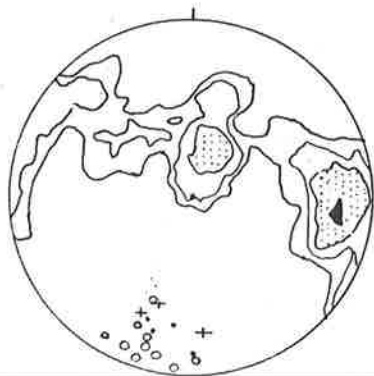
A



B



C



D

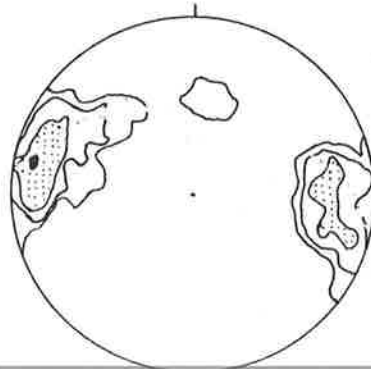


Fig. 6.15 Cross section of  $F_1$  folding at Cascade Creek (AA') and also parasitic folds in Apollyon chiasmolite schist in the western limb of this fold further south (BB', CC'). See Map 3 for location.

---

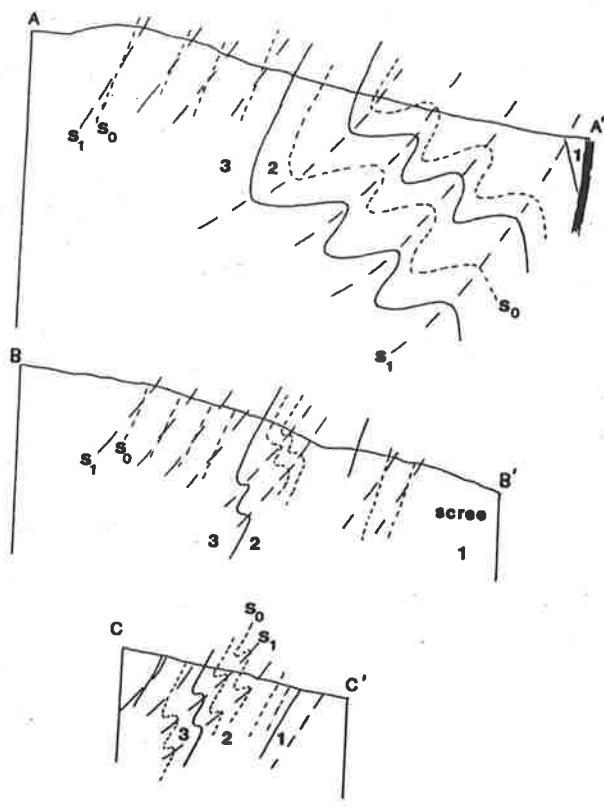


Fig. 6.16 Bedding overturn south of Cascade Creek.

Equal area diagrams.

- A. Poles to  $S_1$  indicate an orientation of  $356^\circ 65^\circ W$ .  
99 points, contours at 0.85, 1.69, 3.39, 6.77,  
13.55; maximum 14.65%.
- B. Poles to  $S_0$  show a maximum corresponding to  
 $002^\circ 76^\circ W$ , but also show a slight bulge,  
indicating steep easterly dips (c.  $80^\circ$ ) as beds  
rotate through the vertical.  
112 points, contours at 0.70, 1.39, 2.79, 5.57,  
11.15; maximum 12.05%.
-



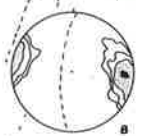
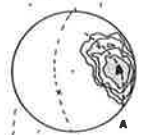
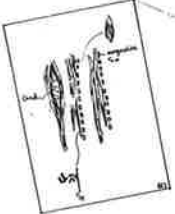
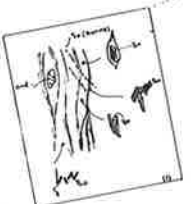


Fig. 6.17 Parasitic  $F_1$  fold in the western limb of  $F_3$  synform.  
Note that  $F_3$  folding of  $F_1$  axial surface traces  
locally destroys their parallelism with  $S_1//S_0$  in  
Area 3. Poles to  $S_0 + S_1$  indicate steeply east  
plunging axes.  
See Map 4 for location.

---

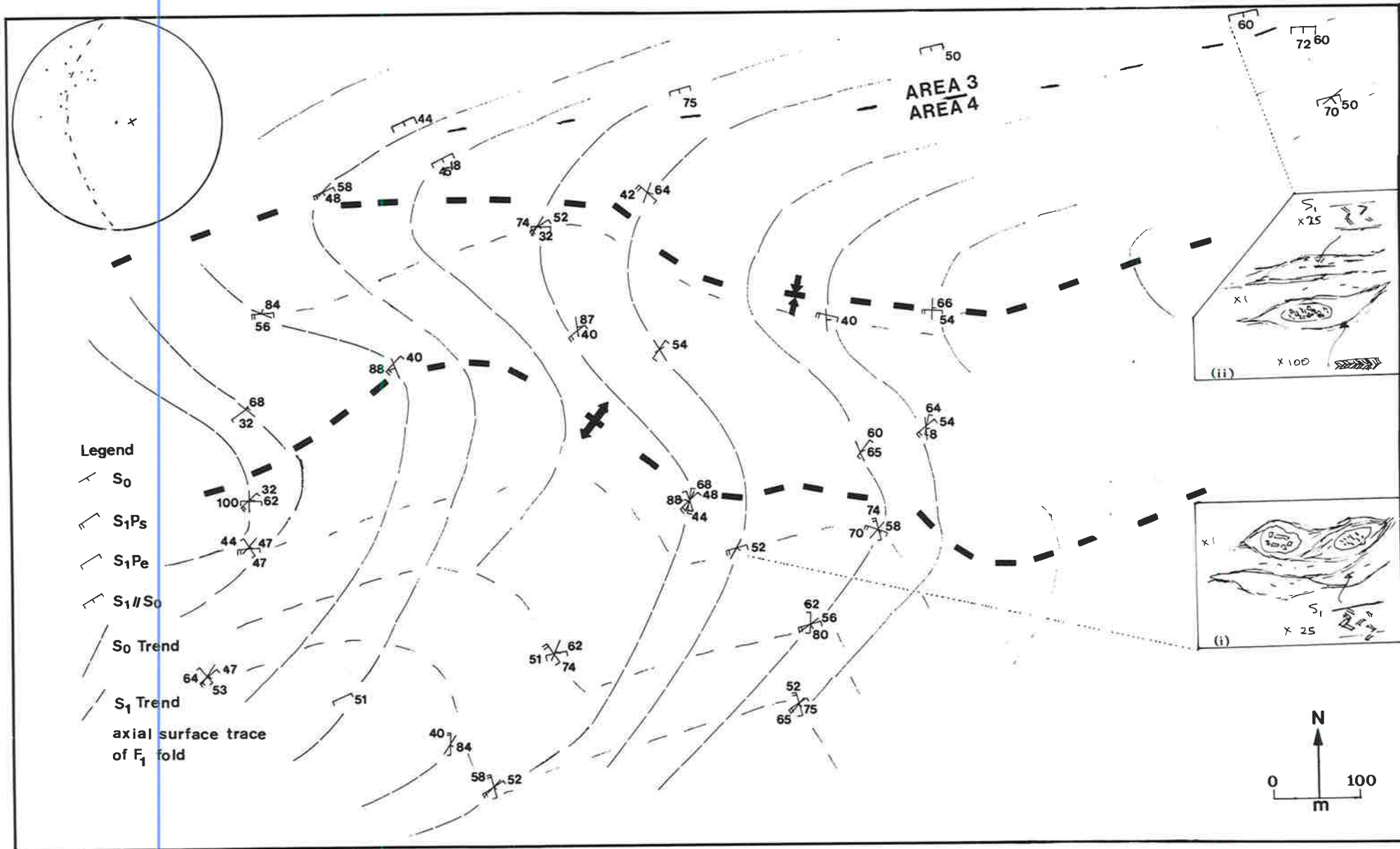


Fig. 6.18 Boundary between Area 4 ( $S_{1N}$  relations) and Area 3 ( $S_{1P}$  relations).

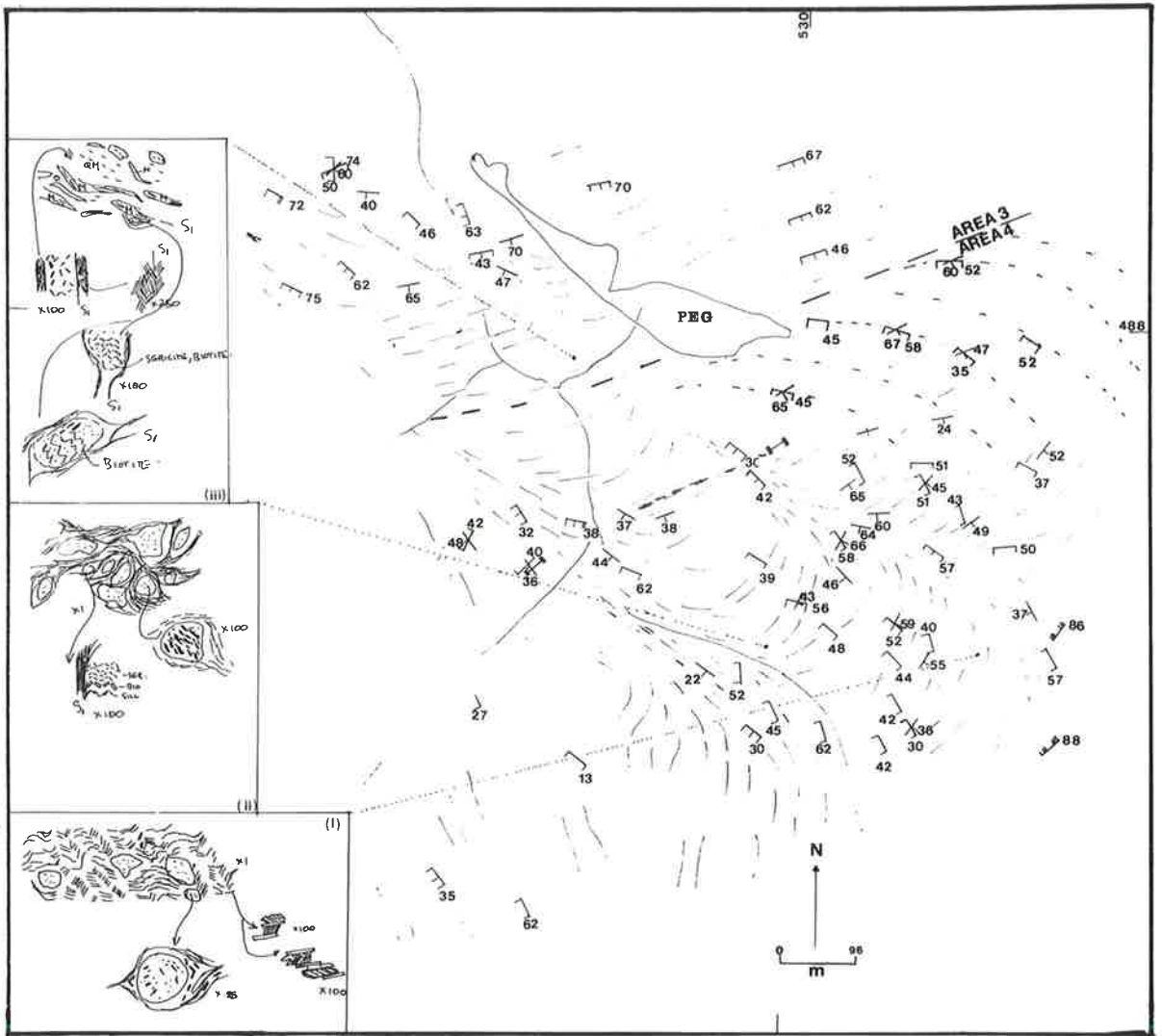
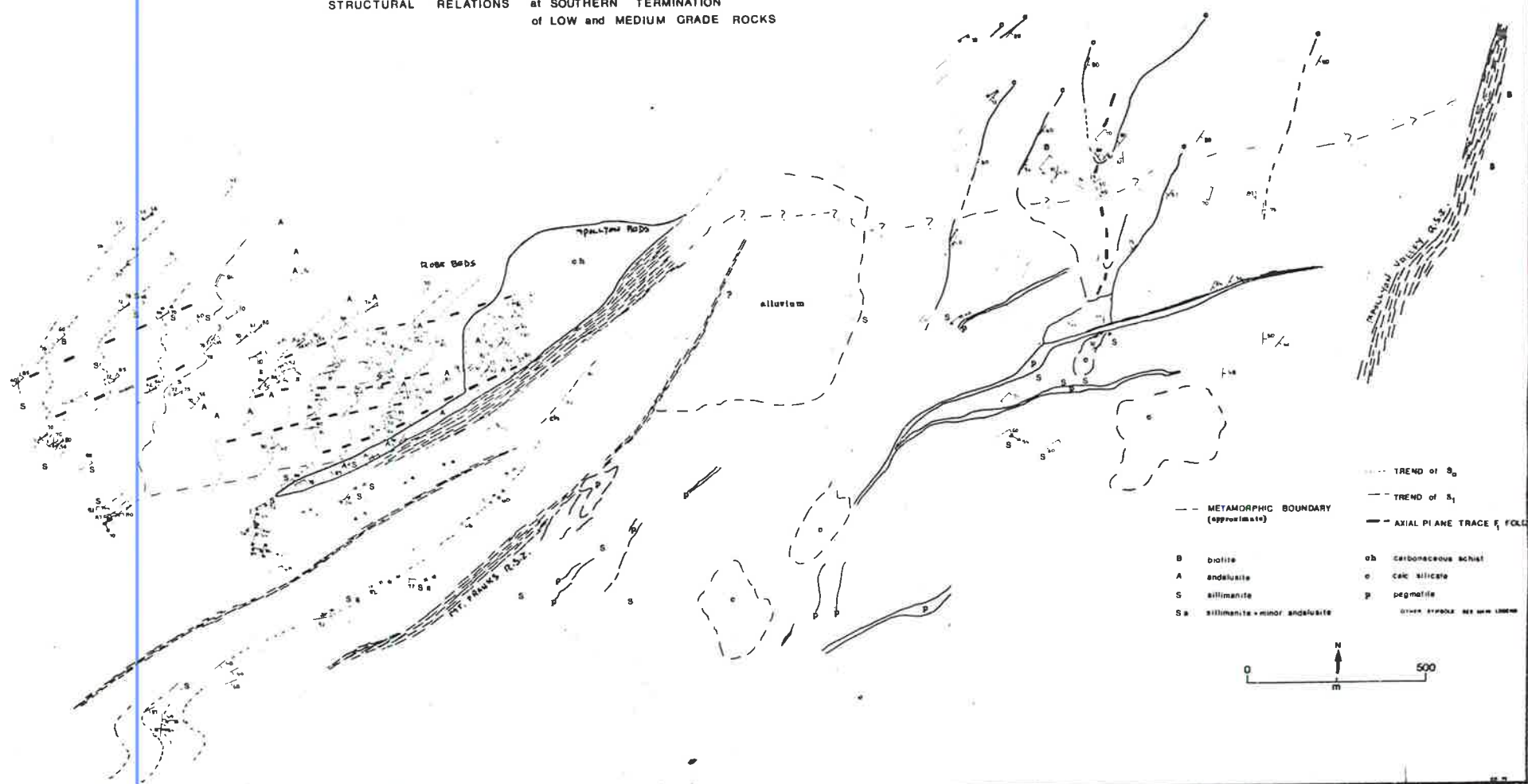


Fig. 6.19 Structural relations in south of area at termination of low and medium grade rocks in an area of steeply north plunging  $F_1$  folds. Sillimanite-incoming line only approximately shown in central block.

STRUCTURAL RELATIONS at SOUTHERN TERMINATION  
of LOW and MEDIUM GRADE ROCKS



- METAMORPHIC BOUNDARY (approximate)
- TREND of S<sub>0</sub>
- TREND of S<sub>1</sub>
- AXIAL PLANE TRACE of FOLDS
- B biotite
- A andalusite
- S sillimanite
- Sa sillimanite + minor andalusite
- ob carbonaceous schist
- c calc. silicate
- p pegmatite
- OTHER SYMBOLS SEE NEW SERIES

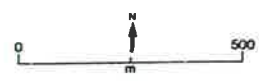
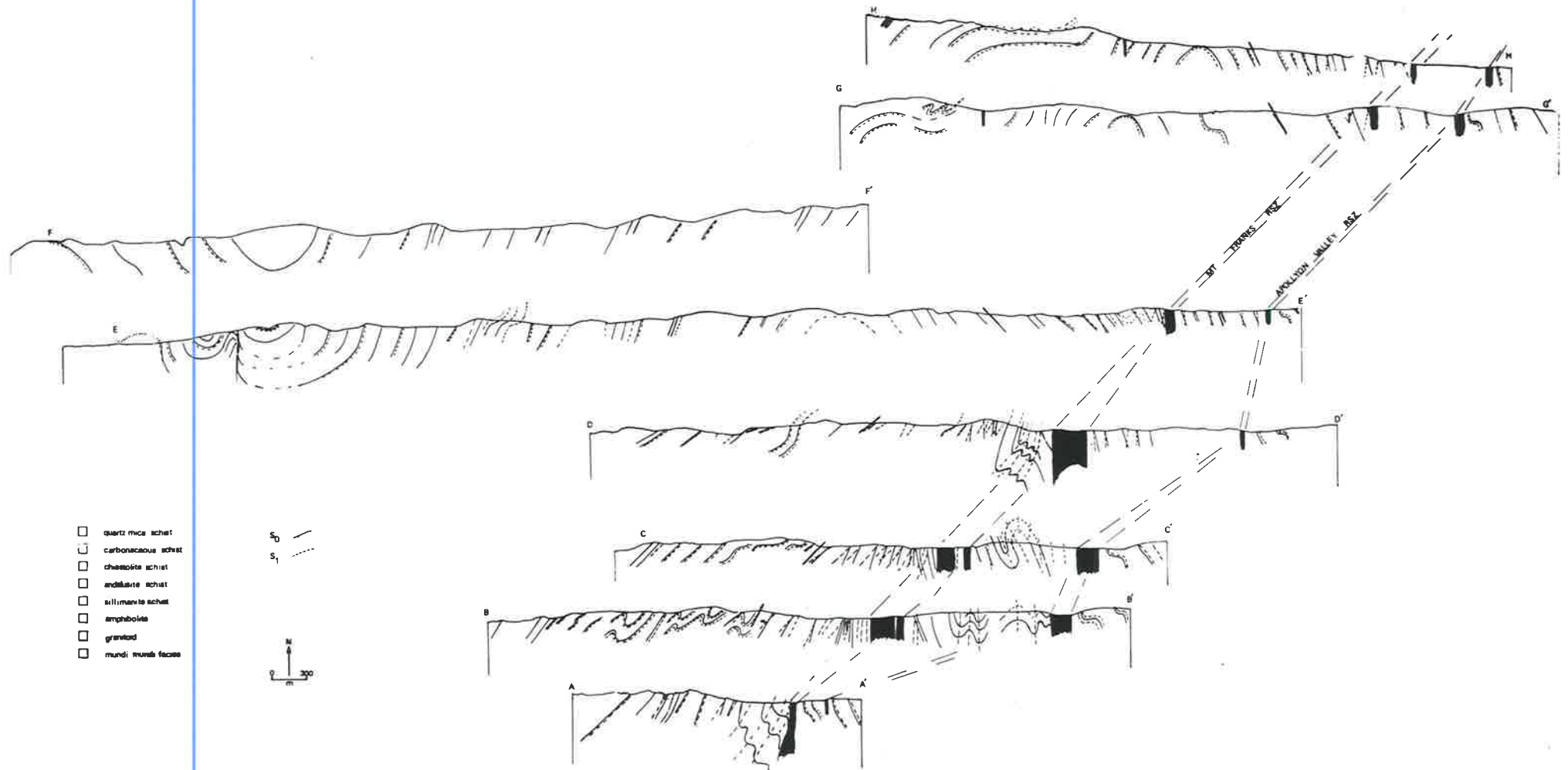


Fig. 6.20 Serial cross sections.

For locations, see Map 1.

Note south to north change in  $S_0$  and  $S_1$  orientation in western block from westerly to easterly dipping.





- quartz mica schist
- ▨ carbonaceous schist
- ▤ chlorite schist
- ▥ andalusite schist
- ▧ sillimanite schist
- ▩ amphibolite
- granitoid
- ▬ rudi. fluviat. facies



Fig. 6.21 Three dimensional sketch of bedding surfaces in  
Mt Franks - Mundi Mundi Area.

---

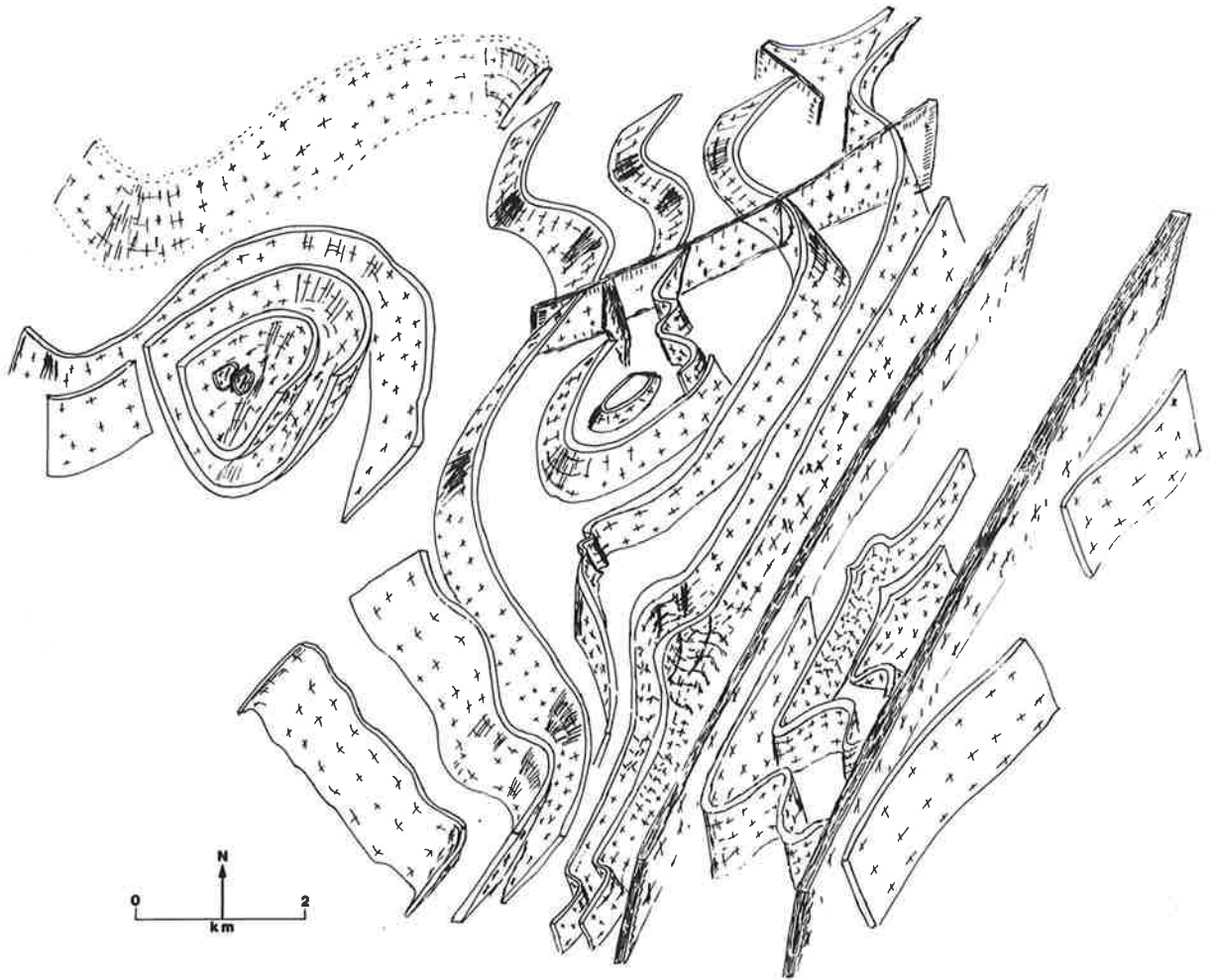


Fig. 6.22 Change in orientation of  $S_1/S_3$  intersections from subarea 6a, 6b to subareas 10 and 13. The shallowing of intersection orientation indicates that  $S_1$  was non planar before  $F_3$  folding. (see Appendix III for details).

Fig. 6.23 Reconstructed shape of major  $F_1$  syncline. See text for details.

---

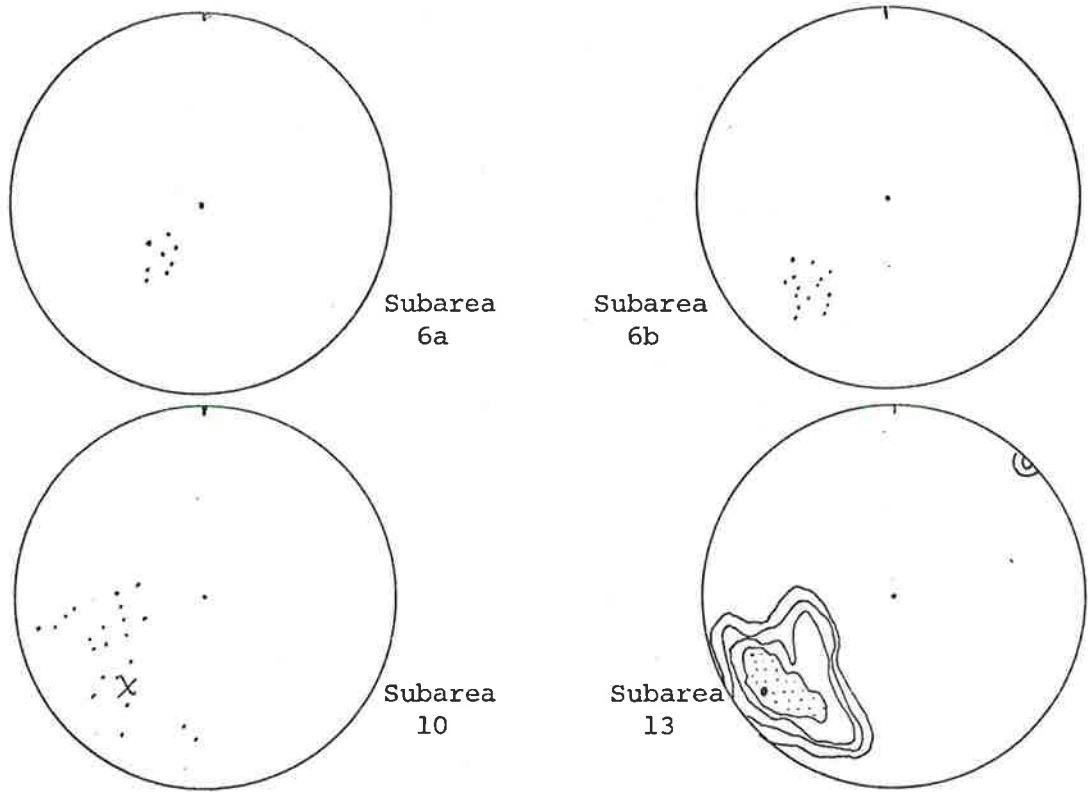


Fig. 6.22

South of Mt Franks

North of Mt Franks

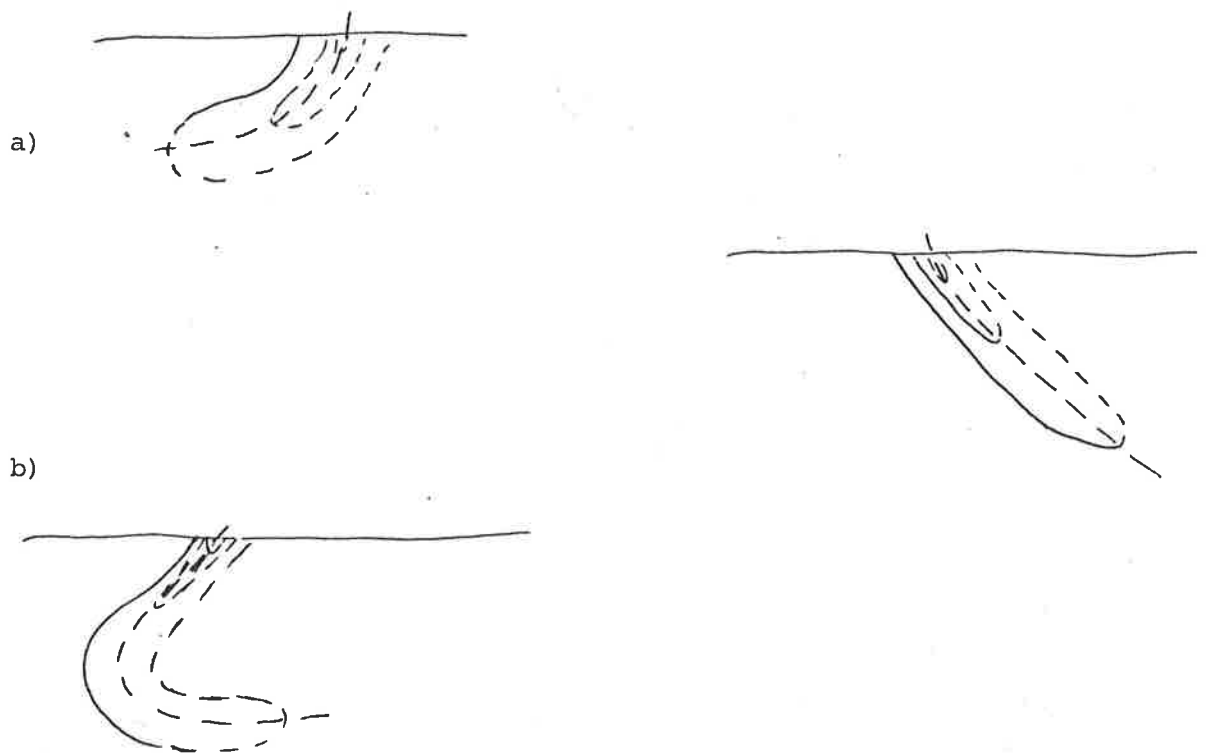


Fig. 6.23

Fig. 6.24 Schematic model of non isoclinal  $F_1$  folding resulting in continued sillimanite (re)crystallisation after folding. See text for details.

Fig. 6.25 Equal area plots of data in Mt Franks Retrograde Schist Zone.

- a. Poles to  $S_R$  indicate an orientation of  $039^\circ 90^\circ$ .  
71 points, contours at 2.24, 4.48, 8.96, 17.91, 35.83; maximum 38.73%.
- b.  $L_M$ , mineral lineation within  $S_R$  plunging at  $70^\circ$  to  $211^\circ$ .  
32 points, contours at 1.72, 3.43, 6.87, 13.73, 27.46; maximum 29.69%.
- c.  $F_{R+I}$  folds in  $S_R$ .  
37 points, contours at 1.09, 2.19, 4.38, 8.75, 17.50; maximum 18.92%.

surface

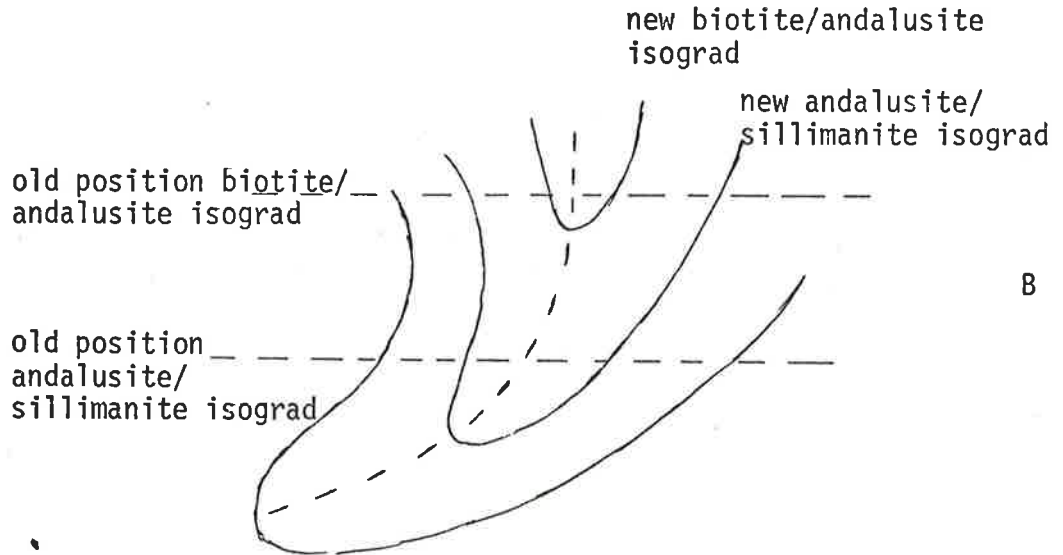


biotite/andalusite



A

andalusite/sillimanite



B

FIG 6.25

FIG 6.26

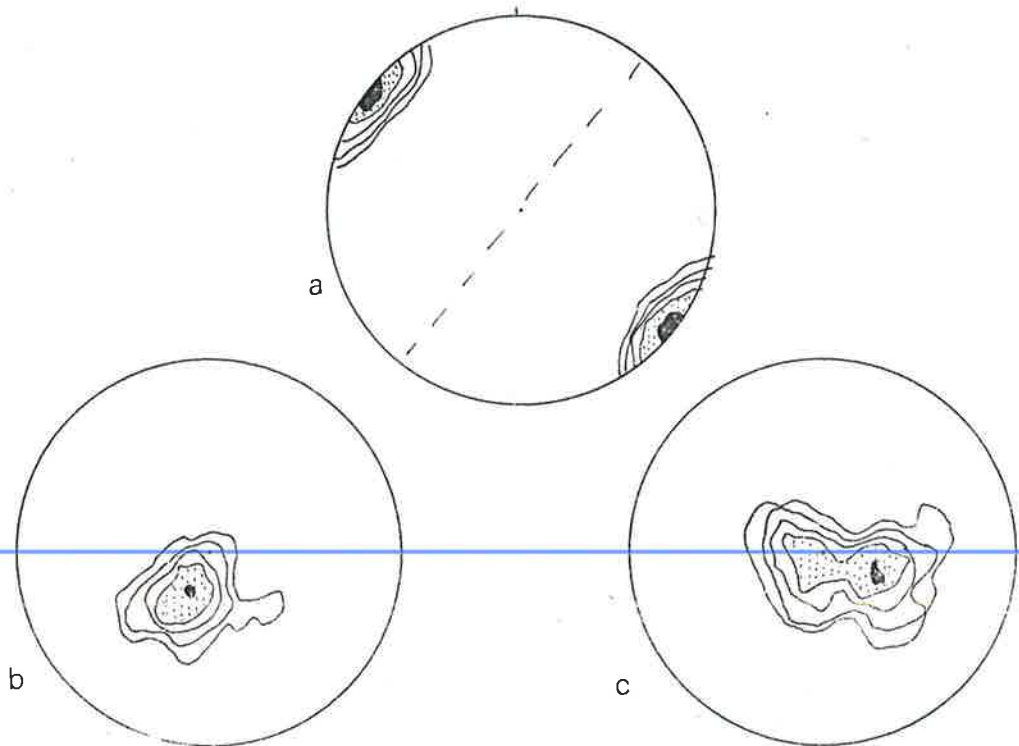
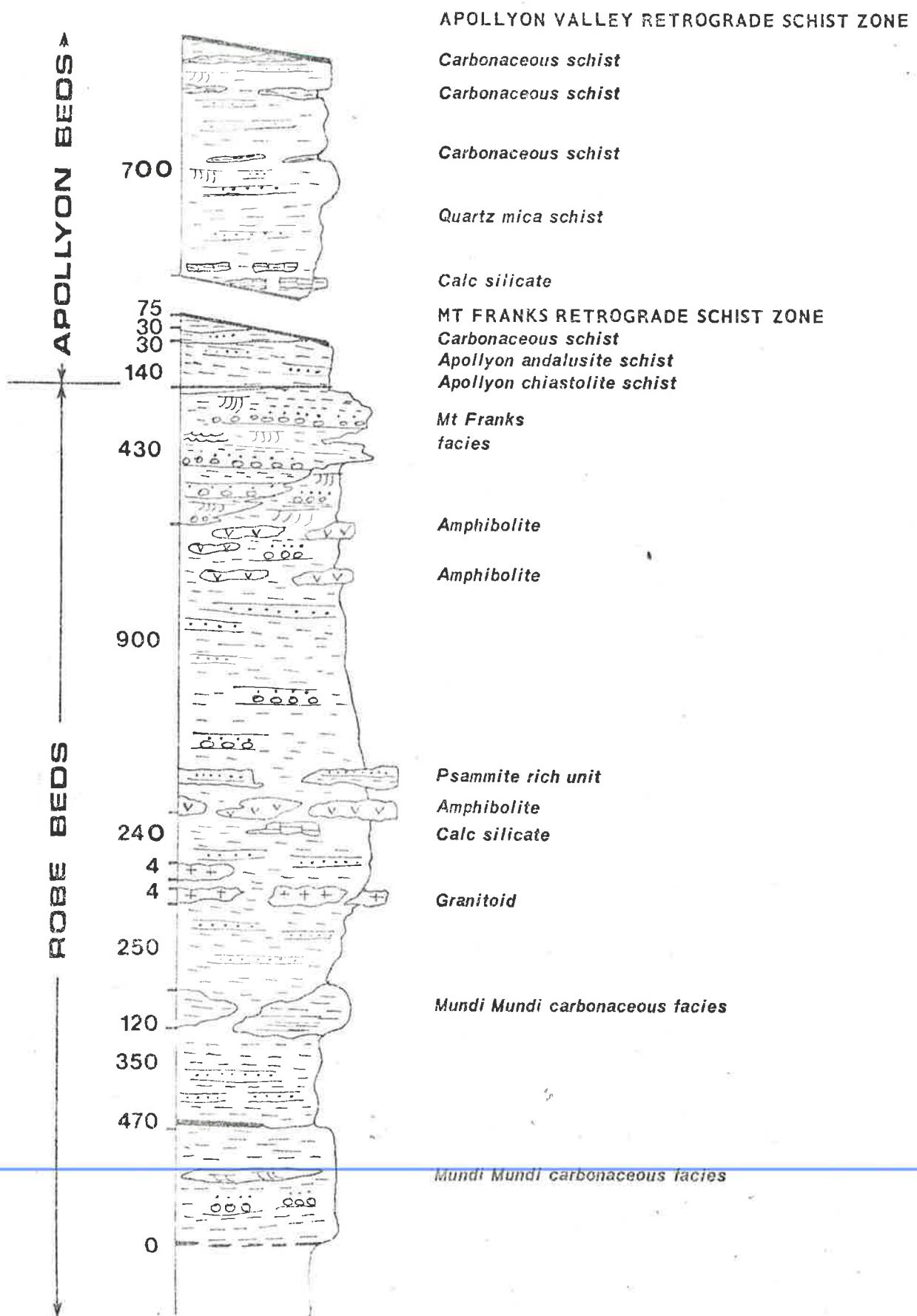


Fig. 6.26 Reconstructed stratigraphic succession west of Apollyon Valley Retrograde Schist Zone. See Section 6.5 and 6.3 for details.

---





CHAPTER 7      STRUCTURAL AND METAMORPHIC SYNTHESIS OF  
THE NORTHWESTERN PART OF THE WILLYAMA COMPLEX,  
AND CORRELATION WITH OTHER AREAS

7.1 INTRODUCTION.

The first part of this chapter extends the mesoscopic, microscopic and macroscopic findings of the Mt Franks - Mundi Mundi area to the north, and presents a structural and metamorphic synthesis of the northwestern part of the Willyama Complex. It is suggested that the regional  $F_1$  syncline recognised in the last chapter can be traced throughout this part of the Willyama Complex.

The second part of this chapter demonstrates that lithological, structural and metamorphic correlations can be made with sequences of low to high grade rocks in the Euriowie Inlier (Tuckwell, 1975), and in the Yanco Glen area, and that structural correlations can be made with granulite facies rocks in the Mine Area and Parnell Area (Laing, 1977; Laing et al, in press, Marjoribanks et al, in prep.).

7.2 STRUCTURAL AND METAMORPHIC RELATIONS IN THE NORTHWESTERN PART OF  
THE WILLYAMA COMPLEX.

The extent of this region is shown in Fig. 7.1. Along its northern margin, it is overlain by alluvium and by younger Adelaidean cover. In the west, it is bounded by the Mundi Mundi Plain, and on the east by the Apollyon Valley Retrograde Schist Zone. Although this zone is generally obscured by alluvium north of the Mt Franks - Mundi Mundi Area, it is defined in scattered outcrop east and south of the Gum Creek Granite (Thomson, 1976) and at Brewery Well where it separates Laing's (1969) transitional and retrogressed zones (see also Willis, 1976). Continuity of the Apollyon Valley Retrograde Schist Zone between these areas is provided by landsat imagery (see frontispiece) and Bureau of Mineral Resources Australia aeromagnetic data (D. Isles, pers. comm., 1976).

Data from the region north of the Mt Franks - Mundi Mundi Area were

gained from traversing, sample collection and from literature study (Leslie and White, 1955; Anderson, 1966, 1971; Tuckwell, 1968; Cooper, 1969; Laing, 1969; Price, 1969; Roberts, 1969; Reynolds, 1975; Splatt, 1975; J. Thomson, 1976, 1977 and W. D'Arcy\* (pers. comm., 1976).

Because of the limited amount of work carried out north of the Mt Franks - Mundi Mundi Area, conclusions reached in this chapter are not as soundly based as ideas discussed in earlier chapters of this thesis. Nevertheless, the ideas in the first part of this chapter are offered as a first attempt at synthesising the geology of this region.

For purposes of data examination, the northwestern part of the Willyama Complex will be divided into four areas (Fig. 7.1):

- 1) Mt Franks - Mundi Mundi area,
- 2) the Mt Robe area - from area 1 north to the Kantappa Retrograde Schist Zone,
- 3) the Brewery Well area - from area 2 north to the southern margin of the Brewery Well Granite, and
- 4) the Kantappa Area - from area 3 north.

#### 7.2.1 Stratigraphy

The stratigraphy recognised west of the Apollyon Valley Retrograde Schist Zone in the Mt Franks - Mundi Mundi area is consistent with local sequences developed throughout the northwestern part of the Willyama Complex (Fig. 7.2).

Direct continuity of mapping between the Mt Robe area and the area to the south (Anderson, 1966), and scattered observations of sedimentary younging direction (see Section 7.2.3.3) suggest that the oldest rocks in the Mt Robe area are equivalent to the Robe Beds further south.

---

\* W. D'Arcy is currently carrying out a Ph.D. study of the rocks in the Kantappa Area.

They consist of psammites, psammopelites and pelites of andalusite and sillimanite grade which are associated with local non sillimanite bearing metasediments (Anderson, 1966; Reynolds, 1975) and with amphibolites and granitoids. A well defined horizon of amphibolite within the andalusite schist is associated with local gneisses (Reynolds, 1975) and local tourmaline schists lie above them. Price (1969) reported the presence of calc silicates from the northern part of this area. Scree fragments of chiastolite schist reported northeast of Black Prince Mine are probably continuous with the main chiastolite schist unit (the Apollyon chiastolite schist) further south (Anderson, 1966), and a well laminated fine grain quartz rich rock reported just east of the Gum Creek Granite by Splatt (1975) may be equivalent to Apollyon quartz mica schists in the Mt Franks - Mundi Mundi Area.

Although the sequence in the Brewery Well and Kantappa areas is repeated about a major fold axis (Fig. 7.1), it is consistent with that developed further west. Basal knotted (andalusite) schists are separated from sillimanite schists by the Kantappa and Apollyon Valley Retrograde Schist Zones, and three separate chiastolite schist bands within the knotted schists were recognised east of Brewery Well by Leslie and White (1955). Equivalent units across the fold axis to the west occur just along the western edge of the Gum Creek Granite and were recognised from further north by Price (1969). They are correlated here with the Apollyon chiastolite schists. Price also recognised a calc silicate unit at this general stratigraphic level. These units are overlain by well-bedded quartz-mica schists with phyllite interbeds (Apollyon Bed equivalents), and then by a thick unit of grey laminated or spotted phyllites with lenticular carbonaceous bands and local 'cherty' horizons. These constitute the youngest exposed rocks of the Willyama Complex and are best exposed between Kantappa and Brewery Well where they are not truncated by the Apollyon Valley Retrograde Schist Zone.

Significant features of this stratigraphic succession include the

TABLE 7.1 STRUCTURAL CORRELATION ACROSS THE NORTHWESTERN PART OF THE WILLYAMA COMPLEX

|                                      | Mt Franks - Mundi Mundi area<br>(area 1)  | Mt Robe area<br>(area 2)   | Area between Brewery Well and<br>Kantappa Retrograde Schist Zone<br>(area 3)                            | Kantappa area<br>(area 4)  |
|--------------------------------------|---|--|---|--|
| Pre-S <sub>1</sub><br>schistosity    | Biotite, local sillimanite, muscovite;<br>parallel and non-parallel to S <sub>0</sub> ;<br>ilmenite in andalusite                                 | Implied:<br>ilmenite in andalusite   |   |  |
| Pre-S <sub>1</sub><br>porphyroblasts | Biotite, andalusite, sillimanite,<br>mineral aggregates   | Biotite, andalusite  | Biotite, cordierite(?)<br>(Laing), andalusite   | Biotite, andalusite, mineral aggregates<br>after cordierite(?) (D'Arcy)                                    |
| S <sub>1</sub>                       | Homogeneous to layered: muscovite,<br>local biotite, sillimanite, rotated biotite;<br>parallel and non-parallel to S <sub>0</sub>                 | Layered: local biotite,<br>muscovite, sillimanite, rotated<br>biotite: parallel to S <sub>0</sub>                                | Relicts only visible: muscovite,<br>rotated biotite, local biotite;<br>subparallel(?) to S <sub>0</sub> | Homogeneous: muscovite, some<br>biotite, some rotated biotite;<br>generally non-parallel to S <sub>0</sub> |
| F <sub>1</sub>                       | Upright to overturned: tight to<br>isoclinal: variable plunge   | Overturned;<br>tight to isoclinal  |   | Upright;<br>tight: variable plunge   |
| L <sub>1</sub>                       | Not common in non-sillimanite<br>schist: sillimanite, quartz - muscovite,<br>mineral aggregates   | Sillimanite, quartz,<br>muscovite  |   | Mineral aggregates   |
| S <sub>2</sub>                       | Localized in F <sub>2</sub> hinges;<br>biotite, sillimanite, muscovite  |  | Dominant: muscovite,<br>opaque stringers  |  |
| F <sub>2</sub>                       | Local, tight;<br>overturned to west   | Local, tight; overturned<br>to west; not recognized<br>by Splatt or Reynolds   | Tight, upright  | North-plunging crenulation<br>of Roberts   |
| S <sub>3</sub>                       | Common in east of area: muscovite,<br>rotated biotite, rotated sericite clots<br>pseudomorphic after andalusite;<br>ENE. - NE. trend, subvertical | Generally rare; muscovite;<br>rotated biotite, rotated clots of<br>sericite after andalusite (Splatt);<br>NE. trend; subvertical | Not common, more a fracture;<br>axial plane to F <sub>3</sub> folds;<br>NE. trend, subvertical          | Generally absent   |
| F <sub>3</sub>                       | Upright: open kink style;<br>ENE. - NE. trend: generally SW.<br>plunge some NE. plunge  | Upright: open kink<br>style; NE. trend:<br>generally SW. plunge.   | Upright: open kink<br>style; NE. trend;<br>subvertical plunge   |  |
| L <sub>3</sub>                       | Muscovite, quartz,<br>aggregates  |  |   |  |

restriction of amphibolites to the older rocks, the increase in graphite towards the top of the sequence, and the decrease in grain size towards the top of the sequence.

### 7.2.2 Mesosopic and Microscopic Relations

Before an attempt can be made to extrapolate the macroscopic structures of the Mt Franks - Mundi Mundi area northwards, it is necessary to establish a correlation within this whole region on both a mesoscopic and microscopic scale.

Table 7.1 presents a suggested correlation of structural events between the four areas of this region. This forms the basis for the macroscopic synthesis in Section 7.2.3.

Critical aspects of the meso and microfabric in each of the three northern areas, and the assumptions involved in correlating between different areas will now be discussed. The Mt Robe Area is discussed first, and then the Kantappa Area. Because of schistosity complications, the Brewery Well Area is discussed last.

#### 7.2.2.1 The Mt Robe Area and Correlation with the Mt Franks - Mundi Mundi Area

The dominant schistosity in this area is axial planar to rare isoclinal folds in bedding, and thus generally lies parallel to bedding (Anderson, 1966; Price, 1969; Reynolds, 1975; Splatt, 1975). This schistosity is defined by muscovite + quartz  $\pm$  biotite  $\pm$  sillimanite. A sillimanite lineation is common (Anderson, 1966). Price (1969) first drew attention to the segregated nature of this schistosity and suggested that it had formed by the crenulation of an earlier schistosity. Evidence for a phase of earlier fabric development is provided by the presence of oriented ?ilmenite inclusion trails in pre-S<sub>1</sub> andalusites (Splatt, 1975). Splatt also reported the presence of pre-S<sub>1</sub> biotites kinked about S<sub>1</sub>.

Second generation effects in this area are restricted to the rare

northwest trending folds in  $S_0$ ,  $S_1$  and  $L_1$  reported by Anderson (1966). These folds are tight with an overturned axial surface; according to Anderson they lack an  $S_2$  fabric.

$F_3$  folds of Anderson (1971) are correlated with  $F_2$  folds of Reynolds (1975) and Splatt (1975) on the basis of style and orientation.  $F_3$  folds form characteristic southwest plunging kink type crenulations in  $S_1$ . The hinges of larger folds are generally marked by co-axial crenulations and a northeast trending, subvertical mica fabric may be present. Splatt (1975) noted that there was a re-alignment of sericite clots after andalusite into  $S_3$ , and Reynolds (1975) noted that  $F_3$  folds were co-axial with  $L_1$  and he further suggested that a new lineation ( $L_3$ ) formed by the re-alignment of muscovite and hornblende in amphibolites. Formation of chlorite, chloritoid and cross cutting muscovite laths was probably associated with this event (Browne, 1922).

Interference folds probably related to  $D_3$  were described by Anderson (ibid) and Splatt (ibid), and Reynolds described minor post  $D_3$  folding.

Correlation between the Mt Robe Area and the Mt Franks - Mundi Mundi Area is based on five lines of evidence:

- 1) the presence of pre- $S_1$  mineral growth in both areas,
- 2) the macroscopic continuity of  $S_{1P}$  between both areas,
- 3) the similar mineralogy of  $S_{1P}$ ,
- 4) the correlation of  $F_2$  folds by style and orientation, and
- 5) the correlation between  $D_3$  effects in style, orientation and metamorphic grade.

---

#### 7.2.2.2 The Kantappa Area, and Correlation with the Mt Franks - Mundi

##### Mundi Area

The dominant schistosity in this area is a sub-vertical, homogeneous schistosity which is axial planar to variably plunging first generation

open to tight folds (W. D'Arcy, pers. comm., 1976). The schistosity ( $S_1$ ) is defined by the crystallographic alignment of muscovite and some biotite, and by the shape alignment of quartz and some biotite. A

lineation defined by biotite aggregates may also be present. Evidence for a pre- $S_1$  mineral growth in these rocks is provided by:

- 1) kinking of biotite parallel to  $S_1$ ,
- 2) the presence of rotated or corroded biotites in  $S_1$  which lack a crystallographic preferred orientation (cf. Section 4.3.7.2),
- 3) the alteration of biotite to muscovite in  $S_1$ ,
- 4) the formation of  $S_1$  pressure shadows, and the wrapping of  $S_1$  around now retrogressed porphyroblasts, and
- 5) the re-alignment of graphite into  $S_1$ .

W. D'Arcy (pers. comm., 1976) has suggested that retrogressed porphyroblasts may originally have been andalusite and cordierite.

Post  $S_1$  deformation in this area is restricted to north plunging crenulations in  $S_1$  which only occur west of the Brewery Well granite (Roberts, 1969), and to offsets of bedding on  $S_1$  which D'Arcy (1977) attributed to reactivation during the deformation of the Adelaidean sediments.

Correlation between this area and the Mt Franks - Mundi Mundi Area is hindered by separation of many kilometres and cannot be firmly made. Nonetheless, it is suggested that  $D_1$  structures in the low grades of the Mt Franks - Mundi Mundi area may be equivalent to those in the Kantappa Area.  $F_1$  folds in both areas are variably plunging upright, and  $S_1$  in both areas lies at an angle to bedding.  $S_1$  ( $S_{1N}$  in the Mt Franks - Mundi Mundi area) in both areas is preceded by biotite and porphyroblast growth, but as yet there is no evidence for a pre- $S_1$  fabric in the Kantappa Area.

---

In both areas,  $S_1$  is defined by muscovite with a variable biotite component, and contains a subvertical mineral elongation defined by elongate aggregates containing pre- $S_1$  biotite.



### 7.2.2.3 The Brewery Well Area and Correlation with the Kantappa and Mt Robe Areas

Laing (1969), working immediately south of the Brewery Well Granite, and Price (1969), working further west in andalusite schists just below the Adelaidean Unconformity, both noted that the dominant schistosity in their areas is segregated and overprints internal porphyroblast fabrics. They thus suggested it was  $S_2$  in age, and Laing (1969) showed that it was overprinted by northeast trending, steeply plunging  $F_3$  kink folds which he correlated with the  $F_3$  folds of Anderson (1966) in the Mt Robe Area. Further west, Price (1969) reported north/south trending  $F_3$  folds. If there is a direct correlation between  $F_3$  of Price and Laing, a period of post  $D_3$  rotation must be postulated for the western area. Thomson (1976, 1977) has established the existence of a major north/south trending fold in bedding and layer parallel schistosity here but the geology of this area is not well established. This western area, bounded to the south by the Kantappa Retrograde Zone, is possibly also to the east by the continuation of the Mt Franks Retrograde Schist zone (King and Thomson, 1953; Thomson 1976). Evidence for late stage movement along the Kantappa Retrograde Zone to the south of this area is provided by the presence of fault blocks of Adelaidean Sediments (Fig. 7.1).

The  $S_2$  schistosity of Laing (1969) is axial planar to  $F_2$  folds in  $S_0$  and an early schistosity, and is overprinted by  $F_3$ . Microfabric studies clearly demonstrate the development of  $S_2$  from the early  $S_1$  schistosity. Crenulated  $S_1$  is defined by laths of muscovite and biotite, as well as by a shape orientation of biotite. In addition there is some evidence that muscovite laths in  $S_1$  overprint retrogressed porphyroblasts which Laing (1969) suggested represented cordierites. Price (1969) also reported that  $S_2$  deformed retrogressed porphyroblasts, and was associated with a lineation formed by porphyroblast beards.

No definite correlation can be made between the Brewery Well and Kantappa

Areas, and two possible alternatives are:

- 1)  $S_1$  in the Kantappa Area corresponds to  $S_1$  in the Brewery Well Area which is overprinted by  $S_2$ , and
- 2)  $S_2$  at Brewery Well corresponds to  $S_1$  in the Kantappa Area, and there is no equivalent to the  $S_1$  schistosity (first suggested by Laing, 1969). Model 1) is favoured by two lines of evidence:  $S_1$  in both areas is a muscovite + biotite schistosity and overprints early porphyroblasts, and  $S_2$  in the Brewery Well Area contains no biotite. In this case,  $S_2$  dies out to the northwest where it might be represented by the crenulations in  $S_1$  reported by Roberts (1969).

The ultimate correlation between the Kantappa and Brewery Well Areas depends on the relation of  $S_2$  and  $F_2$  to the major synclinal hinge which can be traced into the Brewery Well Area from the northwest. This hinge is regarded as  $F_1$  in the Kantappa Area (see below). At present, the known restriction of  $F_2$  and  $S_0/S_2$  relations in the Brewery Well Area is insufficient to establish congruency relations or otherwise.

The correlation of  $S_1$  and  $S_2$  of Laing (1969) with the pre- $S_1$ ,  $S_1$  and  $S_2$  schistositities in the Mt Robe Area is constrained by the unequivocal correlation of  $D_3$  structures. In both areas  $S_3$  is northeast trending and subvertical. Price (1969) suggested that  $S_2$  in the Brewery Well Area corresponds to  $S_1$  in the Mt Robe Area. However, Price (1969) did not recognise pre- $S_1$  porphyroblast growth in the Brewery Well Area, and if this episode is correlated with pre- $S_1$  growth in the Mt Robe Area, it may suggest equivalence of  $S_1$ , which is a muscovite + biotite schistosity, between both areas. This correlation is consistent with findings of a traverse carried out across the Kantappa Retrograde Schist Zone which suggested that north plunging crenulations in  $S_1$  leading to new schistosity formation (? $S_2$ ) north of the zone had no correlations south of the zone.

If model 2 involved in both correlations, viz. that  $S_2$  in the Brewery

Well Area correlates with  $S_1$  in the northwest and southwest, is correct, then  $S_1$  in the Brewery Well Area correlates with a pre- $S_1$  fabric in the Mt Robe Area but has, as yet, no recognised correlative in the Kantappa Area. The Brewery Well Area would then possess the best evidence for preferred early mineral growth in this part of the Willyama Complex.

The macroscopic synthesis of the next section does not depend on micro-fabric relations in the Brewery Well Area, and either correlation discussed above is consistent with it.

### 7.2.3 Macroscopic Synthesis

#### 7.2.3.1 The Kantappa - Lakes Nob Syncline

The last section suggested that:

1) there is a direct correlation between  $D_1$ ,  $D_2$  and  $D_3$  effects in the Mt Franks - Mundi Mundi and Mt Robe areas,

2)  $D_1$  effects can be correlated between the Kantappa and Mt Franks - Mundi Mundi areas, and

3)  $D_1$  and  $D_3$  effects may be correlated between the Brewery Well and Mt Franks - Mundi Mundi Areas. Alternatively,  $D_2$  structures in the Brewery Well Area correlate with  $D_1$  structures in the Mt Franks - Mundi Mundi Area. The variable development of  $D_2$  structures across the Kantappa Retrograde Schist Zone suggests that this zone, or its precursor was already active in  $D_2$  time. Laing (1977) has similarly suggested that "proto" British and De Bavay Shears in the Mine Area were active in  $D_2$  time.

Bearing in mind the above structural correlation and the continuity of marker units (Section 7.2.1), it is suggested that the regional  $D_1$  syncline obscured by the Apollyon Valley Retrograde Schist Zone in the Mt Franks - Mundi Mundi Area corresponds to the major syncline exposed in the Kantappa Area (where it is  $F_1$  in age) and in Brewery Well Area (where it is  $F_1$  or  $F_2$  in age), but which runs into the schist zone southeast of the Gum Creek Granite (Fig. 7.1). That is, the Mt Franks - Mundi Mundi and Mt Robe Areas lie in the western limb of this syncline, with the hinge and eastern limb

exposed only in the two northern areas.

In the Kantappa Area, the hinge of this macroscopic upright syncline is outlined by repetition of lithological units and by variation in bedding orientation. North of Campbells Creek, this syncline and parasitic folds on its eastern limb are south plunging and best outlined by lenticular carbonaceous schists. South of Campbells Creek, the syncline is northerly plunging (Thomson, 1976, 1977; W. D'Arcy, pers. comm., 1976). These folds are regarded as  $F_1$  structures because:

- 1)  $S_1$  is congruent to, and changes sense across, the fold,
- 2) small  $F_1$  folds change shape across the fold, and
- 3) their axes lie parallel to  $F_1$  small folds and  $S_0/S_1$  intersections which also change plunge through the horizontal.

Laing (1969) traced the hinge of this syncline into the northwestern part of the Brewery Well Area, where it is refolded by  $F_3$  folds. Using the mapping of Thomson (1976) this hinge can be traced through the Brewery Well Area around the shared limb of an  $F_3$  fold pair, and then further south where it either runs down the eastern side of the Gum Creek Granite or is obscured by it (Fig. 7.1).

Because of  $S_2$  development in the Brewery Well Area, the relationships between this axis and  $F_1$  folds is unknown: the major syncline pre-dates or is the same age as  $S_2$ , and sedimentary youngings indicate that it is upward facing. South of the Gum Creek Granite, the lack of lithological repetition suggests that the synclinal axis is truncated by the Apollyon Valley Retrograde Schist Zone (Fig. 7.1).

This major syncline which dominates the northwestern part of the Willyama Complex is called the Kantappa - Lakes Nob Syncline.

#### Characteristics of the Kantappa - Lakes Nob Syncline

Minor  $D_1$  structures indicate that the Kantappa - Lakes Nob Syncline changes plunge from southerly to northerly between Kantappa and Brewery Well.

In the Mt Robe Area, plunges are probably shallow since moderate southerly plunges occur on and just north of Mt Franks. South of Mt Franks, minor folds change plunge through the horizontal to become northerly plunging in both the Apollyon and Robe Beds just north of Lakes Nob. Despite these plunge variations, the overall plunge of the syncline is probably northerly since rocks highest in the succession are exposed in the north of the region, in the Kantappa Area.

The original orientation of the axial surface of the Kantappa - Lakes Nob Syncline can be estimated from the orientation of  $S_1$  in areas unaffected by later folds and by the attitude of  $S_1/S_2$  and  $S_1/S_3$  intersections and  $F_2$  and  $F_3$  small folds.

In the low grade rocks  $S_1$  is sub vertical. As a result  $F_2$  folds are vertically plunging in the Brewery Well area and  $F_3$  folds are sub vertical here. In the low grade rocks in the Mt Franks - Mundi Mundi area,  $S_1/S_3$  intersections vary from steep NE to steep SW plunging. Because of  $S_2$  formation in the Brewery Well Area, and  $F_3$  folding in the Mt Robe Area, the orientation of  $S_1$  in the underlying rocks is best seen in the Mt Franks - Mundi Mundi Area. In Section 6.3.2 it was shown that  $S_1$  is curvilinear in these rocks, that  $F_2$  folds are moderately west plunging and that  $F_3$  folds are moderately westward and southwest (or even northeast) plunging. In the Mt Franks - Mundi Mundi Area, it was suggested that the western limb of this syncline became overturned with depth (Section 6.3.3). Although andalusite schists in the Kantappa and Brewery Well areas are east dipping in this limb (i.e. right way up), relations in the Mt Robe Area are obscured by lack of outcrop and by  $F_3$  refolding (see below). However, consistent with relations to the south, it is suggested that the eastern limb of the Mt Robe Synform is overturned (Section 6.3.1).

#### 7.2.3.2 Relation between Metamorphic Zones and the Kantappa - Lakes Nob Syncline

In the Mt Franks - Mundi Mundi Area, it was suggested (Section 6.3.4)

that if the metamorphic zones are pre- $S_1$  in age, they should be folded about the regional syncline. Distribution of metamorphic zones over the whole region (Fig. 7.1) supports this. In the Brewery Well Area, low grade rocks in the core of the Kantappa - Lakes Nob Syncline are flanked by andalusite grade schists which are faulted against sillimanite schists. The boundary between low and medium grade rocks lies parallel to bedding in the Kantappa - Brewery Well Area but is localised along the Mt Franks Retrograde Schist Zone further south. In the Mt Robe and Mt Franks - Mundi Mundi Areas, the eastern margin of these low grade rocks is faulted against high grade rocks lying east of the Apollyon Valley Retrograde Schist Zone.

The andalusite/sillimanite boundary is fault controlled in the Kantappa - Brewery Well area. In the Mt Robe area, it generally lies parallel to bedding but cuts across bedding in the hinge of the  $F_3$  Mt Robe Synform. Thomson's (1976) mapping in this area has shown that the isograd does not simply cut through the hinge, but is partially folded (parallel to bedding) before cutting through the hinge in a NNE orientation and then itself being intersected by the Kantappa Retrograde Zone. Thomson (1976) suggested that the change in orientation of the isograd resulted from new sillimanite growth during  $S_3$  time. No evidence of new sillimanite growth was found further south, and two other possible explanations are:

1) that the isograd lies non parallel to bedding in this area and its orientation sub parallel to  $S_3$  is a coincidence, or

2) that the isograd is controlled by a NNE trending  $D_3$  lineament.

However no offset of amphibolite units or of bedding has been detected around this hinge.

Further south in the Mt Franks - Mundi Mundi Area, the andalusite/sillimanite isograd generally lies parallel to bedding, and is folded round  $F_1$  and  $F_3$  folds (see Section 6.3.3). Andalusite schists terminate in the south of the area in north plunging folds. Biotite schists further to the east are cut off in an area of north plunging  $F_1$  folds.

It can thus be seen that the belt of low and medium grade rocks in the northwestern part of the Willyama Complex is so located because of its position in a tight  $F_1$  syncline. The general depth control on metamorphism and change in style of  $D_1$  structures with the folded distribution of these metamorphic zones suggests that the tectonic - level model developed in Section 6.3.5 can be applied to the northwestern part of the Willyama Complex.

### 7.2.3.3 Macroscopic $F_3$ Folds in the Western Limb of the Kantappa - Lakes Nob Syncline

#### The Mt Robe Synform

Anderson (1966) described the Mt Robe Synform as an open fold with a steep west dipping or east dipping eastern limb and steep western limb. Bedding in the main hinge was folded around an axis plunging at  $50^\circ$  to the southwest while further south, shallower ( $30^\circ$ ) plunges were recorded. Anderson (ibid) suggested that the western limb of synform was truncated by a northwest trending Mt Robe fault passing through the Mt Robe Area (Fig. 7.1). He suggested that this fault continued along strike to the east, but noted that there was no disruption of amphibolites in the eastern limb of the Mt Robe Synform. Recently produced aeromagnetic maps across this area (B.M.R., 1976) show an ESE trending lineament in this locality, and it can be seen extending further east, across the Gum Creek alluvial flat.

Younging directions in the eastern limb north of Black Prince Mine and at Silver King Mine (see also Splatt, 1975) suggest that the steeply west-dipping, eastern limb of this synform is overturned. In Section 6.2.3.3 it was suggested that  $S_0//S_1$  in the eastern limb of this synform became overturned in the Black Prince Area. Variations in younging east of Silver King reported by Splatt (1975) were attributed by him to small  $F_1$  folds. This is justified if younging reversals occur about a consistently dipping  $S_0$ . However, this area is dominated by folds with an axial plane crenulation schistosity similar to  $S_3$  elsewhere, and it is not known if these folds are

the sole cause of Splatt's younging reversals.

Relations in the central part of the Mt Robe Area need clarification. South of the Mt Robe fault, Reynolds (1975) reported upward youngings on Mt Robe itself. Because of this faulting, the relation between these youngings to those in the eastern limb of the main synform is unknown; it may be due to  $F_3$  folding. Thomson (1976) has located a synformal hinge just near the Mt Robe mine and shallow dips occur from Mt Robe south to Eldee Creek. It is accordingly suggested that the axial trace of the Mt Robe synform continues to the southwest through these areas, and passes through the southwest plunging synform located near Mundi Mundi Creek in the Robe Beds (Fig. 7.1). This whole structure is thus called the Mt Robe Synform.

However, it must be pointed out that the exact location of the hinge in the area just south of Mt Robe is only inferred, and further work needs to be done to clarify relations in this area, and in particular to examine evidence for any  $F_1$  features.

This interpretation differs from that of Anderson (1966) who suggested that NE trending fault in the Black Prince area displaced the hinge of the Mt Robe Synform into this area where it was repeated as a steeply ( $70^\circ$ ) southwest plunging structure. However, in Section 6.2.3.3 it was suggested that structures in the Black Prince Area consisted of an  $F_3$  fold pair - an eastern anticline and western neutral fold overprinted by  $F_4$  crenulations and an  $F_4$  fault. It was also shown that these structures were critical in joining the Mt Robe Synform with the structures to the south since  $S_0$  changed dip from east to west around these folds.

#### Mt Robe Antiform

Anderson (1971) suggested that the Mt Robe Antiform lying west of the Mt Robe Synform could be traced southwest to Eldee Creek. He noted that the hinge is partially obscured by pegmatite but showed that the main axis plunges at  $20^\circ - 30^\circ$  to the southwest near Mt Eltie, but further north,



plunges north because of  $F_2$  folding (Anderson, 1966). Confirmation of this structure was found south of Mt Eltie during the present study.

It is suggested that the trace of this antiform, which may be downward facing from the evidence of one northward younging sedimentary structure, can be extended further southwest into the hinge area mapped just north of Mundi Mundi Creek near the Mundi Mundi Plain (Fig. 7.1). However, more detailed work is needed north and south of Eldee Creek in this area.

The major  $F_3$  folds in the Brewery Well area consist of a western antiform and eastern synform which lie along the axial surface trend of the Mt Robe Antiform and Mt Robe Synform respectively. It is suggested that these structures may be linked across the Kantappa Retrograde Schist Zone. However, these folds are not apparent in the intervening andalusite schist west of the Gum Creek Granite, and north of the Kantappa Retrograde Schist Zone and this absence, coupled with the discordance between the orientation of  $F_3$  structures of Anderson (1971), Price (1969) and Laing (1969), might be accounted for by post- $D_3$  faulting.

#### 7.2.4 Granitoids in the Northwestern Part of the Willyama Complex

Sillimanite grade rocks, in the Mt Franks - Mundi Mundi area, are dominated by migmatite complexes, and by large bodies of pegmatite aligned roughly parallel to  $S_1$ . In many cases a gradation between migmatite and pegmatite can be observed. In the lower grade rocks, granitoids occur as pegmatite/granite sills parallel to  $S_0$ ,  $S_1$  or  $S_3$ .

In the Mt Robe Area, Anderson (1966, 1971) noted that some pegmatites were folded around  $F_2$  and  $F_3$  folds, while other bodies were emplaced parallel to  $S_3$  axial planes. Because some of the late stage bodies cut across the Mt Robe fault, Anderson argued that they were intruded after the  $D_3$  event. In the Silver King area, Splatt (1975) reported that in addition to pre- $F_3$  pegmatites which were parallel to  $S_0$  and  $S_1$ , there were larger cross cutting bodies. In the Mt Robe area, Reynolds (1975) noted that massive discordant pegmatites obliterated  $F_3$  fold hinges.

In the Brewery Well Area, plutonic activity has resulted in the formation of granites of the Mundi Mundi suite - the Brewery Well granite and the Gum Creek Granite (Fig. 7.1).

The Brewery Well Granite studied by Leslie and White (1955) and Laing (1969) is an alaskitic rock (Vernon, 1969) intruding Willyama metasediments and unconformably overlain by basal Adelaidean conglomerates. Leslie and White (ibid) reported a narrow aureole of feldspathised and hornfelsed country rock but Laing (ibid) did not observe any feldspathisation. The body consists of massive unfoliated granite but contains several sets of fractures.

Veins of aplite and pegmatite are associated with the southern contact and pass out into the country rock where they penetrate along  $S_2$  or  $S_0$ , and sometimes outline  $F_3$  folds (Laing 1969).

The Gum Creek Granite is elliptical in plan with fault bounded eastern and western margins. It is a fine grained granite consisting (Splatt, 1975) of quartz, microcline, plagioclase ( $An_{10}$ ), muscovite and biotite. Splatt (ibid) noted that the biotites were locally deformed. Although the body is generally massive, at least two sets of fractures are present, trending  $310^\circ 90^\circ$ , and  $030^\circ 70^\circ W$ , and the contacts are foliated. This foliation is parallel to the margins of the granite body; on the eastern and western sides it is parallel to  $S_3$  in the metasediments. Inclusions of country rock in the granite are either hornfelsed or partially resorbed, and hornfels also occur along the granite contacts.

The granitoid bodies scattered throughout the northwestern part of the Willyama Complex fall into two ages - syn- $S_1$  migmatites and pegmatites and late-stage cross cutting pegmatites, and granites which are believed to be associated with the  $D_3$  event. Evidence for the syn- $D_1$  age of the migmatites and some granitoids is provided by

- 1) their parallelism to  $S_1$ ,
- 2) their folding around  $F_2$  and  $F_3$  folds, and

3) the presence of pegmatite veins parallel to  $S_1$  containing micas crenulated during  $D_3$  folding.

Their formation during this deformation is consistent with an ultimate origin by partial melting during the high grade metamorphism (see Section 5.2.4, and also Reynolds, 1975; Splatt, 1975; and Phillips, 1975).

Evidence for a  $D_3$  age for the late stage bodies is provided by

1. emplacement parallel to  $S_3$ ,
2. emplacement in  $F_3$  fold hinges (Brewery Well Granite, Robe Granite), cf. model by Gresens (1967, Fig.4) for emplacement of pegmatites in "structurally low pressure zones,"

3. foliated margins of the Gum Creek Granite,
4. the presence of pegmatite veins with quartz stringers and micas aligned parallel to  $S_3$  in the enclosing metasediments,
5. the ellipsoidal shape of the Gum Creek Granite which has its long axis parallel to  $S_3$  and its short axis perpendicular to  $S_3$ , and
6. the faulted western margin of the Brewery Well Granite as revealed by examination of Landsat 1 photos (see frontispiece).

It is thus suggested that late stage magmas were generated during the  $D_3$  deformation with the resultant crystallisation of syn- $D_3$  and post  $D_3$  granites and pegmatites.

A. White (pers. comm., 1976) has suggested that the Mundi Mundi granite suite is an S-type granite, formed by partial melting of sediments. P,T conditions during  $D_3$  time were unfavourable for partial melting not only in the northwestern part of the Willyama Complex, but also in the stratigraphically lower area around Broken Hill (Laing, 1977), and thus an origin by partial melting at depth must be invoked. Magma generated at depth would rise towards areas of lower enclosing pressure and would thus migrate towards the top of the sedimentary pile. The site of emplacement of these magma bodies is largely dependent upon the fluid content. Bodies with a minor fluid phase content would be able to ascent higher in the pile

before crystallising than would bodies with a higher content of fluids. It is thus suggested that these fluid poor magmas are represented by the fine grained granites of the Mundi Mundi suite which have been emplaced in the upper parts of the sedimentary pile whereas other magmas crystallising further down result in the formation of coarse grained pegmatites. The Mundi Mundi granites are surrounded by narrow contact aureoles whereas the pegmatites emplaced at greater depths are surrounded by a broad envelope of highly sericitised metasediments of  $D_3$  age.

### 7.3 CORRELATION WITH OTHER AREAS OF LOW TO MEDIUM GRADE METAMORPHISM.

#### 7.3.1 The Bijerkerno Area

Work in this area by Meares (1969) and Tuckwell (1975) has established a sequence of low to high grade metamorphics which is similar to that occurring in the northwestern part of the Willyama Complex.

##### 7.3.1.1 Lithology

Tuckwell (1975) established a 6000 m thick sequence of sediments which pass upward from graded pelites and psammities into quartzites with local calcareous units. These are overlain by three chiasmolite horizons which mark the top of his Wookookaroo Beds (K. Tuckwell, pers. comm., 1977). The overlying Bijerkerno Beds begin at the base of a prominent calc silicate horizon and consist of fine grain carbonaceous siltstones, phyllites and quartzites. This stratigraphic sequence is similar to that established in the northwestern part of the Willyama Complex. The Robe/ Apollyon boundary in that area would correspond to the base of the lowest chiasmolite schist unit at Bijerkerno.

##### 7.3.1.2 Metamorphism

~~In the Bijerkerno area, Meares (1969) and Tuckwell (1975) recognised three prograde metamorphic zones based on the successive appearance of biotite, andalusite, and sillimanite. A line denoting the incoming of garnet occurs close to the andalusite - in line. Both these workers recognised~~

that these isograds lie parallel to bedding, not  $S_1$ , and that bedding,  $S_1$  and isogradic surfaces are folded around an  $F_2$  fold. Tuckwell (1975) explained this feature by suggesting that the isograds were imposed on flat lying bedding, and were subsequently folded about  $F_1$ .

The following metamorphic and microstructural scheme was then set up (Tuckwell, 1975):

|                          |  |
|--------------------------|--|
| pre- $S_1$ metamorphism: | andalusite, biotite, ?sillimanite  |
| syn- $S_1$ metamorphism: | mineral spots (incipient andalusite), some andalusite, garnet, ?sillimanite. |
| post $S_1$ :             | chlorite, sericite, chloritoid, opaques.                                     |
| syn- $S_2$ :             | chlorite, biotite, muscovite, chloritoid.                                    |
| post $S_2$ :             | big cross cutting muscovite laths.   |

Tuckwell (1975) reported the occurrence of andalusite in layers parallel to bedding, and showed that these crystals contained inclusions of graphite, quartz, biotite and muscovite which were also parallel to bedding.

### 7.3.1.3 Structure

Tuckwell (1975) suggested that the Bijerkerno areas lie on the right way up limb of a flat lying  $F_1$  anticline which closes to the east and which is folded around his  $F_2$  Bijerkerno Syncline. He noted that  $S_0/S_1$  relations vary from non parallel in andalusite grade rocks to parallel in sillimanite grade rocks; low grade rocks in the core of the syncline contain an upright  $S_2$  schistosity.

### 7.3.2 Yanco Glen Area

This area lies in the main part of the Willyama Complex, south of the Corona fault which bounds the Euriowie Inlier (Fig. 1.2). Rocks in this area consist of sillimanite grade psammites and pelites overlain on the east by andalusite grade metasediments. Corbett (pers. comm., 1975) working in the southern part of this area notes the presence of pre-tectonic andalusites which overlap into his main schistosity. The dominant fabric

is regarded as  $S_2$  (Corbett, written comm., 1977) because of its layered nature.

### 7.3.3 Discussion and Correlation

The sequence in the west limb of the Kantappa - Lakes Nob Syncline has very close similarities to Tuckwell's (1975) sequence. Two exceptions are the lack of carbonaceous schists well down in Tuckwell's sequence (Mundi Mundi equivalents) and the lack of amphibolites in Tuckwell's area. On this basis of porphyroblast overprinting criteria and on the nature of  $S_0/S_1$  relations it is suggested that  $S_1$  of Tuckwell may correspond to  $S_1$  of this study. However, Tuckwell found no evidence for a pre- $S_1$  schistosity although he noted that inclusions in andalusite layers were oriented parallel to bedding. Tuckwell's  $F_2$  folds may correlate with  $F_3$  of this study on the basis of style, associated schistosity and to a limited extent orientation; in this case there is no  $F_2$  equivalent at Bijerkerno. Both areas are marked by the folding of bedding parallel isograds.

Corbett's  $S_2$  may be correlable with  $S_1$  of the present study and the pre- $S_1$  fabric in this study would be correlated with his  $S_1$ . Both Tuckwell's (1975) and Corbett's (pers. comm. 1976) areas lie on the upright limb of large scale flat lying anticlines, and if the correlations presented above are accurate, this corresponds to the opposite limb occupied by the sequence in the Kantappa - Lakes Nob Syncline and suggests these areas may be linked by  $F_1$  folding.

### 7.4 CORRELATION BETWEEN THE MT FRANKS - MUNDI MUNDI AREA AND HIGH GRADE ROCKS BETWEEN THE MINE AREA AND THE PARNELL AREA.

Glen et al (1977, Appendix I) suggested that rocks around the Mine and Parnell areas lie stratigraphically below rocks in the northwestern part of the Willyama Complex. Although rocks in the Mine Area have a metamorphic grade of granulite facies (Binns, 1964; Laing, 1977) and are therefore much

higher than that of rocks described in this study, it is considered that they occur in the high temperature field of the P,T gradient discussed in Section 5.

The mesoscopic structural history of this area has recently been evaluated by Rutland and Etheridge (1975), Laing, (1977), Laing et al (in press) and Marjoribanks et al (in prep.) and three major deformations are now recognised.

#### 7.4.1 Structural History of High Grade Rocks in the Mine - Parnell Area

##### 7.4.1.1 $D_1$ Effects

The principal effects of  $D_1$  is the deformation of an almost ubiquitous bedding-parallel schistosity and a mineral lineation mainly defined by biotite and sillimanite. The only macroscopic closure so far identified is in the Parnell Track Area (Laing, 1977) but Marjoribanks (pers. comm., 1975) has recognised macroscopic domains of upward and downward facing beds which he regards as limb areas of large scale isoclinal, recumbent  $F_1$  folds. The absence of recognisable hinges between these limbs may be attributed to the presence of axial surface thrusts or slides.

##### 7.4.1.2 $D_2$ Effects

$D_2$  effects in the Mine Area have led to the formation of tight to isoclinal  $F_2$  folds which are overturned to the east and which are downward facing on  $S_1$ . The axes of these folds plunge at about  $35^\circ$  to the southwest while the axial surfaces dip at  $70^\circ$  to the northwest. West of the Mine Area there is considerable change in style of  $F_2$  folds. The Stirling Vale synform, another  $F_2$  structure (R. Marjoribanks, pers. comm., 1976) is an upright, more open fold south of the Stephens Creek Retrograde Schist Zone. North of this zone, there is another marked change in the style of  $F_2$  folds: they become very open, almost monoclinial with flat lying axial surfaces refolded by  $F_3$  structures.  $S_2$ , axial planar to these folds, is readily recognisable in hinge areas as a high grade, sillimanite + biotite schistosity,

and may be accompanied by the formation of  $L_2$ . In limbs of isoclinal  $F_2$  folds,  $S_2$  cannot be differentiated from  $S_1$ , and a composite schistosity is then developed.

#### 7.4.1.3 $D_3$ Effects

$F_3$  folds in the Mine - Parnell area are open, northeast trending, upright structures which either plunge to the southwest, parallel to  $L_1$ , or to the northeast.  $S_3$  lies axial planar to  $F_3$  folds and trends northeast with vertical dips. It is generally a low grade schistosity, characterised by rotation of  $S_1$  or  $S_2$  and by incomplete recrystallisation, and is outlined by muscovite, chlorite, some chloritoid, new quartz and biotite (Laing, 1977). Laing has suggested that there is a genetic relationship between  $S_3$  and  $S_R$  within the northeast trending Globe Vauxhall and Western retrograde schist zones.

#### 7.4.1.4 $D_4$ Effects

$D_4$  folds occur in the north mine area (Laing, 1977) but are generally only of minor significance.

#### 7.4.2 Correlation

Possible correlations between the Mt Franks - Mundi Mundi Area and the Mine - Parnell area can be treated in two groups depending on the significance placed on microscopic evidence for  $S_{1N}/S_{1P}$  equivalence in the Mt Franks - Mundi Mundi Area.

If  $S_{1N}$  and  $S_{1P}$  are regarded as equivalent (the preferred interpretation) then two possible correlation schemes can be devised between these two areas:

|         | Mt Franks - Mundi Mundi<br>Area | Mine - Parnell Area |
|---------|---------------------------------|---------------------|
| MODEL 1 | pre- $S_1$                      | not known           |
|         | $S_1$                           | $S_1$               |
|         | $S_2$                           | $S_2$               |
|         | $S_3$                           | $S_3$               |



|         |                    |                |
|---------|--------------------|----------------|
| MODEL 2 | pre-S <sub>1</sub> | S <sub>1</sub> |
|         | S <sub>1</sub>     | S <sub>2</sub> |
|         | S <sub>2</sub>     | not known      |
|         | S <sub>3</sub>     | S <sub>3</sub> |

Alternatively, if S<sub>1N</sub> is regarded as overprinting S<sub>1P</sub> (consistent with macro- but not microscopic data) then a third model can be devised:

|         | Mt Franks - Mundi Mundi Area     | Mine - Parnell Area |
|---------|----------------------------------|---------------------|
| MODEL 3 | pre-S <sub>1P</sub> fabric       | not known           |
|         | S <sub>1P</sub>                  | S <sub>1</sub>      |
|         | S <sub>1N</sub>                  | S <sub>2</sub>      |
|         | S <sub>2</sub> = S <sub>1N</sub> |                     |
|         | S <sub>3</sub>                   | S <sub>3</sub>      |

All three of these models are constrained by a very good correlation between D<sub>3</sub> events in both areas. This correlation is on a basis of orientation, style, grade of metamorphism and relation to a set of retrograde schist zones. Models 1 and 3 both suffer from the absence of a pre-S<sub>1</sub> fabric in rocks between the Mine Area and Parnell Area, and Model 2 suffers from the absence of an S<sub>2</sub> correlative in the Mine - Parnell Area. These models will now be discussed in detail.

#### MODEL 1 Evidence

1) The main feature of this model is the correlation of S<sub>1</sub> in both areas. Although no pre-S<sub>1</sub> schistosity is known as yet from the Mine-Parnell Area, there is some evidence that S<sub>1</sub> in the Mine - Parnell Area overprints early andalusites which can probably be correlated with andalusites in the northwestern part of the Willyama Complex which are interkinematic between the pre-S<sub>1</sub> and the S<sub>1</sub> schistosities. This evidence is provided by:

i) the presence of square shaped sillimanite pseudomorphs in the mine area (Hodgson, 1974, Fig. 16; Laing, 1977),

ii) the presence of relict andalusite in bedding-parallel S<sub>1</sub>

sillimanite schist just east of the Apollyon Valley Retrograde Schist Zone (Section 5.

iii) the presence of square-shaped sillimanite pseudomorphs between the Parnell area and the Apollyon Valley Retrograde Schist Zone (G. Bradley, pers. comm., 1977), and

iv) the presence of andalusite wrapped around by bedding-parallel  $S_1$  in the Parnell Area (B. Stevens, pers. comm., 1976).

The presence of pre- $S_1$  kinked biotites in layers in bedding-parallel sillimanite schists just east of the Apollyon Valley Retrograde Schist Zone suggests an earlier period of biotite growth as well.

Thus it appears that a pre- $S_1$  thermal event can be reasonably established east of the Apollyon Valley Retrograde Schist Zone. Absence of a pre- $S_1$  schistosity (if present) might be explained by the high grade nature of the  $S_1$  schistosity which is dominated by complete and crystallisation and recrystallisation of new minerals (W. Laing, pers. comm., 1976).

2) K feldspar in the Mt Franks - Mundi Mundi Area generally has a shape orientation parallel to  $S_1$ , and contains inclusion trails of biotite cross cut by, or aligned parallel to  $S_1$ . In the Mine Area, Laing (1977) has reported equant to elongate K feldspar in  $S_1$  with inclusion trails of biotite and quartz parallel to  $S_1$ .

3) In the Mine - Parnell area,  $S_1$  is bedding - parallel and is associated with large scale changes in younging so that  $F_2$  and  $F_3$  folds are both upward and downward facing.  $S_1$  in the northwestern part of the Willyama Complex is also bedding-parallel in high grade rocks and  $F_3$  folds in this area are both upward and downward facing.

4)  $D_1$  folds in the Mine - Parnell area are inferred to be isoclinal and recumbent. In the northwestern part of the Willyama Complex there is an inferred change in style of the major  $F_1$  syncline from tight and upright in low grade rocks to isoclinal and overturned in high grade rocks.

5)  $D_2$  folds in the Mine Area are tight and overturned to the west. They

are comparable in style, and broadly in orientation, with  $F_2$  folds in the Shepherds Hut Area.

### Implications

The main implication of this model is that visible, macroscopic  $F_1$  folds in the northwestern part of the Willyama Complex can be correlated with  $F_1$  recumbent folds inferred from macroscopic changes of younging in the Mine - Parnell Area. Thus the change in nature of fold styles from isoclinal, and probably disrupted, to tight, and the change in the nature of  $S_1/S_0$  relations from bedding parallel to non parallel passing up the sedimentary pile is a reflection of the tectonic levels concept discussed before. This model also implies that there was a period of widespread andalusite grade metamorphism in the high grade rocks before the formation of  $S_1$ , and that there was an even earlier period of schistosity formation throughout the area. Relations between the pre- $S_1$  schistosity, interkinematic porphyroblasts and the  $S_1$  schistosity in the Mt Franks - Mundi Mundi area suggest that they might have been part of a complex early event. This model also implies that there is a direct correlation of later age structures across the Willyama Complex. This is supported by the similarity in style of  $F_2$  folds in both areas.

### MODEL 2 Evidence

The lack of a pre- $S_1$  fabric in the Mine - Parnell Area might suggest that the pre- $S_1$  fabric in the Mt Franks - Mundi Mundi Area correlates with  $S_1$  of Laing et al (in press) and Marjoribanks et al (in prep.) and that  $S_1$  correlates with  $S_2$  of these authors.

Evidence for this model is:

- 1) the lack of pre- $S_1$  fabric in the Mine - Parnell Area,
- 2) the layered nature of both  $S_1$  in Mt Franks - Mundi Mundi area and  $S_2$  in Parnell - Mine Area,
- 3) the presence of both  $S_1$  in Mt Franks - Mundi Mundi Area and  $S_2$  in Mine - Parnell area parallel to bedding in isoclinal folds (this evidence

is not compelling, see point 3) above).

#### Evidence Against this Model.

1. the pre- $S_1$  schistosity in the Mt Franks - Mundi Mundi area is not everywhere parallel to bedding whereas  $S_1$  in the Mine - Parnell area is everywhere parallel to bedding
2. the pre- $S_1$  schistosity in the northwestern part of the Willyama Complex is overprinted by andalusite.  $S_1$  in the Mine - Parnell area overprints andalusite
3.  $F_2$  folds in the Mine - Parnell area are upward and downward facing on  $S_1$ . In the Mt Franks - Mundi Mundi area, correlable folds ( $F_1$  of this study) are always upward facing on  $S_1$  and there is no pre- $F_1$  small scale inversion of sedimentary younging directions
4. there would be no correlatives in the Mine - Parnell area to the  $F_2$  folds in the northwestern parts of the Willyama Complex
5.  $F_2$  folds in the Mine - Parnell Area die out as the Apollyon Valley Retrograde Schist Zone is approached from the east (Marjoribanks et al, in prep.)
6.  $S_2$  in the Mine - Parnell Area is not an obvious schistosity and is best seen in  $F_2$  fold hinges; in limb areas it lies parallel to  $S_1$ . In contrast, the correlable schistosity further west ( $S_1$  of this study) is the dominant fabric, and is bedding-parallel over large areas.

#### Implications

This model would imply that the youngest, lowest grade rocks of the Willyama Complex are dominated by a second generation schistosity which is more strongly developed than in the underlying sequence. It also implies that bedding-parallel  $S_1$  in the Mine - Parnell area becomes non parallel to bedding in the younger rocks, where it becomes transposed into  $S_2$ . A further implication of this model is that the Kantappa - Lakes Nob Syncline recognised in the northwestern part of the Willyama Complex is related to the  $F_2$ , not the  $F_1$  event. This also implies that peak of metamorphism

as revealed by the folded isograds in this area is interkinematic between  $F_1$  and  $F_2$  (new nomenclature) although the isograds themselves lie parallel to  $S_0$ . This is in contrast to Laing (1977) who found that peak metamorphism in the Mine area was syn- $S_1$  in age.

#### MODEL 3

This model suffers the same problem as Model 1: there is no early fabric identified in the Mine - Parnell Area. The main advantage of this model is the correlation of the layer parallel schistosity in both areas - but this is also a feature of Model 1. If this model is correct, then the Kantappa - Lakes Nob Syncline is  $F_2$  in age and other implications of Model 2 are valid.

#### 7.4.2.1 Discussion

At the present state of understanding, no absolute correlation can be made between the northwestern part of the Willyama Complex and the Mine - Parnell Area. However, some microstructural criteria can be used to infer a direct equivalence of structural events which is consistent with the macroscopic evidence.








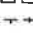





---

Fig. 7.1 Geological relations in the northwestern part of the Willyama Complex.

Drawn by cartographic section, N.S.W. Geological Survey.

---

a amphibolite  
 ch chistolite schist  
 cs calc silicate  
 m mundi mundi facies

-  Low-grade quartz-mica schist, phyllite, carbonaceous schist
-  Medium-grade andalusite schist
-  High-grade sillimanite schist - includes local areas of relict andalusite
-  Granitoid
-  Alluvium
-  Retrograde schist zone
-  Andalusite/sillimanite boundary
-  Axial surface trace, F<sub>1</sub> fold
-  Axial surface trace, F<sub>2</sub> fold
-  Bedding trend and dip direction
-  Sedimentary younging direction
-  Antiform
-  Synform

Data north of area 1 from  
 Anderson (1956); Lang (1959);  
 Leslie and White (1953); Price (1969);  
 Reynolds (1975); Thomson (1976)

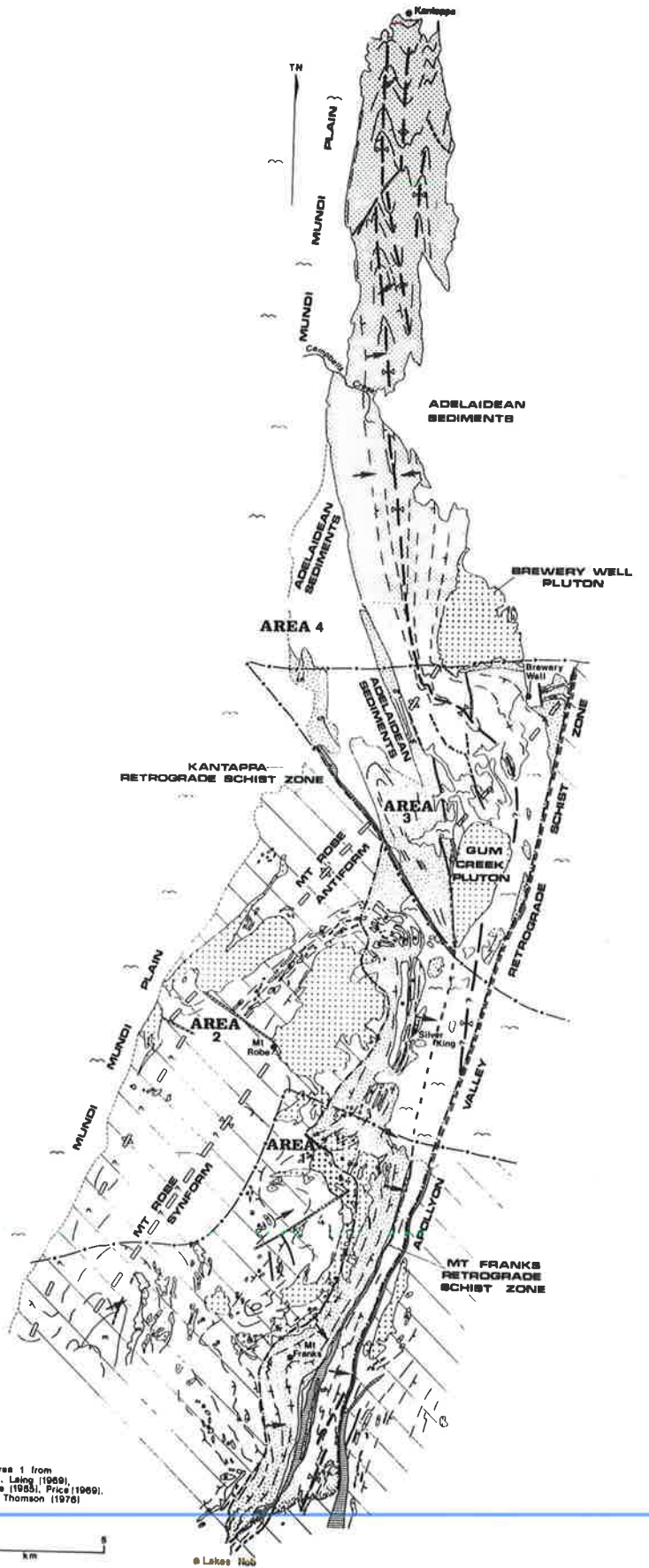


Fig. 7.2      Generalised stratigraphy of the northwestern part of the Willyama Complex. Stratigraphic relations from Area 3 and 4 have been combined with data from Area 1 (the Mt Franks - Mundi Mundi area).

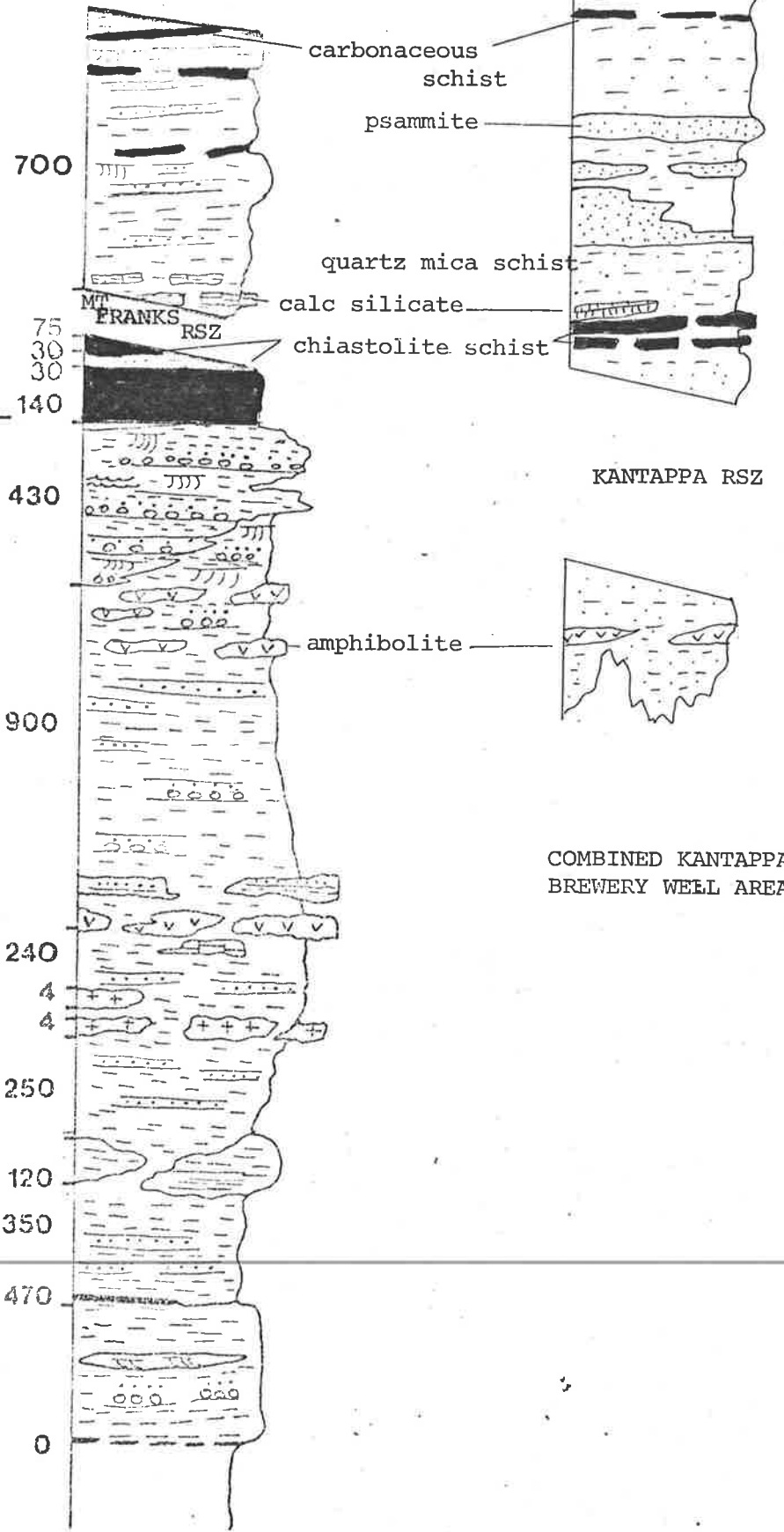
---



MT FRANKS-MUNDI MUNDI  
 AREA. (Middle part includes  
 MT ROBE AREA)

APOLLYON BEDS

ROBE BEDS



1. The oldest event which can be recognised in the area is the deposition of rocks of the Willyama Complex - an event estimated at c. 1800 Ma. by Pidgeon (1967) and Shaw (1968). The basement on which these rocks were deposited has not been identified but Glen et al (1977; Appendix I) have suggested that this basement consisted of continental crust, possibly of Archaean age.
2. The oldest rocks in the Mt Franks - Mundi Mundi area, the Robe Beds, are dominantly non carbonaceous, and consist of interbedded pelites, psammities and psammopelites, with horizons of amphibolites, local quartz-mica gneisses, calc silicate rocks and carbonaceous schists. These rocks are now at andalusite and sillimanite grade; migmatites are also present. The overlying Apollyon Beds, by contrast, consist of mappable units of carbonaceous and non carbonaceous schist. They pass upwards from carbonaceous and non carbonaceous andalusite bearing schists into quartz-mica schists, carbonaceous schists and phyllites, and calc silicate rocks. The Parnell Beds are similar to the Robe Beds but are now separated from it by a major shear zone - the Apollyon Valley Retrograde Schist Zone. In all these rocks, bedding is the dominant layering.
3. The quartz + mica + alumino silicate content of metasediments of the Robe and Parnell Beds together with the lack of lithics and conglomerates suggests an origin as mature clay sands deposited in a "distal" environment. The presence of graded as well as sharp bedding boundaries in the Robe and Parnell Beds is consistent with formation on a shelf-slope or basin. The increasing presence of current activity higher up the sequence may indicate shallowing, and the disappearance of amphibolites near the top of the Robe Beds may suggest cessation of basic volcanism. The Apollyon Beds are more quartz rich and finer grained than the underlying beds. Carbonaceous schists probably formed away from the main source of deposition and calc silicates formed as limy marls (Edwards, 1958).

4. The first recognisable deformational event is the formation of a preferred orientation defined by biotite  $\pm$  sillimanite  $\pm$  sericite. This preferred orientation is preserved only on a microscopic scale and varies in orientation from non parallel to parallel to bedding. No folds have been found with this fabric and its dynamic significance is unknown. If it is a discrete event and is related to a folding episode, these folds must have limb areas larger than those of  $D_1$  folds (see below). Alternatively this fabric may be an early phase of a complex  $M_1, D_1$  event.

5. This pre- $S_1$  mineral preferred orientation is succeeded by a period of static mineral growth (biotite, andalusite, sillimanite, sericite, ?garnet, ?cordierite) and then by the main  $D_1$  fabric forming ( $S_1, L_1$ ) and folding ( $F_1$ ) episode. The complex, progressive nature of this whole  $D_1$  event is indicated by the crystallisation of biotite, sericite, sillimanite and andalusite at various stages in "pre- $S_1$ " to "syn- $S_1$ " time.

6. The low, medium and high grade metamorphic zones distinguished in the field are characterised by the index minerals biotite, biotite + andalusite + garnet and biotite + sillimanite + garnet respectively. Although andalusite probably grew from components rather than from porphyroblast breakdown, the exact reaction cannot be identified. Relations at the andalusite/ sillimanite isograd can be explained in terms of a Carmichael (1969) type model with the reaction taking place via a sericite phase. Andalusite persists as metastable relicts in the sillimanite grade zone and is best preserved in carbonaceous schists where the reaction to sillimanite is hindered by low  $P_{H_2O}$ . These index minerals are all pre- $S_1$  to syn- $S_1$  in age and indicate that the metamorphic zones predate  $D_1$  folding and schistosity formation. However, the rise of geotherms reflected by this metamorphism is not a static event since it is associated with a pre- $S_1$  mineral preferred orientation.

---

The general parallelism of isograds with bedding may either be due to a hypothetical large isoclinal folds or a variation in grade of metamorphism with depth.

7.  $F_1$  folding was not accompanied by mesoscopic transposition of bedding. The main effect of the  $D_1$  event is the formation of the regional Kantappa - Lakes Nob Syncline which can be traced throughout the northwestern part of the Willyama Complex. Previously formed metamorphic zones are folded around this structure so that the core of the fold, occupied by low grade rocks, is underlain by medium and high grade rocks. Most of the hinge and eastern limb of this syncline were possibly disrupted in an early slide which localised formation of the Apollyon Valley Retrograde Schist Zone in  $D_3$  time. The regional syncline thus controls the distribution of low and medium grade rocks in this part of the Willyama Complex. To the north these lower grade rocks disappear under alluvium; to the south they terminate in steep north plunging  $F_1$  folds.

8. The Kantappa - Lakes Nob Syncline was formed with variable plunge and is characterised by a change in fold style from open - tight in low grade rocks in the core to tight - isoclinal in the underlying high grade rocks in the exposed western limb. This is accompanied by a change in  $S_0/S_1$  relations from non parallel to parallel with depth. The Kantappa - Lakes Nob Syncline is also characterised by a curved axial surface, which changes orientation from vertical in the low grade rocks to inclined at depth. As a result, the exposed limb also changes orientation - from right way up to overturned at depth. Although the effect of any hypothetical pre- $F_1$  fold cannot be ruled out, this change in orientation is attributed to  $F_1$  overturning and to late stage  $D_1$  effects which rotated  $S_1$  through the vertical. This rotation may be related to subsequent modification of originally formed vertical  $F_1$  folds, and is associated with the rotation of the extension direction ( $L_1$ ) from subvertical in low grade rocks to inclined in high grade rocks. This was possibly caused by a change in the direction of mass transfer from vertical to inclined or subhorizontal in the underlying, more plastic rocks. This change was also accompanied by an inferred rotation of fold axes into parallelism with  $L_1$  from low grade to high grade rocks.

9. A new schistosity,  $S_1$ , was formed axial planar to  $F_1$  folds and now dominates the area. (Re)crystallisation to muscovite + quartz + biotite grade occurred in low and medium grade rocks, but (re)crystallisation up to sillimanite + K feldspar grade and the formation of migmatites occurred in the high grade rocks.

Where a pre- $S_1$  fabric is mainly defined by white mica (low grades, carbonaceous schists of the medium grades) extensive  $D_1$  recrystallisation has taken place and  $S_1$  occurs as a generally homogeneous schistosity. Where a pre- $S_1$  fabric is dominated by biotite on the other hand,  $S_1$  forms a segregated schistosity with the alternation of M (mica) and QM (quartz + mica) domains. The spacing of these domains reflects the wavelength of  $F_1$  microfolds; M domains define limb areas - areas of high rotational strain, mass transfer, volume decrease and crystallisation - whereas QM domains define hinge areas and have suffered much less intense strain and mineral corrosion.  $S_1$  was probably not formed precisely parallel to the XY plane of the  $D_1$  strain ellipsoid.

10. The  $D_2$ ,  $M_2$  event was of only local significance in this area and resulted in the formation of overturned, tight  $F_2$  folds and the localised development in hinge areas of an  $S_2$  fabric. This is defined by white mica + opaques + biotite + sillimanite and developed by rotation and recrystallisation of earlier  $M_1$  minerals.

11. The  $D_3$  event in this area formed as a result of NW-SE shortening and resulted in the formation of large, open, variably plunging upright  $F_3$  folds with northeast trends. They clearly refold  $D_1$  and  $D_2$  structures and where southwest plunging, lie sub parallel to  $L_1$ . The northwestern part of the Willyama Complex is dominated by two major  $F_3$  folds - which in the area examined are downward facing on  $S_3$  - the Mt Robe Synform and the Mt Robe Antiform. The nature of the  $D_3$  event was controlled to a large extent by  $S_0/S_1$  relations: macroscopic folds predominate where  $S_1$  lies parallel to  $S_0$  whereas small scale crenulation leading to schistosity formation predominates

in areas of non parallelism. Where  $S_0$  after the  $D_1$  event lies parallel to the XY plane of the  $D_3$  event, it remains unfolded. Rather,  $S_1$  (lying at angles to  $S_0$ ) is folded across  $S_0$  and outlines macroscopic folds.  $S_3$  formed during this event as a muscovite + quartz  $\pm$  biotite schistosity axial planar to  $F_3$  folds. It locally contains a mica lineation,  $L_3$ . Four different deformational and schistosity forming processes can be identified in  $S_3$  formation:

- 1) recrystallisation of old minerals,
  - 2) mass transfer mechanisms leading to the shape modification of early formed minerals, to the formation of "stylolites," and when coupled with the mimetic growth of muscovite, to the formation of a segregated  $S_3$ ,
  - 3) the rotation of early minerals by slip or by kinking, and
  - 4) the small scale rotation of muscovite layers in  $S_1$  which, when coupled with mass transfer processes leads to the formation of a rotational fabric  $S_3'$  which itself rotates into  $S_3$ .
- Chloritoid, staurolite and chlorite are also features of this event, and granitoid formation also occurred during this time.

12. During late stages of  $D_3$ , the Mt Franks Retrograde Schist Zone formed as an intense zone of ductile deformation. Together with the Apollyon Valley Retrograde Schist Zone, these zones share a common orientation of mineral lineation and a retrograde schistosity with  $L_3$  and  $S_3$  in the surrounding country rock.

13. The  $D_4$  event formed minor open folds and crenulations which lie parallel to crenulations in the retrograde schistosity of retrograde schist zones.

14. The  $D_1$ - $D_4$  events summarised above are regarded as part of the Olarian Orogeny (see Glen et al, 1977; Appendix I for recent discussion). The  $D_1$  event is broadly comparable to the high grade event around the mine area, dated at c. 1695 Ma. by Shaw (1968). The  $D_2$  event is undated but may be close to the  $D_1$  event in time. The  $D_3$  event is associated with the emplace-

ment of the Mundi Mundi granite - dated at c. 1520 Ma. by Pidgeon (1967). All these events predate the deformation of Adelaidean rocks in the Delamerian Orogeny (c. 500 Ma. - Glen et al, 1977; Appendix I). During this Palaeozoic Orogeny, the Apollyon Valley Retrograde Schist Zone was re-activated and localised folds in the Adelaidean, and Thackaringa - type deposits in the basement. Other retrograde zones were probably (re)activated at this time.

---

## REFERENCES

- ALBEE, A.L., and CHODOS, A.A., 1969. Minor element content of co-existent  $Al_2SiO_5$  polymorphs. *Am. J. Sci.* 267:310-316.
- ALLISON, I. and La TOUR, T.E., 1977. Brittle deformation of hornblende in a mylonite: a direct geometrical analogue of ductile deformation by translation gliding. *Can. J. Earth Sci.*, 14, 1953-1958.
- ALTHAUS, E., 1969. Experimental evidence that the reaction of kyanite to form sillimanite is at least bivariant. *Am. J. Sci.*, 267; 273-277.
- ANDERSON, D.E., 1966. The structural and metamorphic petrology of the Mount Robe district, Broken Hill, N.S.W. Ph.D. thesis, University of Sydney (unpubl.)
- \_\_\_\_\_, 1971. Kink bands and major folds, Broken Hill, Australia. *Geol. Soc. Am. Bull.* 82, 1841-1862.
- ANDREWS, E.C., 1922. The geology of the Broken Hill District. *Mem. Geol. Surv. N.S.W.* 8. 432 pp.
- \_\_\_\_\_, 1923. Supplementary note on the geology of the Broken Hill district in The geology of the Broken Hill District. *Mem. Geol. Surv. N.S.W.*, (8), (supplement) 27 pp.
- B.M.R., 1976. Total magnetic intensity map Broken Hill New South Wales (detailed Survey) preliminary edition.
- BELL, P.M., and NORD, G., 1973. Microscopic and electron diffraction study of fibrolite sillimanite in *Ann. Rpt. Dir. Gphys. Lab. Wash.* in *Carnegie Inst. Year Book*, 444-448.
- BELL, T.H., and ETHERIDGE, M.A., 1976. The deformation and recrystallisation of quartz in a mylonite zone, Central Australia. *Tectonophysics*, 32:235-267.
- BEUTNER, E.C., in press. Slaty Cleavage and related strain in Martinsburg Slate, Delaware Water Gap, New Jersey (pre-print).
- BINNS, R.A., 1963. Some observations on metamorphism at Broken Hill, N.S.W. *Proc. Australas. Inst. Min. Metall.*, 207, 239-259.
- \_\_\_\_\_, 1964. Zones of progressive regional metamorphism in the Willyama Complex, Broken Hill district, New South Wales. *J. Geol. Soc. Aust.*, 11, 283-330.
- \_\_\_\_\_, and MILLER, 1963. Potassium-argon age determinations on some rocks from the Broken Hill region of New South Wales. *Nature* 199 (4890), 274-275.
- BLACK, P.M., 1976. Regional high-pressure metamorphism in New Caledonia. *Abs. 25th Inst. Geol. Congr.*, Sydney, 671.
- BORRADAILE, G.J., 1972. Variably oriented co-planar primary folds. *Geol. Mag.*, 109(2), 89-98.



REFERENCES (cont'd)

- BRIDGES, M.B., and ETHERIDGE, M.A., 1974. A Computer program to contour orientation density (Uni. of Adelaide limited circulation).
- BROWNE, W.R., 1922. Report on the Petrology of the Broken Hill Region, excluding the Great Lode and its Immediate Vicinity in The Geology of the Broken Hill District, Mem. Geol. Surv. N.S.W., 8, 295-353.
- CAMERON, W.E. and ASHWORTH, J.R., 1972. Fibrolite and its relationship to sillimanite. Nature Phys. Sci., 235, 134-136.
- CARMICHAEL, D.M., 1969. On the mechanisms of prograde metamorphic reactions in quartz-bearing pelitic rocks. Contr. Miner. Petr. 20, 244-267
- CHENHALL, B.E., 1973. Some aspects of prograde and retrograde metamorphism at Broken Hill. Ph.D. thesis, Univ. of Sydney (unpubl.)
- CHINNER, G.A., 1961. On the Origin of sillimanite in Glen Cova. J. Petrol., 2, 312-323.
- \_\_\_\_\_, 1966. The significance of the aluminium silicates in metamorphism. Earth.-Sci. Rev., 2, 111-126.
- \_\_\_\_\_, 1973. The selective replacement of the aluminium silicates by white mica: a comment. Contr. Miner. Petr., 41, 83-87.
- \_\_\_\_\_, SMITH, J.V., and KNOWLES, C.R., 1969. Transition metal contents of  $Al_2SiO_5$  polymorphs. Am. J. Sci., 267A, 96-113.
- COBBOLD, P.R., COSGROVE, J.W., and SUMMERS, J.M., 1971. Development of internal structures in deformed anisotropic rocks. Tectonophysics, 12, 23-53.
- COOPER, P.F., 1969. The geology of Alberta Creek, Barrier Ranges, N.S.W. B.Sc.(Hons.) thesis, Univ. of N.S.W. (unpubl.)
- \_\_\_\_\_, 1975. Explanatory Notes on the Broken Hill 1:250,000 Geological sheet SH54-15. 56 pp. New South Wales Geological Survey, Sydney.
- COSGROVE, J.W., 1976. The formation of crenulation cleavage. J. Geol. Soc. Lond., 132, 155-178.
- de SITTER, L.U., 1960. Conclusions and conjectures on successive tectonic phases. Geologie Mijnb., 39, 195-197.
- \_\_\_\_\_, and ZWART, H.J., 1960. Tectonic development in supra- and infrastructures of a mountain chain. Rep. 21st Int. Geol. Congr., Copenhagen 18, 248-256.
- D'ARCY, W.F., 1977. Structures and metamorphism of the northern tip of the Willyama Complex, Broken Hill, N.S.W. abs 2nd Aust. Geol. Conv., 53.
- DEER, W.A., HOWIE, R.A., and ZUSSMAN, J., 1966. An introduction to the rock forming minerals. Longmans, London, S2P pp.

REFERENCES (cont'd)

- DIETRICH, J.H., 1969. Stress history of folding. *Am. J. Sci.*, 267, 155-165.
- DUNN, P.R., PLUMB, K.A., and ROBERTS, H.G., 1966. A proposal for a time - stratigraphic subdivision of the Australian Precambrian. *J. Geol. Soc. Aust.*, 13, 593-608.
- DUNNET, D., 1969. A technique of finite strain analysis using elliptical particles. *Tectonophysics*, 7, 117-136.
- DURNEY, D.W., 1972. Solution-transfer, an important geological deformation mechanism. *Nature*, 235, 315-317.
- EDWARDS, A.B., 1958. Amphibolites from the Broken Hill district, *J. Geol. Soc. Aust.*, 5, 1-32.
- ELLIOTT, D., 1973. Diffusion flow laws in metamorphic rocks. *Geol. Soc. Amer. Bull.*, 84, 2645-2664.
- ETHERIDGE, M.A., 1971. Experimental investigations of the mechanisms of mica preferred orientation in foliated rocks. Ph.D. thesis, A.N.U., Canberra (unpubl.).
- \_\_\_\_\_, and HOBBS, B.E., 1974. Chemical and deformational controls on the recrystallization of mica. *Contr. Miner. Petr.*, 43, 111-124.
- \_\_\_\_\_, HOBBS, B.E., and PATERSON, M.S., 1973. Experimental deformation of single crystals of biotite. *Contr. Miner. Petr.*, 38, 21-36.
- \_\_\_\_\_, PATERSON, M.S. and HOBBS, B.E., 1974. Experimentally produced preferred orientation in synthetic mica aggregates. *Contr. Miner. Petr.*, 44, 275-294.
- EUGSTER, H.P., 1970. Thermal and ionic equilibria among muscovite, K-feldspar and aluminosilicate assemblage. *Fortschr. Miner.* 47(1):106-123.
- \_\_\_\_\_, and SKIPPEN, 1967. Igneous and metamorphic reactions involving gas equilibria. *in* Albeson, P.H. (ed) *Researches in Geochemistry*. J. Wiley and Sons, New York, vol. 2, 492-520.
- EVANS, B.W., 1965. Application of a reaction-rate method to the breakdown equilibria of muscovite and muscovite plus quartz. *Am. J. Sci.*, 263, 647-667.
- EVENDEN, J.F., and RICHARDS, J.R., 1961. Potassium-argon ages at Broken Hill, Australia. *Nature*, 192 (4801), 446.
- FLEMING, P.D., 1973. Mg-Fe distribution between co-existing garnet and biotite, and the status of fibrolite in the andalusite-staurolite zone of the Mt Lofty Ranges, South Australia. *Geol. Mag.*, 109, 477-482.
- FLETCHER, R.C., 1977. Quantitative theory for metamorphic differentiation in development of crenulation cleavage. *Geology*, 5, 185-187.

REFERENCES (cont'd)

- FLINN, D., 1965. On the symmetry principle and the deformation ellipsoid. Geol. Mag., 102(1), 36-45.
- FRANCIS, G.H., 1956. Facies boundaries in pelites at middle grades of regional metamorphism. Geol. Mag., 93, 353-368.
- FRENCH, B.M., 1966. Some geological implications of equilibrium between graphite and a C-H-O gas phase at high temperature and pressure. Rev. Geophys., 4, 223-254.
- GLEN, R.A., 1978. Large-scale early folding and tectonic levels in the northwestern part of the Willyama Complex, New South Wales. New South Wales Geological Survey - Quarterly Notes, 31, in press.
- \_\_\_\_\_, and LAING, W.P., 1975. The significance of sedimentary structures in the Willyama Complex, New South Wales. Proc. Australas. Inst. Min. Metall., 256, 15-20.
- \_\_\_\_\_, LAING, W.P., PARKER, A.J., and RUTLAND, R.W.R., 1977. Tectonic relationships between the Proterozoic Gawler and Willyama Orogenic Domains, Australia. J. Geol. Soc. Aust., 24(3), 125-150.
- GEOLOGICAL SUB-COMMITTEE, 1910. Geology, Broken Hill Lode. A.I.M.E., 161-236.
- GRAY, D., 1976. A model for cleavage development in crenulated low to medium grade metamorphics. Abs. 25th I.G.C., Sydney, 122.
- GRAY, D.R., 1977. Differentiation associated with discrete crenulation cleavages. Lithos 10, 89-101.
- GREEN, J.C., 1963. High-level metamorphism of pelitic rocks in northern New Hampshire; Amer. Min., 48, 991-1023.
- GRESENS, R.L., 1967. Tectonic hydrothermal pegmatites: II an example. Contr. Miner. Petr., 16: 1-28.
- GUSTAFSON, J.K., BURRELL, H.C., and GARRETTY, M.D., 1950. Geology of the Broken Hill ore Deposit, N.S.W., Australia. Geol. Soc. Amer. Bull., 61, 1369-1438.
- HALLER, J., 1971. Geology of the east Greenland Caledonides. Wiley-Interscience, New York, 413 pp.
- HARKER, A., 1939. Metamorphism. Methuen and Co., London, 362 pp. (second edition).
- HOBBS, B.E., 1966a. The structural environment of the northern part of the Broken Hill orebody. J. Geol. Soc. Austr., 13, 315-338.
- \_\_\_\_\_, 1966b. Microfabric of tectonites from the Wyangala Dam area, New South Wales, Australia. Geol. Soc. Am. Bull., 77, 685-706.
- \_\_\_\_\_, 1972. Deformation of non-Newtonian materials in Heard, H.C., et al. (eds) Flow and Fracture of Rocks. Am. Gphys. Union, 243-258.

REFERENCES (cont'd)

- \_\_\_\_\_, MEANS, W.D., and WILLIAMS, P.F., 1976. An outline of Structural Geology. John Wiley and Sons, New York. 571 pp.
- \_\_\_\_\_, RANSOM, D.M., VERNON, R.H., and WILLIAMS, P.F., 1968. The Broken Hill ore body, Australia. A review of recent work. Mineral Deposita, 3, 293-316.
- \_\_\_\_\_, and VERNON, R.H., 1968. The structural and metamorphic history of the area around the northern half of the Broken Hill Lode. Eight Comm. Min. Metall. Congr., 1965 Vol.6: Proceedings-General, 1419-1428.
- HODGSON, C.J., 1974. The geology and geological development of the Broken Hill lode in the New Broken Hill Consolidated Mine, Australia. Part I: Structural geology. J. Geol. Soc. Aust., 21(2), 413-430.
- HOLDAWAY, M.J., 1971. Stability of andalusite and the aluminium silicate phase diagram. Am. J. Sci., 271, 97-131.
- IWAMATSU, A., 1975. Folding styles and their tectonic levels in the Kitakami and Abukuma Mountainous Lands, northeast Japan. Jnl. Fac. Sci. Tokyo, 11, 19(2), 95-131.
- JAUQUET, J.B., 1894. Geology of the Broken Hill Lode and Barrier Ranges mineral field, New South Wales. Mem. Geol. Surv. N.S.W., 5, 149 pp.
- JOESTEN, R., 1974. Local equilibria and metasomatic growth of zoned calc-silicate nodules from a contact aureole, Christmas Mountain, Big Bend Region Texas. - Am. J. Sci. 274:P76-901.
- JOPLIN, G.A., 1968. A petrography of Australian metamorphic rocks. Angus and Roberson, Sydney, 262pp.
- KANSEWICH, E.R., 1962. Approximate age of tectonic activity using anomalous lead isotopes. Geophys. J.R. Astron. Soc., 7, 158-168.
- KATZ, M.B., 1976a. Broken Hill - a precambrian hot spot? Precambrian Research 3, 91-106.
- \_\_\_\_\_, 1976b. Lineament tectonics of the Willyama Block and its relationship to the Adelaide Aulacogene. J. Geol. Soc. Aust., 23, 275-285.
- KERRICK, D.M., 1968. Experiments on the upper stability limit of pyrophyllite at 1.8 Kb and 3.9 Kb water pressure. Am. J. Sci., 266: 204-214.
- \_\_\_\_\_, 1972. Experimental determination of muscovite and quartz stability with  $P_{H_2O} < P_{Total}$ . Am. J. Sci., 272: 946-958.

REFERENCES (cont'd)

- KING, H.F., and THOMSON, B.P., 1953. The geology of the Broken Hill District in Edwards, A.B., (ed) Geology of Australian Ore Deposits, 1st Ed., 5th Empire-Min. Metall. Congr., Melb., 533-577.
- KWAK, T.A.P., 1974. Natural staurolite breakdown reactions at moderate to high pressures. Contrib. Mineral. Petrol., 44, 57-80.
- LAING, W.P., 1969. The geology of the Brewery Well area, northern Barrier Ranges, western New South Wales, B.Sc.(Hons.) thesis, University of Sydney (unpubl.).
- \_\_\_\_\_, 1977. Structural and Metamorphic Geology of a critical area adjacent to the Broken Hill Orebody, Willyama Complex, Australia. Ph.D. Thesis, Univ. of Adel., (unpubl.).
- \_\_\_\_\_, MARJORIBANKS, R.W., and RUTLAND, R.W.R., in press. Structural evidence relating to the genesis of the Broken Hill orebodies. Geol. Soc. Am. Bull.
- LESLIE, R.B., and WHITE, A.J.R., 1955. The "Grand" Unconformity between the Archaean (Willyama Complex) and Proterozoic (Torowangee Series) north of Broken Hill, New South Wales, Trans. R. Soc. S. Aust., 78, 121-133.
- LEWIS, B.R., FORWARD, P.S., and ROBERTS, J.B., 1965. Geology of the Broken Hill Lode reinterpreted. in Geology of Australian Ore Deposits (ed J. McAndrew). Eighth Comm. Min. Metall. Congr., 319-332.
- LUNDGREN, L.W., Jr., Muscovite reactions and partial melting in southeastern Connecticut. J. Petrol., 7(3): 421-453.
- MARLOW, P.C., and ETHERIDGE, M.A., 1977. Development of a layered crenulation cleavage in mica schists of the Kanmantoo Group near Macclesfield, South Australia. Geol. Soc. Am. Bull., 88, 873-882.
- MARSH, C.W., 1890, Geological notes on the Barrier Ranges silver field Proc. R. Soc. N.S.W., 177-195.
- MARJORIBANKS, R.W., 1976. The relation between microfabric and strain in a progressively deformed quartzite sequence from Central Australia, Tectonophysics; 32:269-293.
- \_\_\_\_\_, GLEN, R.A., LAING, W.P., and RUTLAND, R.W.R., (in press) Structure of the Broken Hill Province, N.S.W., Australia. Mem. Centre for Precambrian Research, Univ. of Adel.
- MAWSON, D., 1907. On the Lower Cambrian age of the Barrier Range (New South Wales), previously regarded as Silurian (?). Abstr. 11th Congr. Aust. N.Z. Ass. Advmt. Sci., Adel. 11, 456.
- \_\_\_\_\_, 1912. Geological investigations in the Broken Hill Area. Trans. R. Soc. S. Aust., 2, 211-319.

REFERENCES (cont'd)

- MEANS, W.D. and PATERSON, M.S., 1966. Experiments on preferred orientation of platy minerals. *Contr. Miner. Petr.*, 13, 108-133.
- \_\_\_\_\_ and WILLIAMS, P.F., 1973. Crenulation cleavage and faulting in an artificial salt-mica schist. *J. Geol.* 80, 569-591.
- MEARES, R.M.D., 1969. The geology of the Bijerkerno Area, Barrier Ranges, New South Wales. B.Sc.(Hons.) thesis, Univ. of N.W.S. (unpubl.)
- MIYASHIRO, A., 1964. Oxidation and reduction in the Earth's Crust with special reference to the role of graphite. *Geochim. Cosmochim. Acta*, 28, 717-729.
- MISAR, Z., 1968. Some occurrences of chloritoid-bearing rocks and their significance in the Broken Hill District, N.S.W. Australia. *Krystalinikum* 8, 109-136.
- O'DRISCOLL, E.S.T., 1968. Notes on the structure of the Broken Hill lode and its tectonic setting, in Radmanovich, M., and Woodcock, J.T., (eds.) Broken Hill Mines - 1968. Monograph 3, Aust. Inst. Min. Metall., 87-102.
- OELE, J.A., 1966. The structural history of the Vall Ferrera Area, the transition zone between the Aston Massif and the Galat - Pallaresa Anticlinorium (Central Pyrenees, France, Spain). *Leidse. Geol. Medd.* 38: 129-164.
- PATERSON, M.S., and WEISS, L.E., 1966. Experimental deformation and folding in phyllite. *Geol. Soc. Am. Bull.*, 72, 841-PP2.
- PETTIJOHN, F.I., 1957. Sedimentary rocks. Harper and Row. New York, 718 pp.
- PHILLIPS, E.R., RANSOM, D.M., and VERNON, R.H., 1972. Myrmekite and muscovite developed by retrograde metamorphism at Broken Hill, New South Wales. *Miner. Mag.* 38: 570-578.
- PHILLIPS, N., 1975. Metamorphism of the Lode horizon in Hobbs, et al., Report to Mine Managers Association.
- \_\_\_\_\_, 1977. Low-intermediate pressure metamorphism at Broken Hill, Abs. 2nd Aust. Geol. Convention, Geol. Soc. Aust., 56-57.
- PIDGEON, R.T., 1967. A rubidium-strontium geochronological study of the Willyama Complex, Broken Hill, Australia. *J. Petrol.*, 8, 283-324.
- PITCHER, W.S., 1965. The aluminium silicate polymorphs. in Pitcher, W.S. and Flinn, G.W. (eds.) Controls of metamorphism. Oliver and Boyd, Edinburgh.
- \_\_\_\_\_, and READ, H.H., 1963. Contact metamorphism in relation to manner of emplacement of the granites of Donegal, Ireland. *J. Geol.*, 71, 261-296.

REFERENCES (cont'd)

- PRICE, G.P., 1969. The geology of the Cartwright's Creek Area, northern Barrier Ranges. N.S.W., B.Sc.(Hons.) thesis, Univ. of Sydney (unpubl).
- RAMSAY, D.M., and STURT, B.A., 1973. An analysis of noncylindrical and incongruous fold pattern from the Eo-Cambrian rocks of Sørøya, Northern Norway. *Tectonophysics*, 18, 81-121.
- RAMSAY, J.G., 1967. Folding and fracturing of rocks. McGraw-Hill, New York, 568 pp.
- \_\_\_\_\_, and GRAHAM, R.H., 1970. Strain variations in shear belts. *Can. J. Earth Sci.*, 7, 786-813.
- \_\_\_\_\_, 1974. Development of Chevron Folds. *Geol. Soc. Am. Bull.*, 85, 1741-1754.
- RANSOM, D.M., 1968. The relationship of lode shape to wall-rock structure in the southern half of the Broken Hill ore body. *J. Geol. Soc. Aust.*, 15, 57-64.
- RAST, N., 1965. Nucleation and growth of metamorphic minerals, in Pitcher, W.S. and Flinn, G.W., (eds) Controls on metamorphism, J. Wiley and Sons., New York, 73-102.
- REYNOLDS, G.D., 1975. The geology of the Mount Robe Area, Broken Hill, N.S.W., B.Sc.(Hons.) thesis, Monash Univ. (unpubl.).
- RICHARDS, J.R. and PIDGEON, R.T., 1963. Some age measurements on micas from Broken Hill. *J. Geol. Soc. Aust.*, 10, 243-260.
- RICHARDSON, S.W., 1968. Staurolite stability in a part of the system Fe-Al-Si-O-H. *J. Petrol.* 9(3), 467-488.
- \_\_\_\_\_, GILBERT, M.C., and BELL, P.M., 1969. Experimental determination of kyanite-andalusite and andalusite-sillimanite equilibria; the aluminium silicate triple point. *Am. J. Sci.*, 267, 259-272.
- RICKARD, M.J., 1961. A note on cleavages in crenulated rocks. *Geol. Mag.*, 98(4), 324-332.
- ROBERTS, B.A., 1969. The geology of the Campbells Creek area, northern Barrier Ranges, N.S.W. B.Sc.(Hons.) thesis, Univ. of New South Wales (unpubl).
- ROBERTS, J.L., 1964. The structure of the Dalradian rocks in the SW Highlands of Scotland. *J. Geol. Soc. London*, 130, 93-124.
- \_\_\_\_\_, and SANDERSON, D.J., 1974. Oblique fold axes in the Dalradian rocks of the Southwest Highlands. *Scotl. J. Geol.*, 9(4), 281-296.
- ROBINSON, D., 1971. The inhibiting effect of organic carbon on contact metamorphic recrystallisation of limestone. *Contr. Miner. Petr.*, 32: 245-250.
- RUSSEL, R.D., and FARQUHAR, R.M., 1960. Dating galenas by means of their

REFERENCES (cont'd)

- isotopic constitutions - II. *Geochim. Cosmochim. Acta*, 19, 41-52.
- \_\_\_\_\_, ULRICH, T.J., and KÖLLAR, F., 1961. Anomalous leads from Broken Hill, Australia. *J. Geophys. Research.*, 66, 1495-1498.
- RUTLAND, R.W.R., 1971. Regional structural analysis of the Willyama Block. Report to Broken Hill Mine Managers Association (unpubl.)
- \_\_\_\_\_, 1973a. A note on major structures in the Willyama Complex, Broken Hill, N.S.W., *Trans. R. Soc. S. Aust.*, 97, 77-90.
- \_\_\_\_\_, 1973b. Tectonic Evolution of the Continental Crust of Australia. *in* Tarling, D.H., and Runcorn S.K. (eds). *Continental Drift, Sea Floor Spreading and Plate Tectonics: implications to the earth sciences*, London, Academic Press, 1003-1025.
- \_\_\_\_\_, 1976. Orogenic evolution of Australia. *Earth-Sci. Rev.*, 12, 161-196.
- \_\_\_\_\_, and ETHERIDGE, M.A., 1975. Two high grade schistositities at Broken Hill and their relation to Major and Minor Structures. *J. geol. Soc. Aust.*, 22(3), 259-274.
- SCHREYER, W., and YODER, H.S., 1961. Petrographic guides to the experimental petrology of cordierite. *Carnegie Inst. Wash. Yearbook* 60, 147-152.
- SEIFERT, F., and SCHREYER, W., 1970. Lower range temperature stability limit of Mg cordierite in the range 1-7Kb water pressure: a redetermination. *Contr. Mineral, Petrol.* 27, 225-238.
- SHAW, S.E., 1968, Rb-Sr isotopic studies of the mine sequence rocks at Broken Hill. *in* Broken Hill mines - 1968. Radmanovich M. and Woodcock, J.T. (eds). *Monograph Series*, 3, Australas. Inst. Min. Metall., 185-198.
- SHROCK, R.R., 1948. *Sequences in layered rocks*. McGraw-Hill. New York 507 pp.
- SORBY, H.C., 1853. On the origin of slaty cleavage. *Edinb. New. Phil. J.*, 55, 137-148.
- \_\_\_\_\_, 1879. Structure and origin of limestone. *Q.J. Geol. Soc. Lond.*, 35, 39-95.
- SPRY, A., 1969. *Metamorphic Textures*. Pergamon Press, Oxford, 350 pp.
- SPLATT, I.A., 1975. *Geology of the Silver King Area, Broken Hill, N.S.W.*, B.Sc.(Hons.) thesis, Monash Univ. (unpubl.).
- 
- STANTON, R.L., 1976. Petrochemical studies of the ore environment at Broken Hill, N.S.W. Part 4: environmental synthesis. *Trans. Inst. Min. Metall.*, 85(B), 221-233.



REFERENCES (cont'd)

- STILLWELL, F.L., 1922. The rocks in the immediate neighbourhood of the Broken Hill Lode and their bearing on its origin in The Geology of the Broken Hill District, Mem. Geol. Surv. N.S.W. 8, 403-416.
- SUESS, E., 1970. Interaction of organic compounds with carbonates. I: Association phenomena and geochemical implications. Geochim. cosmochim. Acta 34: 157-168.
- TECTONIC MAP OF AUSTRALIA, 1960. Bureau of Mineral Resources, Canberra.
- THOMSON, B.P., 1954. Tectonics and Archaen sedimentation of the Barrier Ranges, N.S.W. M.Sc thesis, Univ. of Adelaide (unpubl.).
- \_\_\_\_\_, 1959. Discussion on "Sedimentary structures in the metamorphic rocks and orebodies of Broken Hill" by M.A. Condon. Proc. Australas. Inst. Min. Metall., 191, 201-211.
- \_\_\_\_\_, 1969. Proterozoic Rocks. A. The Barrier Ranges in Packham, G.H. (ed) Geology of New South Wales. J. Geol. Soc. Aust. 16 (1), 55-64.
- \_\_\_\_\_, 1970. A review of the Precambrian and lower Proterozoic tectonics of South Australia. Trans. R. Soc. S. Aust., 94, 193-221.
- \_\_\_\_\_, 1976. Tectonics and regional geology of the Williama, Mount Painter and Denison Inlier Areas in Knight, C.L., (ed) Economic Geology of Australia and Papua New Guinea, 469-476.
- THOMSON, J., 1976. Report on Geological Mapping in the Northwestern portion of the Willyama Complex, Broken Hill. Geological Survey of N.S.W. (unpubl.) GS 76/094.
- TILLEY, C.E., 1924. Contact metamorphism in the Comrie area of the Perthshire Highlands, Q.J. Geol. Soc. Lond., 80, 22-71.
- \_\_\_\_\_, 1925. Petrographical notes on some chloritoid rocks. Geol. Mag., 62, 309-318.
- TOBISCH, O.T., and GLOVER, L., 1971. Nappe formation in part of the Southern Appalachian Piedmont. Geol. Soc. Amer. Bull., 82, 2209-2230.
- TOZER, C.F., 1955. The mode of occurrence of sillimanite in the Glen district, C. Donegal. Geol. Mag., 92, 310-320.
- TUCKWELL, K.D., 1968. The geology of the Western Barrier Range, north of Poolamacca Station, Broken Hill, B.Sc.(Hons.) thesis, Univ. of N.S.W. (unpubl.).
- \_\_\_\_\_, 1975. Structural and metamorphic studies in the Euriovie Block, Broken Hill. Ph.D. thesis, W.L. and L.B. Robinson College, (unpubl.).
- TULLIS, T.E., 1976. Experiments on the origin of slaty cleavage and schistosity. Geol. Soc. Am. Bull., 87, 745-753.

REFERENCES (cont'd)

- TURNER, F.J., 1968. Metamorphic Petrology. Mineralogical and Field Aspects. McGraw-Hill, New York.
- VERNON, R.H., 1968. Microstructures of high-grade metamorphic rocks at Broken Hill, Australia. J. Petrol., 9, 1-22.
- \_\_\_\_\_, 1969. The Willyama Complex, Broken Hill Area. in Packham, G.H. (ed) Geology of New South Wales. J. Geol. Soc. Aust., 16, 20-55.
- \_\_\_\_\_, 1975. Microstructural interpretation of some fibrolitic sillimanite aggregate. Miner. Mag., 40, 303-6.
- \_\_\_\_\_, 1976. Metamorphic Processes - reactions and microstructure development. George Allen and Unwin, London, 247 pp.
- \_\_\_\_\_, 1977. Relationships between microstructures and metamorphic assemblages. Tectonophysics, 39, 439-452.
- \_\_\_\_\_, and RANSOM, D.M., 1971. Retrograde schists of the amphibolite facies at Broken Hill, N.S.W. J. Geol. Soc. Aust., 18, 267-277.
- WATSON, J., 1948. Late sillimanite in the migmatites of Sutherland. Geol. Mag. 85, 149-162.
- WEGMANN, C.E., 1935. Zur Deutung der Migmatite. Geol. Rundschau, 26, 305-350.
- WEISS, L.E., 1968. Flexural slip folding of foliated model materials in Baer, A.J. and Norris, N.K., (eds.) Proc. of Confce on Research in Tectonics. Geol. Sur. Can. Pap. 68, 52, 293-333.
- WILKINSON, C.S., 1884. Report on the silver bearing lodes of the Barrier Ranges in the Albert district, N.S.W. N.S.W. Legislative Assembly Paper, 1076-A, 1883-4 Folio, Sydney.
- WILLIAMS, P.F., 1967. Structural analysis of the Little Broken Hill area, New South Wales. J. Geol. Soc. Aust., 14, 317-331.
- \_\_\_\_\_, 1970. A criticism of the use of style in the study of deformed rocks. Geol. Soc. Am. Bull., 81, 3283-3296.
- \_\_\_\_\_, 1972. Development of metamorphic layering and cleavage in low-grade metamorphic rocks at Bermagui, Australia. Am. J. Sci., 272, 1-47.
- \_\_\_\_\_, 1975. Relationships between axial-plane foliations and strain. Tectonophysics, 30, 181-196.
- \_\_\_\_\_, MEANS, W.D., and HOBBS, B.E., 1977. Development of axial plane slaty cleavage and schistosity in experimental and natural materials. Tectonophysics, 42, 139-158.
- WILLIS, I., 1977. The geology of the Purnamoota - Yanco Glen - Brewery Creek Area, Broken Hill. Rep. Geol. Surv. N.S.W., GS1976/408 (unpubl.).

REFERENCES (cont'd)

- WILSON, C.J.L., 1973. The prograde microfabric in a deformed quartzite sequence, Mount Isa, Australia. *Tectonophysics*, 19, 39-81.
- WINKLER, H.G.F., 1967. Petrogenesis of metamorphic rocks. Springer-Verlag, Berlin, Revised 2nd Ed., 237 pp.
- \_\_\_\_\_, 1974. Petrogenesis of Metamorphic Rocks. Springer-Verlag Berlin. 3rd Ed., 320 pp.
- WOOD, D.S., 1974. Current views of the development of slaty cleavage. *Ann. Rev. Earth. Planetary Sci.*, 2, 369-401.
- WOODLAND, B.G., 1963. A petrographic study of thermally metamorphosed pelitic rocks in the Burke Area, north-eastern Vermont. *Am. J. Sci.*, 261: 354-375.
- ZEN, E-an. 1969. The stability relations of the polymorphs of aluminium silicate, a survey and some comments. *Am. J. Sci.*, 267: 297-309.
- ZWART, H.J., 1960. Relationships between folding and metamorphism in the Central Pyrenees. *Geol. Mijnb.* 39e, 163-180.
-

Glen, R.A., Laing, W.P., Parker, A.J. and Rutland, R.W.R. (1977) Tectonic relationships between the Proterozoic Gawler and Willyama Orogenic Domains, Australia.  
*Journal of the Geological Society of Australia*, v. 24 (3), pp. 125-150, June 1977.

NOTE: This publication is included in the print copy of the thesis held in the University of Adelaide Library.

Glen, R.A. and Laing, W.P.(1975) The significance of sedimentary structures in the Willyama Complex, New South Wales.  
*Australasian Institute of Mining and Metallurgy Proceedings no. 256, pp. 15-20, December 1975.*

NOTE: This publication is included in the print copy of the thesis held in the University of Adelaide Library.

### APPENDIX III

#### GEOMETRICAL ANALYSIS OF THE MT FRANKS - MUNDI MUNDI AREA IN TERMS OF SUB AREAS.

The Mt Franks - Mundi Mundi area has been divided into 25 subareas, the boundaries of which are shown in Map 2. Subarea boundaries were determined in the first instance by the two major northeast trending retrograde schist zones, the Mt Franks Retrograde Schist Zone and the Apollyon Valley Retrograde Schist Zone. In the central block between these two zones, further subdivision was made on the basis of  $F_1$  geometry. Thus, subareas 8a, 8b and 9 define parasitic  $F_1$  folds, whereas subareas 1 and 2 define areas of planar bedding. In the western block, further subdivision of subarea boundaries was made along the boundary between domains  $S_{1N}$  (subareas 3, 4, 5, 6, 7, 12, 18) and  $S_{1P}$  (subareas 10, 11, 13, 14, 15, 16, 17, 19, 20, 21, 22, 23) development. Further subdivision in the  $S_{1N}$  domain was then determined by  $F_1$  fold geometry - limb and hinge areas of  $F_1$  folds, whereas further subdivision in the  $S_{1P}$  domain was determined by variations in  $F_2$  and  $F_3$  fold geometry.

Geometrical features in each subarea will now be discussed. In all cases equal area plots were prepared using the computer program of Bridges and Etheridge (1974). All projections are lower hemisphere.

S<sub>1N</sub> DOMAIN

FABRIC ELEMENTS IN AREAS OF PLANAR BEDDING

Subarea 1 (Fig. 2A). Poles to  $S_0$  plot as a maximum, corresponding to an orientation of  $029^\circ 70^\circ$  SE.

132 points, contours at 0.70, 1.40, 2.80, 5.61, 11.21; maximum 12.12%.

Subarea 2 (Fig. 2B). Poles to  $S_0$  plot as maximum corresponding to an orientation of  $034^\circ 72^\circ$  SE.

56 points, contours at 0.98, 1.96, 3.92, 7.85, 15.69; maximum 16.96%.

Subarea 3a (Fig. 2C). Poles to  $S_0$  plot as maximum corresponding approximately to an orientation of  $029^\circ 74^\circ$  SE.

11 points.

Subarea 3b (Fig. 2D). Similar to subarea 3a.

12 points.

Subarea 3c (Fig. 2E). Poles to  $S_0$  plot as a maximum corresponding to an orientation of  $030^\circ 80^\circ$  SE.

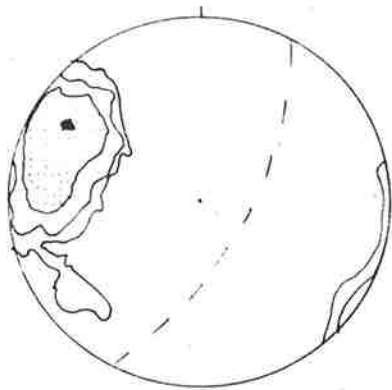
28 points, contours at 1.65, 3.30, 6.61, 13.21, 26.43; maximum 28.57%.

Subarea 3d (Fig. 2F), Poles to  $S_0$  plot as maximum corresponding to an orientation of about  $035^\circ 80^\circ$  SE.

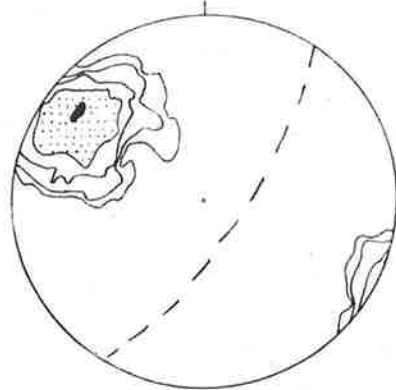
31 points, contours at 1.59, 3.17, 6.34, 12.68, 25.36; maximum 27.42%.

Subareas 3e (Fig. 2G) and 3f (Fig. 2H). Poles to  $S_0$  indicate similar orientations - strike about  $030^\circ$ , dip about  $80^\circ$  SE.

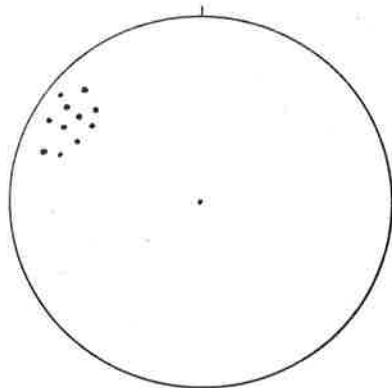
17 and 10 points respectively.



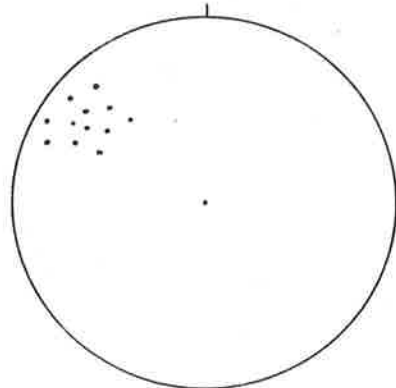
**A**



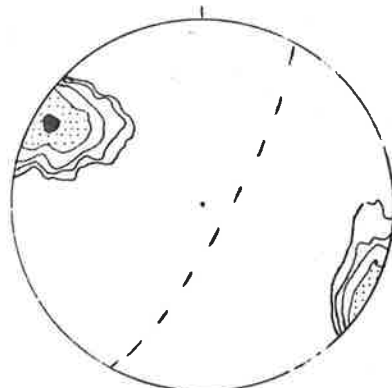
**B**



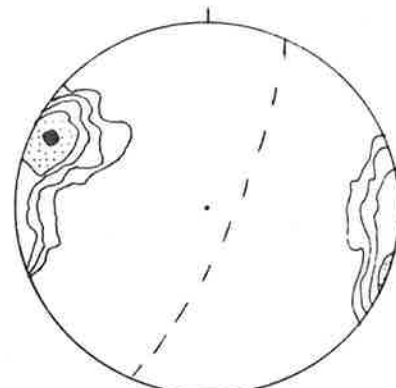
**C**



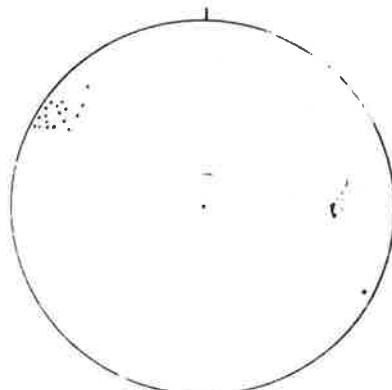
**D**



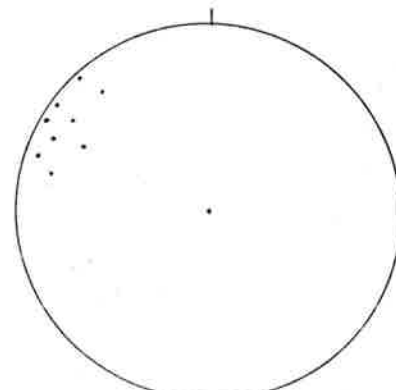
**E**



**F**



**G**



**H**



Subarea 7a (Fig. 3A). Poles to  $S_0$  indicate a point maximum (with a slight spread caused by  $F_1$ ,  $F_3$  or  $F_4$  folding) corresponding to an orientation of  $010^\circ 80^\circ$  SE.

37 points, contours at 0.70, 1.41, 2.81, 5.63, 11.25; maximum 12.16%.

$S_1$ ,  $L_1$  and  $S_0/S_1$  RELATIONS,  $S_{1N}$  DOMAIN

Subarea 1. (Fig. 3B). Poles to  $S_1$  plot as a point maximum, indicating an orientation of  $025^\circ 87^\circ$  SE.

37 points, contours at 2.27, 4.53, 9.06, 18.13, 36.25; maximum 39.19%.

Subarea 2. (Fig. 3C). Poles to  $S_1$  plot as a point maximum indicating an orientation of  $025^\circ 80^\circ$  SE.

51 points, contours at 2.10, 4.19, 8.39, 16.78, 33.55; maximum 36.27%.

Subarea 1. (Fig. 3D).  $L_1$  mineral and aggregate lineations plunges steeply to the south.

36 points.

Subarea 2. (Fig. 3E).  $L_1$  mineral and aggregate lineation plunges steeply to the south.

13 points.

Subareas 1 and 2 (Fig. 3F).  $S_0/S_1$  intersection changes plunge through the horizontal from south and southwest plunging (dots, subarea 1) to north-east plunging (crosses, subarea 2).

15 points, subarea 1,

6 points, subarea 2.

Subareas 3a and 3b (Fig. 3G). Apollyon chistolite schist, west of Mt Franks Retrograde Schist Zone and north of Mt Franks.

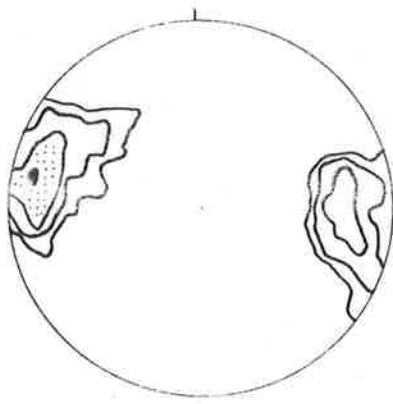
Poles to  $S_1$  indicate an average orientation of  $348^\circ 55^\circ$  SW.

6 points.

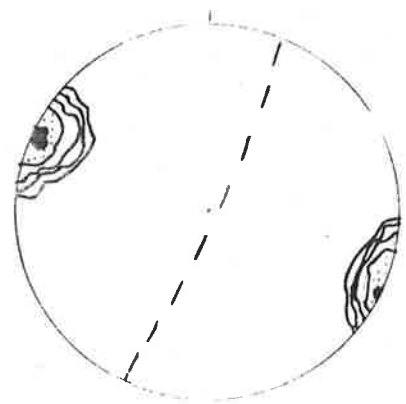
Subarea 3d (Fig. 3H). Robe andalusite schist. Poles to  $S_1$  indicate an orientation of  $004^\circ 86^\circ$  W with a tendency to be folded about a south-west plunging  $F_3$  axis.

79 points, contours at 1.87, 3.73, 7.46, 14.93, 29.86; maximum 32.28%.

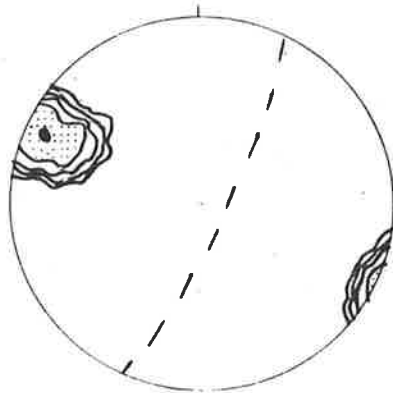
dots =  $F_1$  small folds, and  $S_0/S_1$  intersections.



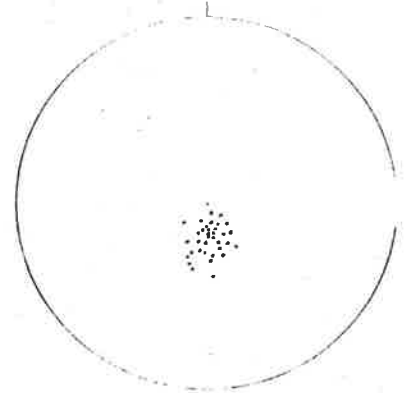
**A**



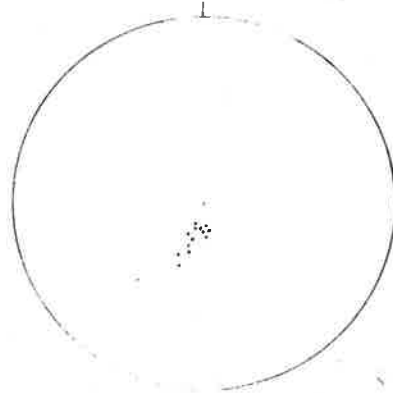
**B**



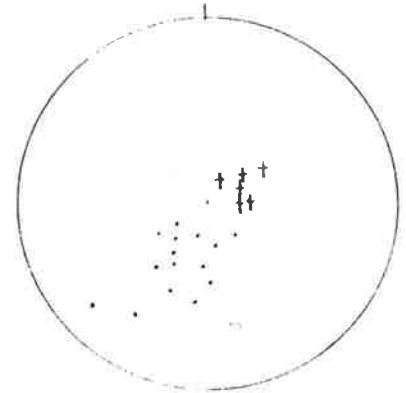
**C**



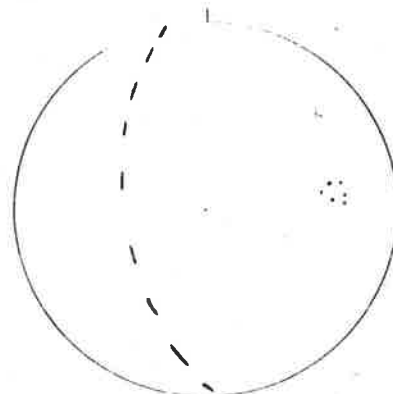
**D**



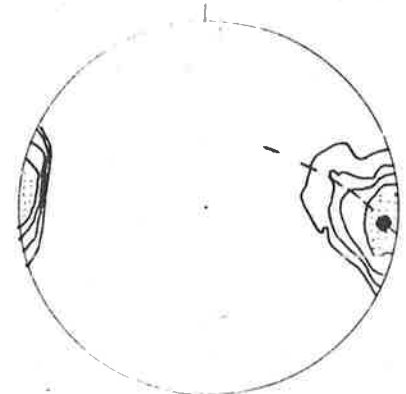
**E**



**F**



**G**



**H**

### S<sub>1</sub> PLOTS, S<sub>1N</sub> DOMAIN

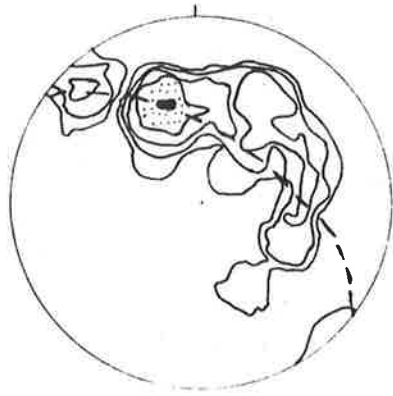
- Subarea 3c (Fig. 4A). Robe andalusite schist. Poles to S<sub>1</sub> are folded about an F<sub>3</sub> axis plunging at 30° to 217°.  
32 points, contours at 0.90, 1.81, 3.61, 7.23, 14.46; maximum 15.62%.
- Subarea 7a (Fig. 4B). South of Mt Franks, Apollyon chiastolite schist. Poles to S<sub>1</sub> have an approximate orientation of 045° 85° NW.  
20 points, contours at 0.91, 1.83, 7.30; maximum 14.61%.
- Subarea 12 (Fig. 4C). South of area. Poles to S<sub>1</sub> indicate an orientation of 055° 88° NW.  
79 points, contours at 1.02, 2.05, 4.10, 8.20, 16.39; maximum 17.29%.

### F<sub>1</sub>, S<sub>0</sub>/S<sub>1</sub> PLOTS, S<sub>1N</sub> DOMAIN

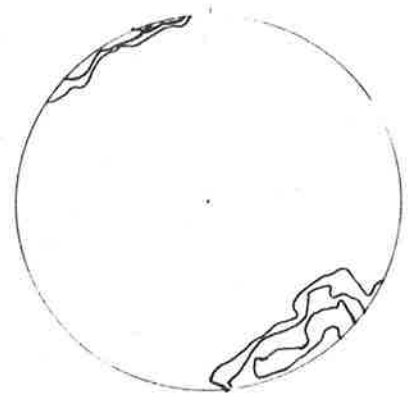
- Subareas 3b, 3c (Fig. 4D). North of Mt Franks. S<sub>0</sub>/S<sub>1</sub> lineations plunge to the southwest at moderate angles.  
8 points.
- Subarea 6a (Fig. 4E). S<sub>0</sub>/S<sub>1</sub> intersections, south of Mt Franks, Apollyon andalusite schist. Intersection lineations change plunge (from north to south) from gently south plunging to gently north plunging.  
37 points, contours at 1.02, 2.03, 4.06, 8.13, 16.25; maximum 17.57%.
- Subareas 6b, 7a (Fig. 4F). S<sub>0</sub>/S<sub>1</sub> intersections change orientation from gently south plunging to north plunging.  
22 points, contours at 0.79, 1.58, 3.15, 6.31, 12.61; maximum, 13.64%.

### D<sub>3</sub> DEFORMATION

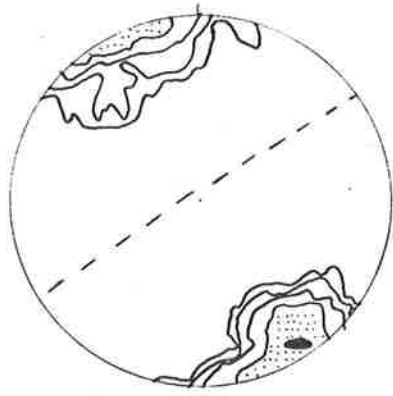
- Subarea 1 (Fig. 4G). Poles to S<sub>3</sub> indicate a statistical orientation of 039° 86° E.  
66 points, contours at 2.28, 4.55, 9.11, 18.22, 36.44; maximum 39.39%.
- Subarea 2 (Fig. 4H). Poles to S<sub>3</sub> indicate a statistical orientation of 040° 83° E.  
63 points, contours at 1.93, 3.85, 7.71, 15.42, 30.83; maximum 33.33%.



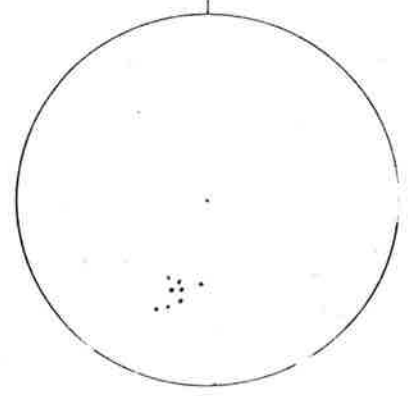
**A**



**B**



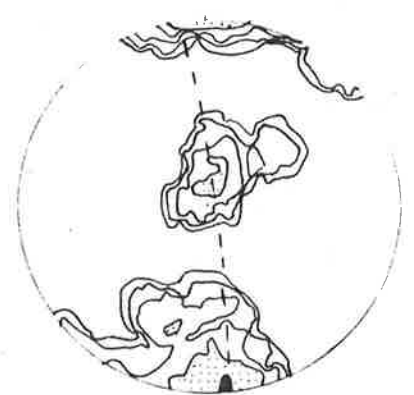
**C**



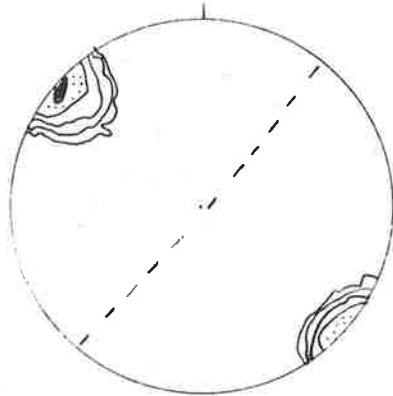
**D**



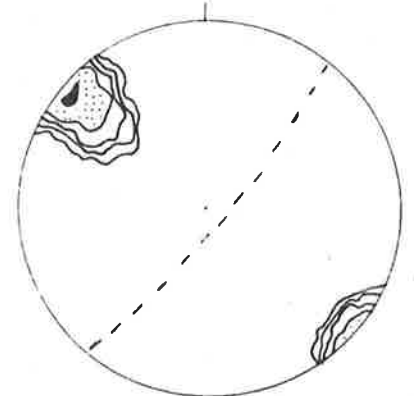
**E**



**F**



**G**



**H**

### D<sub>3</sub> DEFORMATION

Subareas 1 and 2 (Fig. 5A).  $F_3$  folds in  $S_0$  (crosses) are northeast plunging in contrast to  $S_3/S_1$  intersections (crosses and circles) which are southwest plunging and  $L_3$  (dots) which is also southwest plunging.

### D<sub>4</sub>' DEFORMATION

Subarea 1 (Fig. 5B). Poles to  $S_4'$  indicate an orientation of  $057^\circ 90^\circ$ .  
28 points, contours at 2.06, 4.13, 8.26, 16.52, 33.04; maximum 35.71%.

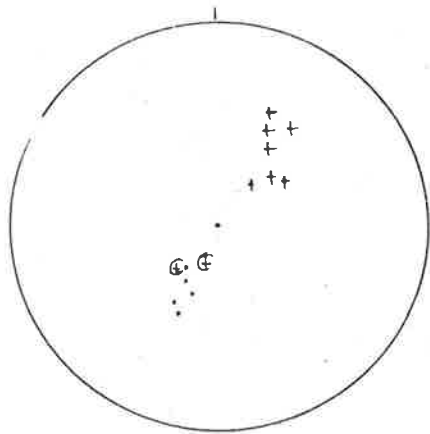
Subarea 2 (Fig. 5C). Poles to  $S_4'$  indicate an orientation of  $060^\circ 82^\circ$  E.  
43 points, contours at 2.15, 4.30, 8.60, 17.21, 34.42; maximum 37.21%.

Subareas 1 + 2 (Fig. 5D). Northeast plunging  $F_4'$  folds (dots) and southeast plunging  $F_4$  folds (dots).  
14 points  $F_4'$ , 10 points  $F_4$ .

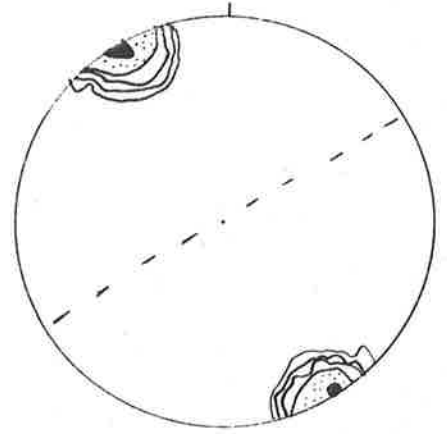
### FABRIC ELEMENTS IN AREAS OF FOLDING

Subarea 8a (Fig. 5E). Anticlinal  $F_1$  hinge. Poles to  $S_0$  (dots = eastern limb, circles = shared limb),  $F_1$  small fold (crosses), axis of folding (X) and  $L_1$  (triangles).

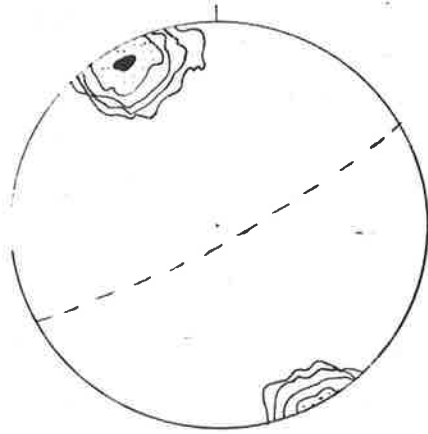
Subarea 8B (Fig. 5F). Synclinal  $F_1$  hinge. Poles to  $S_0$  (dots = western limb, circles = shared limb), axis of folding = X.



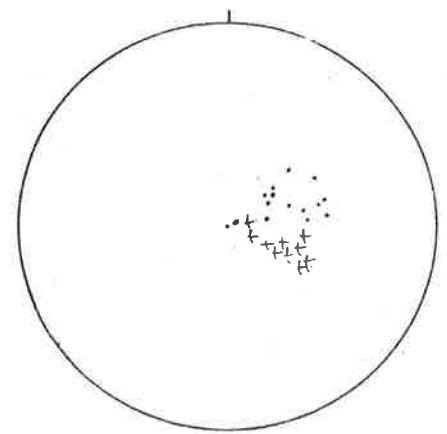
**A**



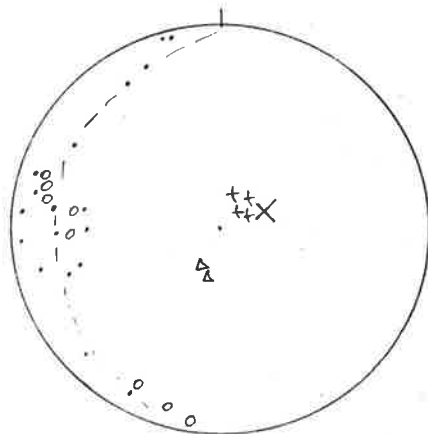
**B**



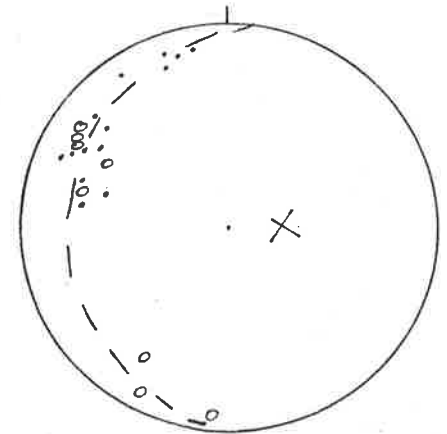
**C**



**D**



**E**



**F**

RELATIONS AROUND F<sub>1</sub> DEXTRAL MT FRANKS FOLD PAIR - ROBE BEDS

Eastern limb (Fig. 6A). Summary S<sub>0</sub>/S<sub>1</sub> relations.

S<sub>0</sub>/S<sub>1</sub> relations are south plunging dextral.

Subarea 3c (Fig. 6B). Poles to S<sub>3</sub> indicate an orientation of 038° 90°.

S<sub>0</sub>/S<sub>3</sub> relations are north plunging sinistral, incongruent to the fold.

52 points, contours at 2.78, 5.56, 11.12, 22.24, 44.47; maximum 48.08%.

Subarea 3d (Fig. 6C). Poles to S<sub>3</sub> indicate an orientation of 036° 85° E.

34 points, contours at 2.47, 4.93, 9.86, 19.72, 39.45; maximum 42.65%.

Subareas 3c + 3d (Fig. 6D). Poles to S<sub>3</sub>' indicate an orientation of 021° 89° v

S<sub>0</sub>/S<sub>3</sub>' relations are southwest plunging dextral.

97 points, contours at 2.74, 5.48, 10.97, 21.93, 43.87; maximum 47.42%.

Eastern limb (Fig. 6E). S<sub>0</sub>/S<sub>3</sub> intersections (observed = dots; calculated = contours) distributed in S<sub>3</sub>.

observed 11 points

calculated 24 points, contours at 0.84, 1.69, 3.37, 6.74, 13.49; maximum 14.58%.

Eastern limb (Fig. 6F). S<sub>0</sub>/S<sub>3</sub>' intersections are southwest plunging at gentle - moderate angles.

12 points, contours at 1.69, 3.37, 6.74, 13.49, 26.98; maximum 29.17%.

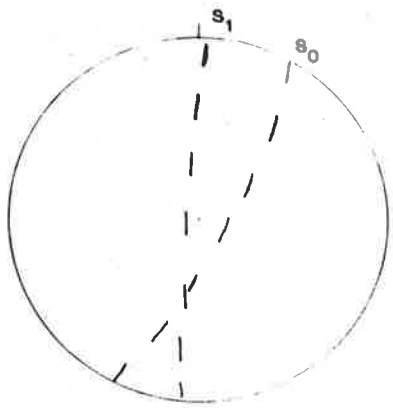
Eastern limb (Fig. 6G). S<sub>1</sub>/S<sub>3</sub> intersections (observed) are

moderately southwest plunging and lie in S<sub>3</sub>.

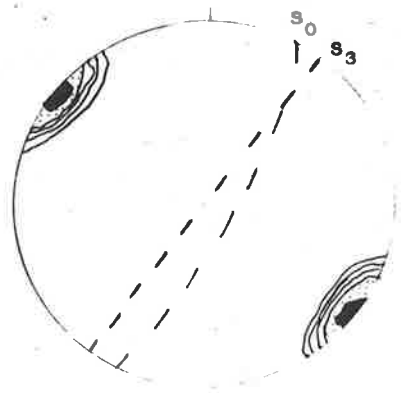
50 points, contours at 1.50, 3.01, 6.01, 12.02, 24.05; maximum 26.00%.

Eastern limb (Fig. 6H). L<sub>3</sub> as a moderately - steeply southwest plunging lineation. Parallel in part to S<sub>1</sub>/S<sub>3</sub> and S<sub>0</sub>/S<sub>3</sub>.

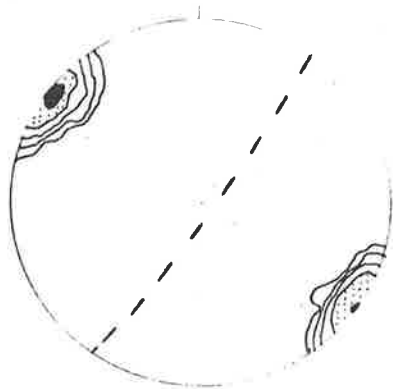
6 points.



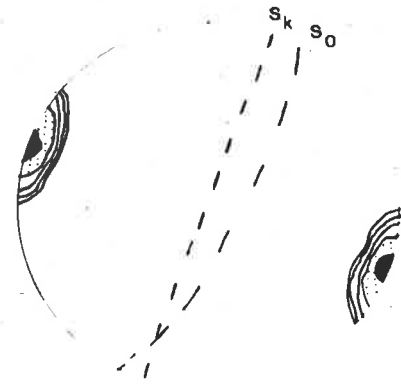
**A**



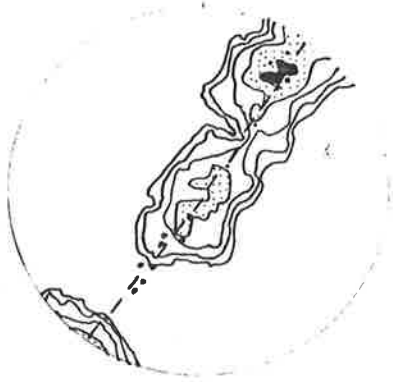
**B**



**C**



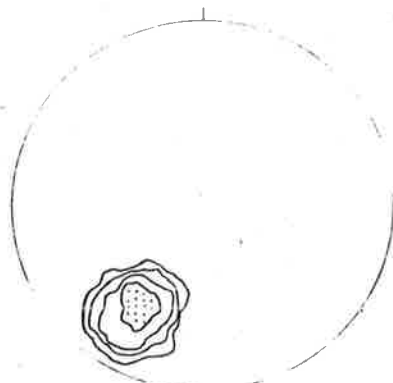
**D**



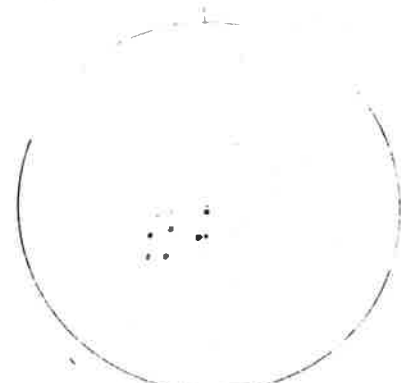
**E**



**F**



**G**



**H**



RELATIONS AROUND  $F_1$  DEXTRAL MT FRANKS FOLD PAIR

Subarea 4c (Fig. 7A). Short limb, main ridge - area of strong  $F_3$  crenulation. Poles to  $S_0$  outline a partial girdle folded about an  $F_1$  axis plunging  $50^\circ$  to  $204^\circ$ .

103 points, contours at 1.07, 2.13, 4.27, 8.53, 17.06; maximum, 18.45%.

Subarea 4b (Fig. 7B). Short limb south of main ridge. Poles to  $S_0$  outline a partial girdle folded about an  $F_1$  axis plunging at  $50^\circ$  to  $204^\circ$ .

63 points, contours at 0.83, 1.65, 3.30, 6.61, 13.21; maximum 14.29%.

Subarea 4c (Fig. 7C). Poles to  $S_1$  in psammite plot as a point maximum (with some tendency to redistribute) indicating an orientation of  $345^\circ$   $45^\circ$  W.

64 points, contours at 1.45, 2.89, 5.78, 11.56, 23.12; maximum 25.00%.

Subarea 4b (Fig. 7D). Poles to  $S_1$  ( $S_{1Ps}$  +  $S_{1Pe}$ ) indicate an  $S_1$  orientation of  $340^\circ$   $44^\circ$  W. The closeness of this value to the value of  $S_{1Ps}$  in subarea 4c suggests there is no refraction or differential rotation.

149 points, contours at 1.38, 2.75, 5.51, 11.02, 22.04; maximum 28.83%.

Subareas 4c + 4b (Fig. 7E).  $S_0/S_1$  intersections from whole of short limb plunge at  $39^\circ$  to  $228^\circ$ .

26 points, contours at 1.45, 2.89, 5.78, 11.56, 23.13; maximum 25.00%.

Subareas 4c + 4b (Fig. 7F). Calculated  $S_0/S_1$  intersections plunge at  $40^\circ$  to  $215^\circ$ .

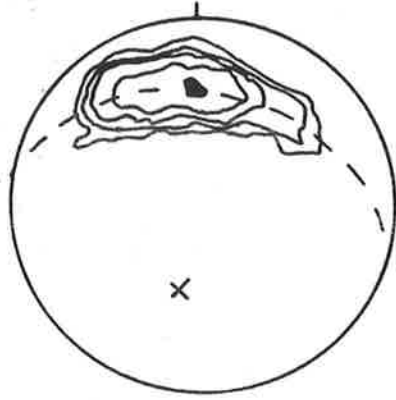
70 points, contours at 1.24, 2.48, 4.96, 9.91, 19.82; maximum 21.43%.

Anticlinal hinge (between subareas 3d, 4b, 4c) (Fig. 7G + Fig. 7H).

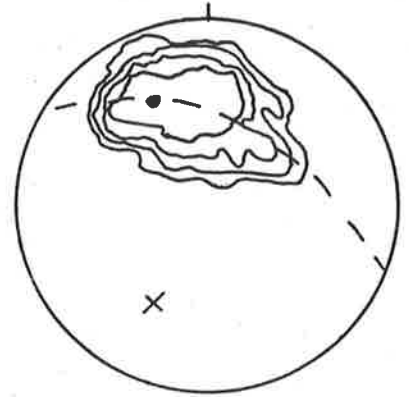
Poles to  $S_0$  indicate an  $F_1$  axis at  $40^\circ$  to  $197^\circ$ . In this area, poles to  $S_1$  indicate an orientation of  $350^\circ$   $52^\circ$  W with a tendency to redistribute about an  $F_3$  axis plunging at  $46^\circ$  to  $211^\circ$ .

Fig. 7G 274 points, contours at 0.61, 1.22, 2.45, 4.90, 9.79; maximum 10.58%.

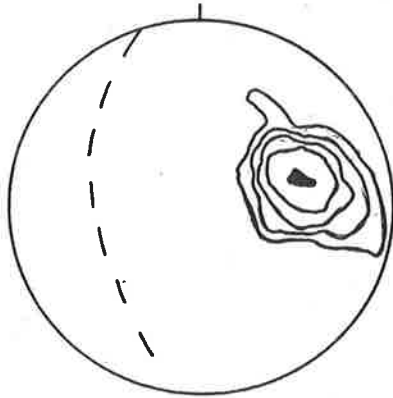
Fig. 7H 71 points, contours at 1.26, 2.52, 5.05, 10.10, 20.19; maximum 21.83%.



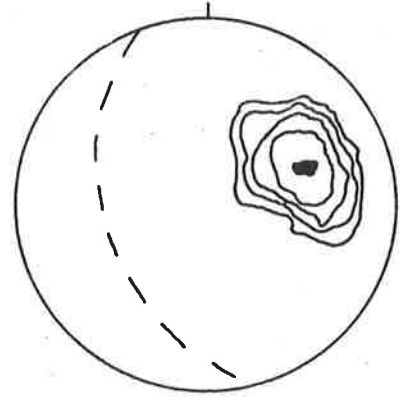
**A**



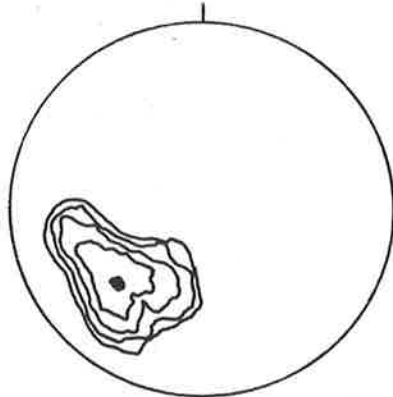
**B**



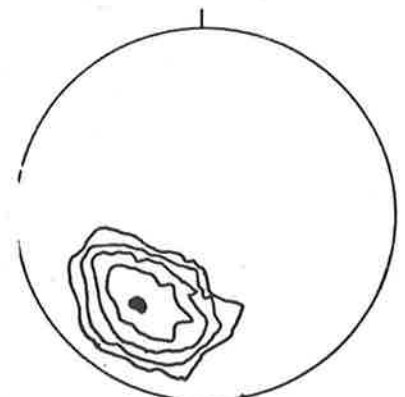
**C**



**D**



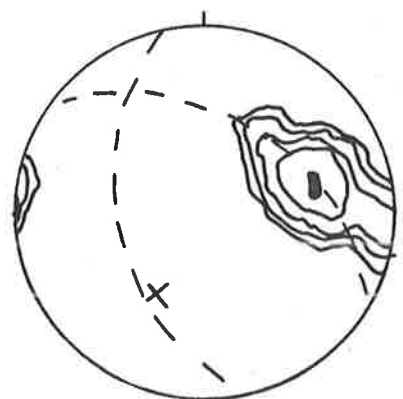
**E**



**F**



**G**



**H**

MT FRANKS FOLD PAIR - SHORT LIMB and ANTICLINAL HINGE

Anticlinal hinge (Fig. 8A). Poles to  $S_1$  in the main ridge indicate an orientation of about  $005^\circ 80^\circ$  W.  
8 points.

D<sub>3</sub> EFFECTS

Subarea 4c (Fig. 8B). Short limb, main ridge. Poles to  $S_3$  indicate an orientation of  $041^\circ, 87^\circ$  E.

99 points, contours at 2.39, 4.79, 9.58, 19.15, 38.31; maximum 41.41%.

Subarea 4b (Fig. 8C). - Short limb excluding main ridge. Poles to  $S_3$  indicate an orientation of  $038^\circ 86^\circ$  E.

28 points, contours at 2.58, 5.16, 10.32, 20.65, 41.29; maximum 44.64%.

Subarea 4c (Fig. 8D). Short limb - main ridge. Poles to  $S_3'$  indicate an orientation of  $037^\circ 84^\circ$  W.

50 points, contours at 1.97, 3.93, 7.86, 15.72, 31.45; maximum 34.00%.

Subarea 4b (Fig. 8E). Short limb excluding main ridge. Poles to  $S_3'$  indicate an orientation of  $023^\circ 80^\circ$  W.

36 points, contours at 1.53, 3.05, 6.10, 12.20, 24.41; maximum 26.39%.

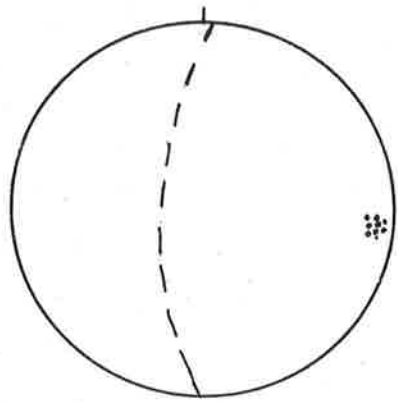
Subarea 4c (Fig. 8F).  $S_0/S_3$  intersections (observed) plunge at  $46^\circ$  to  $220^\circ$ .  
21 points, contours at 2.48, 4.96, 9.91, 19.82, 39.64; maximum 42.86%.

Subarea 4c (Fig. 8G).  $S_0/S_3$  intersections (calculated) plunge at  $44^\circ$  to  $220^\circ$ .

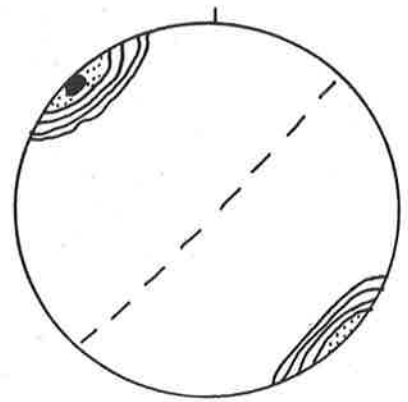
45 points, contours at 1.86, 3.73, 7.45, 14.90, 29.81; maximum 32.22%.

Subarea 4c (Fig. 8H).  $S_0/S_3'$  intersections plunge at  $47^\circ$  to  $208^\circ$ .

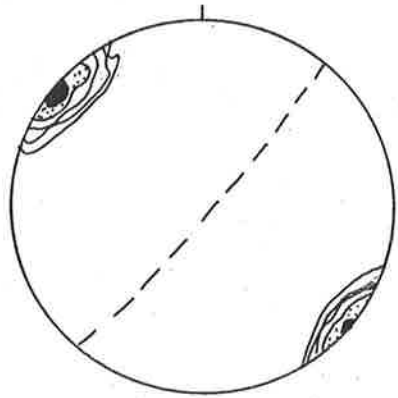
17 points, contours at 1.70, 3.40, 6.80, 13.60, 27.21; maximum 29.41%.



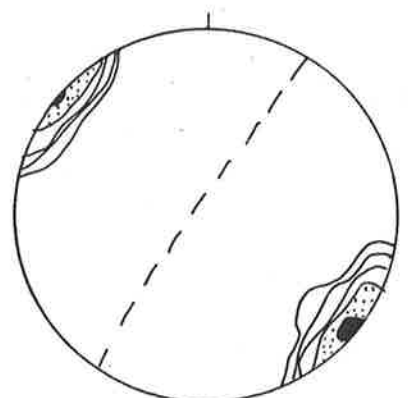
**A**



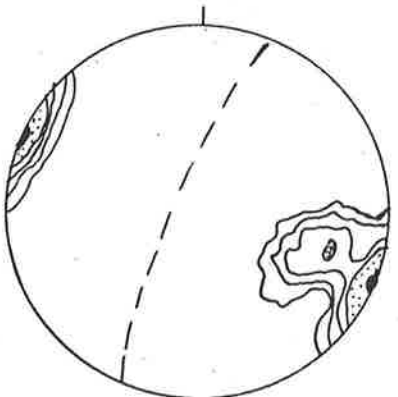
**B**



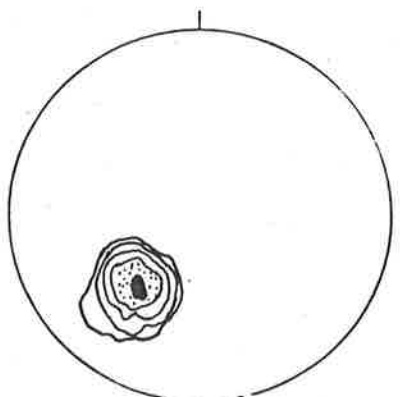
**C**



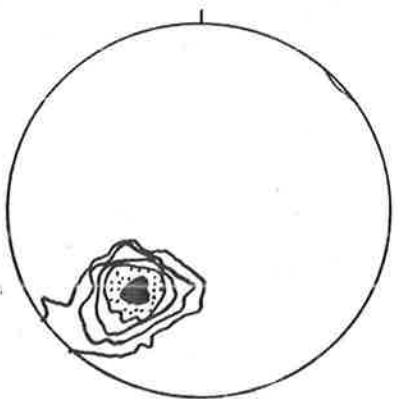
**D**



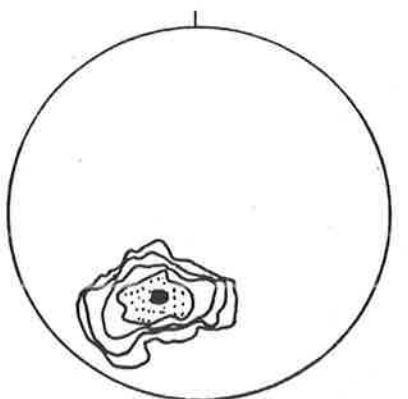
**E**



**F**



**G**



**H**

MT FRANKS FOLD PAIR - SHORT LIMB - D<sub>3</sub> EFFECTS

Subarea 4c (Fig. 9A). Calculated  $S_1/S_3'$  intersections plunge at about  $45^\circ$  to  $208^\circ$ , parallel to observed intersections in the previous figure.  
32 points, contours at 1.26, 2.53, 5.06, 10.12, 20.23; maximum 21.88%.

Subarea 4c (Fig. 9B). Observed  $S_1/S_3$  intersections plunge at  $44^\circ$  to  $232^\circ$ .  
20 points, contours at 1.88, 3.76, 7.52, 15.03, 30.06; maximum 32.50%.

Subarea 4c (Fig. 9C). Calculated  $S_1/S_3$  intersections plunge at  $43^\circ$  to  $224^\circ$ .  
37 points, contours at 1.64, 3.28, 6.56, 13.13, 26.25; maximum 28.38%.

Subareas 4c and 4b (Fig. 9D).  $F_3$  folds in  $S_1$  plunge at  $39^\circ$  to  $229^\circ$ .  
32 points, contours at 1.17, 2.35, 4.70, 9.39, 18.79; maximum 20.31%.

Subareas 3d + 4c + 4b (Anticlinal hinge). (Fig. 9E). Poles to  $S_3'$  indicate an orientation of  $029^\circ, 90^\circ$ ; dots represent  $F_3$  small folds.  
31 points, contours at 1.96, 3.92, 7.83, 15.67, 31.33; maximum 33.87%.

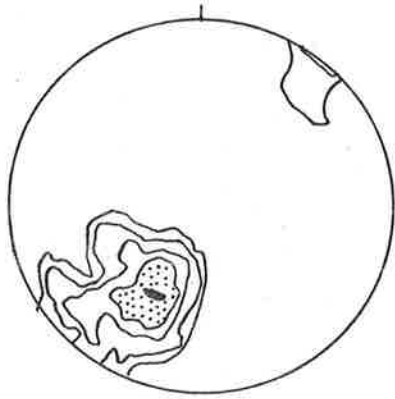
Subareas 3d + 4c + 4b (Anticlinal hinge). (Fig. 9F). Poles to  $S_3$  indicate an orientation of  $040^\circ, 90^\circ$ .  
46 points, contours at 2.26, 4.56, 9.05, 18.10, 36.20, maximum 39.13%.

Subareas 3d + 4c + 4b (Anticlinal hinge). (Fig. 9G).  $F_3$  fold in  $S_1$  in this hinge area define two maxima -  $38^\circ$  to  $209^\circ$ , and  $45^\circ$  to  $231^\circ$ .  
23 points, contours at 1.01, 2.01, 4.02, 8.04, 16.02; maximum 17.39%.

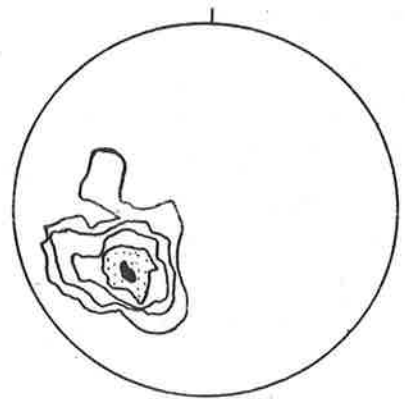
Subareas 3d + 4c + 4b (Anticlinal hinge). (Fig. 9H).  $S_1/S_3$  intersections (crosses) fall within the field of  $F_3$  folds (previous figure)-but do not necessarily lie parallel to  $L_3$  (dots).

12 readings  $S_1/S_3$

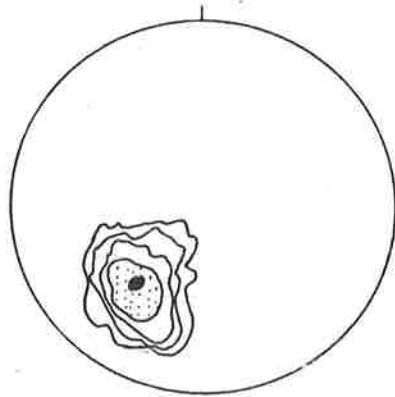
8 readings  $L_3$ .



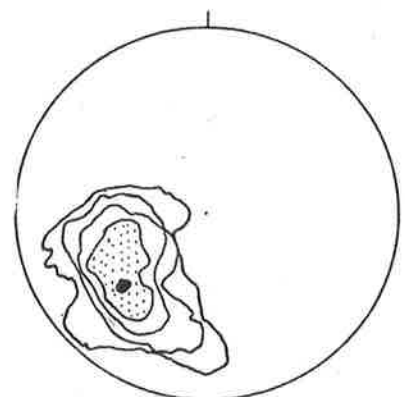
**A**



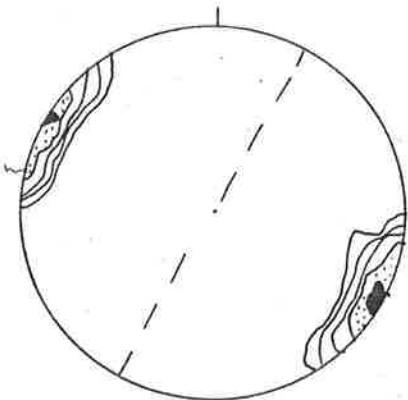
**B**



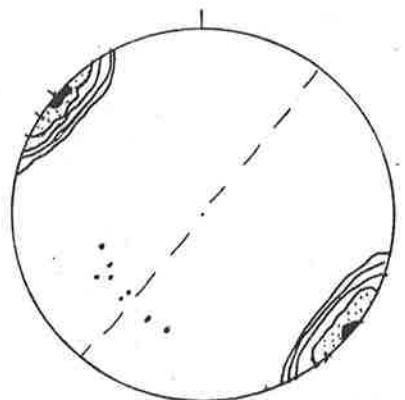
**C**



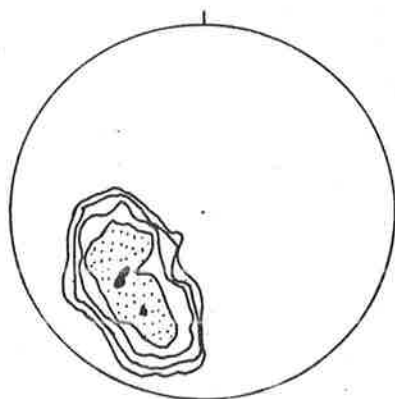
**D**



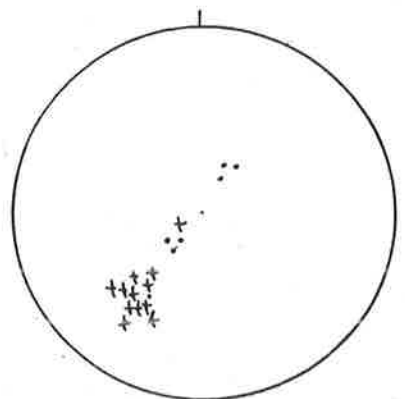
**E**



**F**



**G**



**H**

WESTERN LIMB + SYNCLINAL HINGE

Subarea 5a (Fig. 10B). Poles to  $S_1$  suggest a point maximum indicating an orientation of  $355^\circ 46^\circ$  W despite tendency to refold about an  $F_3$  axis plunging at  $44^\circ$  to  $217^\circ$  and lying in  $S_1$ .

72 points, contours at 0.84, 1.69, 3.37, 6.74, 13.49; maximum 14.58%.

Subarea 5a (Fig. 10C).  $S_0/S_1$  intersections plunge at  $36^\circ$  to  $194^\circ$ .

28 points, contours at 1.03, 2.06, 4.13, 8.26, 16.52; maximum 17.86%.

( $S_0/S_1$  relations in subarea 6c, south of Waterfall Gully shown in text figure here.  $S_0$  dips west at about  $70-80^\circ$  whereas  $S_1$  dips west at  $50-60^\circ$ ).

Subareas 5b + 4b + 4c (synclinal hinge). (Fig. 10D). Poles to  $S_0$  indicate an orientation of the  $F_1$  hinge of  $40^\circ$  to  $193^\circ$ .

27 points, contours at 0.72, 1.43, 2.87, 5.74, 11.48; maximum 12.41%.

Subarea 5a (Fig. 10E). Poles to  $S_3$  indicate an orientation of  $037^\circ 74^\circ$  E.

$F_3$  folds (crosses) and  $L_3$  lineations (dots) are southwest - south plunging at various angles;  $L_3$  is generally steeper than  $F_3$ .

49 points, contours at 2.01, 4.01, 8.02, 16.05, 32.0(; maximum 34.69%.

$L_3$  - 7 points

$f_3$  - 9 points.

Subarea 5a (Fig. 10F). Poles to  $S_3'$  indicate an orientation of  $036^\circ 90^\circ$ .

62 points, contours at 2.52, 5.04, 10.07, 20.14, 40.28; maximum 43.55%.

Subarea 5a (Fig. 10G).  $S_0/S_3$  intersections are distributed in a plane oriented at  $040^\circ 70^\circ$  E ( $S_3$ ).

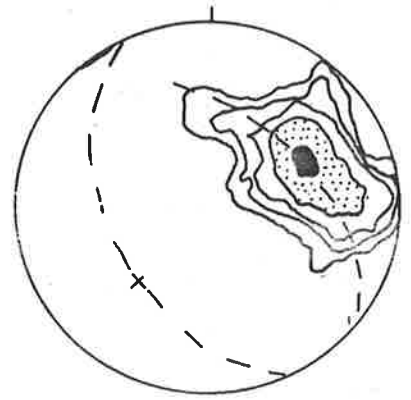
17 points, contours at 0.68, 1.36, 2.72, 5.44, 10.88; maximum 11.76%.

Subarea 5a (Fig. 10H). Calculated  $S_0/S_3'$  intersections are distributed in  $S_3'$ . ( $034^\circ 90^\circ$ ).

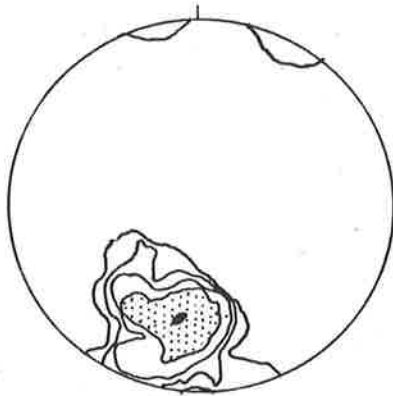
22 points, contours at 1.05, 2.10, 4.20, 8.41, 16.82; maximum 18.18%.



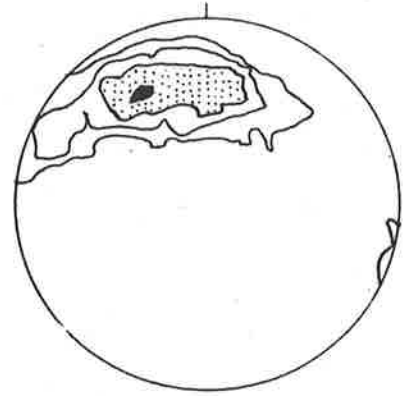
**A**



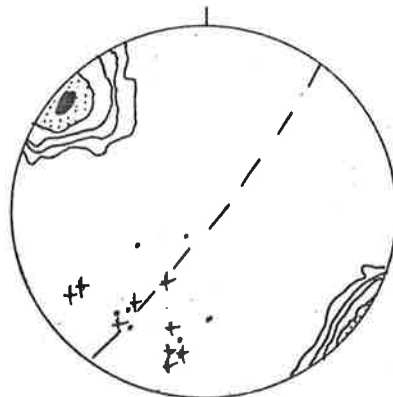
**B**



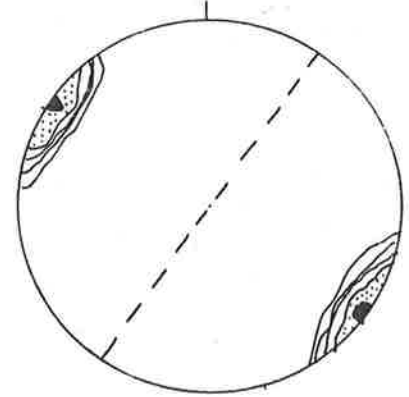
**C**



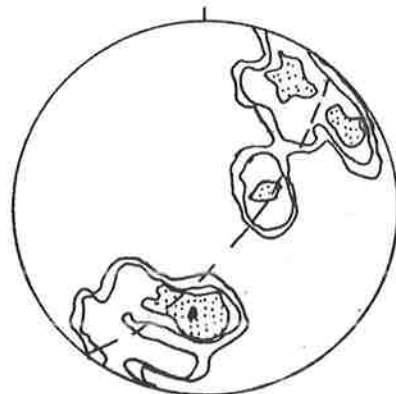
**D**



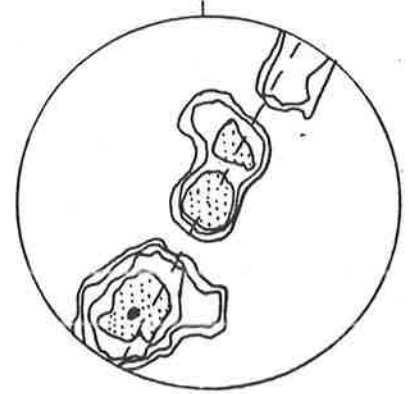
**E**



**F**



**G**



**H**



RELATIONS AROUND F<sub>1</sub> DEXTRAL MT FRANKS FOLD PAIR -

APOLLYON CHIASTOLITE SCHIST

Subarea 3d (east limb) (Fig. 11A). S<sub>0</sub> strikes 029° 74° SE, and has a dextral south plunging intersection with S<sub>1</sub> (348° 55° SW).

Subarea 3d (Fig. 11B). Poles to S<sub>3</sub> indicate an orientation of 035° 90°. 41 points, contours at 2.75, 5.50, 11.00, 22.00, 43.99; maximum 47.56%.

Subarea 3d (Fig. 11C). Poles to S<sub>3</sub>' indicate an orientation of 022° 88° W. 42 points, contours at 2.48, 4.96, 9.91, 19.82, 39.64; maximum 42.86%.

Subarea 3d (Fig. 11D). S<sub>0</sub>/S<sub>3</sub> intersections (crosses) plunge to the northeast; S<sub>0</sub>/S<sub>3</sub>' intersections (circles) plunge to the southwest; L<sub>3</sub> (dots) plunges steeply south.

Subarea 3d (Fig. 11E). S<sub>0</sub>/S<sub>3</sub>' intersections plunge shallowly to the southwest.

17 points, contours at 2.38, 4.76, 9.52, 9.04, 38.09; maximum 41.18%.

Subareas 3d + 4a + 6b (Fig. 11F). Whole fold. Poles to S<sub>0</sub> are folded about an F<sub>1</sub> axis plunging at 30° to 209°. This axis lies within the field of small F<sub>1</sub> folds (crosses).

S<sub>0</sub> 25 points, contours at 0.81, 1.62, 3.24, 6.47, 12.95, maximum 14.00%.

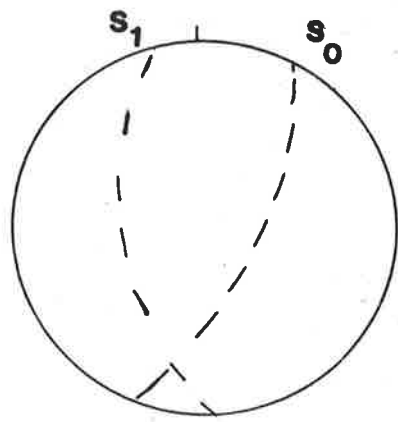
F<sub>1</sub> 10 points.

Subareas 3d + 4a + 6b (Fig. 11G) - whole fold. Poles to S<sub>1</sub> are folded around a southwest plunging F<sub>3</sub> axis lying in S<sub>1</sub>. Two maxima can still be recognised - one at 015° 72° W (unrotated) and the other at 344° 54° W (rotated).

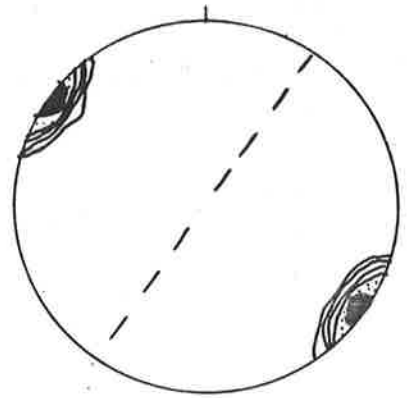
18 points, contours at 1.61, 3.21, 6.42, 12.85, 25.69; maximum 27.78%.

Subareas 3d + 4a + 6b (Fig. 11H). - whole fold. Poles to S<sub>3</sub> indicate an orientation of 032° 88° E. 7 S<sub>0</sub>/S<sub>3</sub> intersections (crosses) plunge to the SW at 20° to 215°.

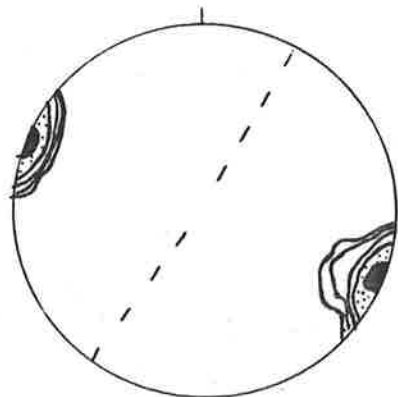
21 points, contours at 2.06, 4.13, 8.26, 16.52, 33.04; maximum 35.71%.



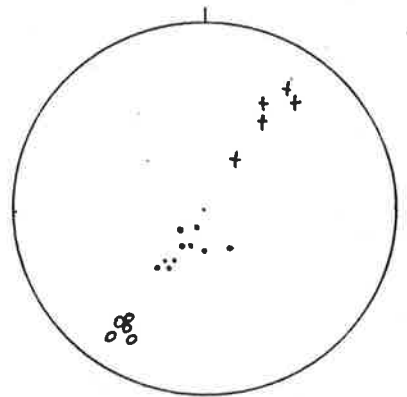
**A**



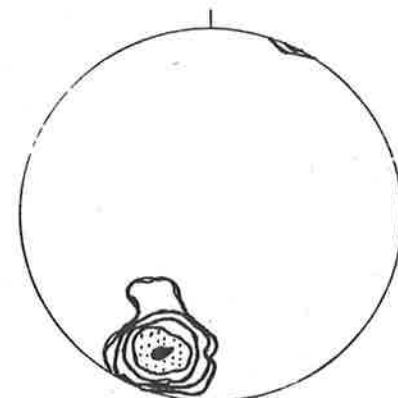
**B**



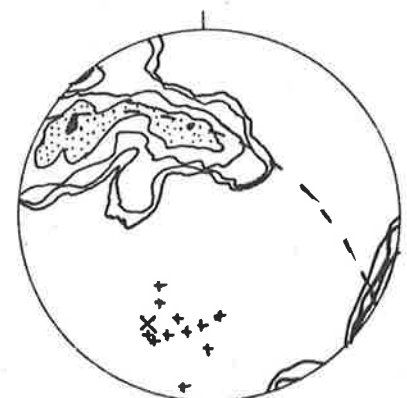
**C**



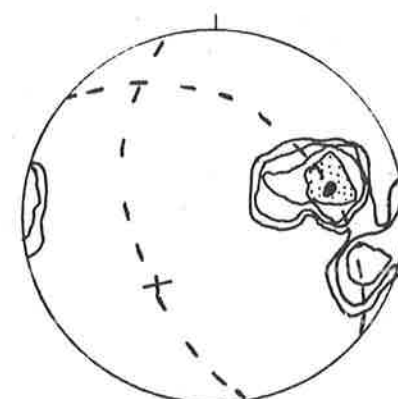
**D**



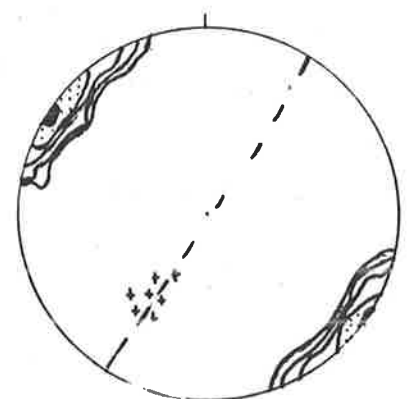
**E**



**F**



**G**



**H**

### S<sub>1N</sub> DOMAIN

Subarea 10. (Fig. 12A). Poles to S<sub>0</sub> show a partial girdle reflecting F<sub>3</sub> folding, and are folded around an axis plunging at 40° to 215°. 56 points, contours at 0.83, 1.65, 3.30, 6.61, 13.21; maximum 14.29%.

Subarea 10 (Fig. 12B). Poles to S<sub>1</sub> show a partial girdle about an F<sub>3</sub> axis plunging at 34° to 215°. This axis lies within the field of small F<sub>3</sub> folds (dots) and S<sub>1</sub>/S<sub>3</sub> intersections (crosses). 109 points, contours at 0.80, 1.59, 3.18, 6.36, 12.73; maximum 13.76%.

Subarea 10 (Fig. 12C). Poles to S<sub>3</sub> plot as a point maximum, indicating an orientation of 040° 90°. 15 points, contours at 1.54, 3.08, 6.17, 12.33, 24.67; maximum 26.67%.

Subarea 11a (Fig. 12D). Poles to S<sub>0</sub> indicate a point maximum at 044° 64° W with minor redistribution. 43 points, contours at 0.81, 1.61, 3.23, 6.45, 12.91; maximum 13.95%.

Subarea 11a (Fig. 12E). Poles to S<sub>1</sub> indicate an orientation of 049° 67° W. (Sampling bias is responsible for its steeper dip than S<sub>0</sub>). S<sub>1</sub> is partially refolded about an SW plunging F<sub>3</sub> axis which lies in the field of F<sub>3</sub> small folds (crosses). triangles = L<sub>1</sub>. 34 points, contours at 1.11, 2.21, 4.42, 8.84, 17.68; maximum 19.12%.

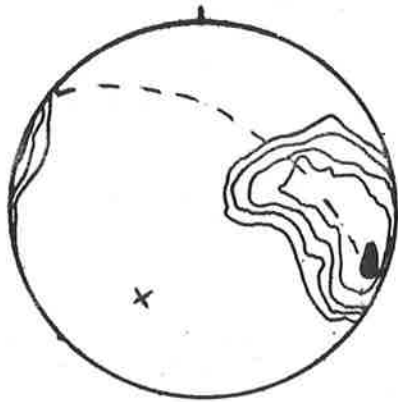
### S<sub>1P</sub> DOMAIN

Subarea 11b - poles to S<sub>0</sub>//S<sub>1</sub> parallel to poles to S<sub>1</sub> in subarea 11a.

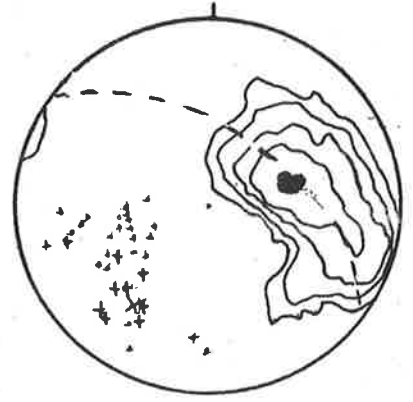
Subarea 13 (Fig. 12F). Poles to S<sub>0</sub> are folded around an F<sub>3</sub> axis plunging at 36° to 231° and lying in S<sub>1</sub>. Despite this a pre-folding S<sub>0</sub> orientation of 337° 38° W is suggested. 110 points, contours at 0.63, 12.6, 2.52, 5.05, 10.0(; maximum 10.91%.

Subarea 13 (Fig. 12G). Poles to S<sub>1</sub> are folded around an F<sub>3</sub>, southwest plunging axis which lies in S<sub>1</sub>. Despite this, an approximate pre-folding S<sub>1</sub> orientation of 345° 40° W is suggested. 89 points, contours at 0.55, 1.10, 2.25, 4.42, 8.83; maximum 9.95%.

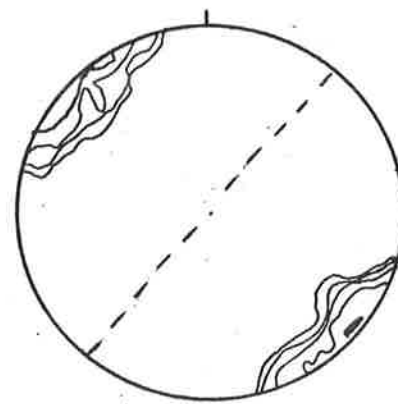
Subarea 13 (Fig. 12H). F<sub>3</sub> folds and S<sub>1</sub>/S<sub>3</sub> intersections plunge at 23° to 238°. Poles to S<sub>3</sub> indicate an approximate orientation of 040° 85° W. 17 points, contours at 1.36, 2.27, 5.44, 10.88, 21.76; maximum 23.53%.



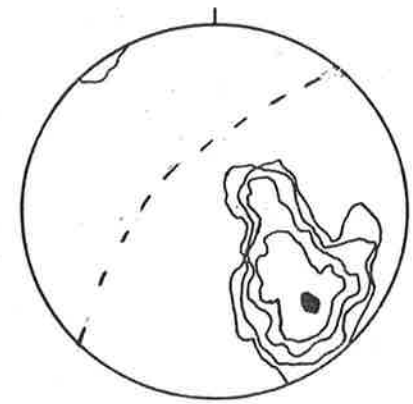
**A**



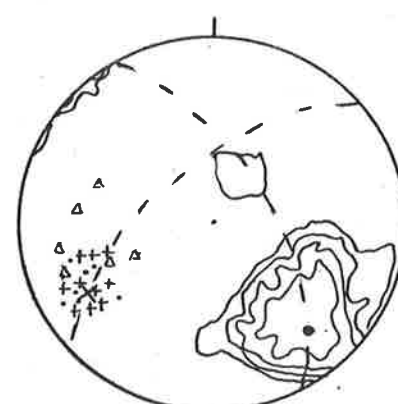
**B**



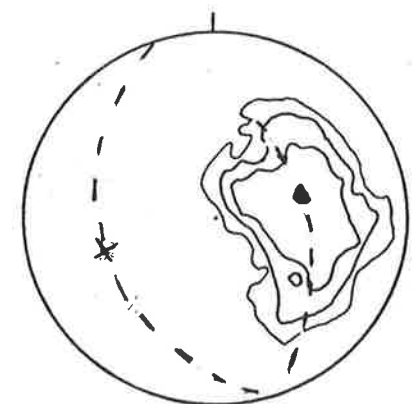
**C**



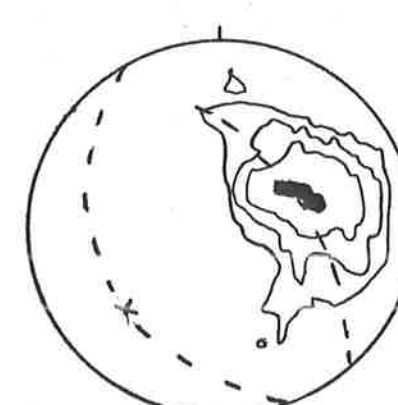
**D**



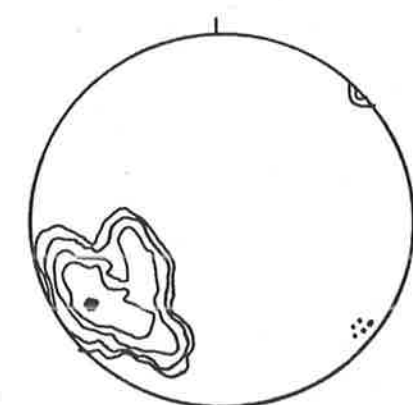
**E**



**F**



**G**



**H**

S<sub>1</sub>P DOMAIN

Subarea 14 (Fig. 13A). Poles to  $S_0$  are folded around an  $F_3$  axis plunging at  $30^\circ$  to  $212^\circ$ .

30 points, contours at 0.48, 0.96, 1.93, 3.85, 7.71; maximum 8.33%.

Subarea 14 (Fig. 13B). Poles to  $S_1$  are folded around an  $F_3$  axis plunging at  $26^\circ$  to  $217^\circ$ .

27 points, contours at 0.75, 1.50, 3.00, 6.00, 11.99; maximum, 12.96%.

Subarea 14 (Fig. 13C). Poles to  $S_0 + S_1$  define an axis of curvature plunging at  $30^\circ$  to  $213^\circ$ .

51 points, contours at 0.57, 1.13, 2.27, 4.53, 9.07; maximum 9.80%.

Subarea 14 (Fig. 13D).  $S_1 / S_3$  intersections plunge at  $33^\circ$  to  $234^\circ$ .

13 points, contours at 2.00, 4.00, 8.00, 16.01, 32.02; maximum 34.62%.

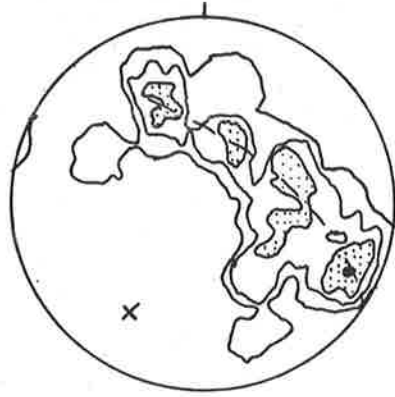
Subarea 15 (Fig. 13E). Poles to  $S_0 + S_1$  define a girdle folded about an  $F_3$  axis plunging at  $60^\circ$  to  $220^\circ$ .

69 points, contours at 0.46, 0.92, 1.84, 3.69, 7.37; maximum 7.97%.

Subarea 15 (Fig. 13F). Small scale  $F_3$  folds (crosses) plunge to the southwest, and lie in  $S_3$ . Diagonal cross represents axis to  $S_0$  poles in previous figure. Poles to  $S_3$  (dots) indicate an approximate  $S_3$  orientation of  $040^\circ$   $90^\circ$ .

Subarea 15 (Fig. 13G).  $F_4$  fold pair in eastern limb of fold.

Subarea 15 (Fig. 13H). Poles to  $S_0 + S_1$  indicate an  $F_4$  axis of folding plunging at  $67^\circ$  to  $291^\circ$ , lying in  $S_4$  (dashed).



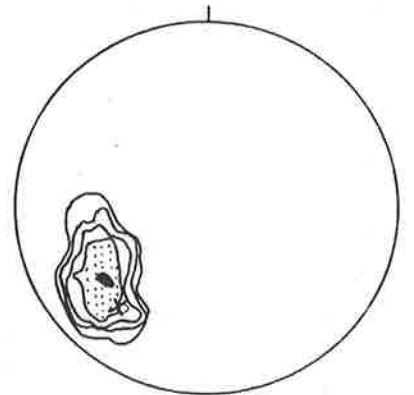
**A**



**B**



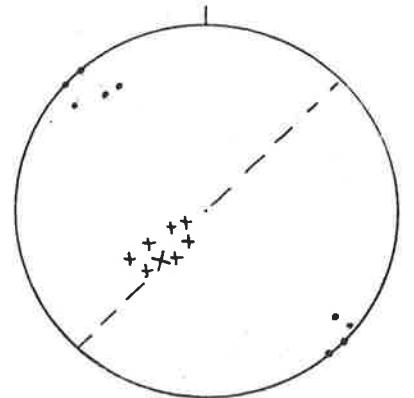
**C**



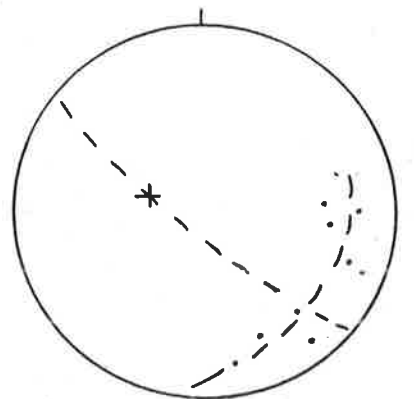
**D**



**E**



**F**



**H**

Subarea 16 (Fig. 14A). Poles to  $S_0 + S_1$  are folded about a poorly defined  $F_3$  axis.

18 points, contours at 0.64, 1.28, 2.57, 5.14, 10.28; maximum at 11.11%.

Subarea 16 (Fig. 14B). Poles to  $S_3$  indicate an orientation of  $035^\circ 90^\circ$ .

Subarea 17 (Fig. 14C). Poles to  $S_0 + S_1$  define a girdle folded around an  $F_3$  axis plunging at  $60^\circ$  to  $223^\circ$ .

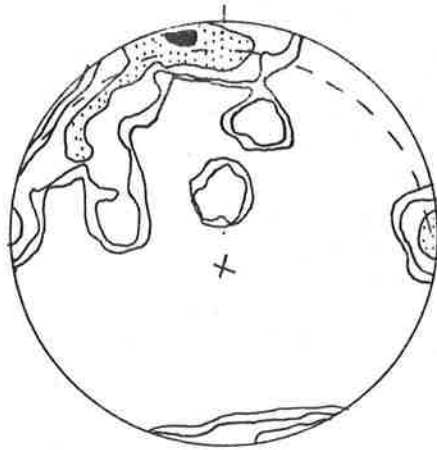
68 points, contours at 0.47, 0.94, 1.87, 3.74, 7.48; maximum 8.09%.

Subarea 17 (Fig. 14D). Poles to  $S_3$  indicate a swing in  $S_3$  orientation with one maximum at  $008^\circ 80^\circ E$ , and another at  $035^\circ 80^\circ E$ .

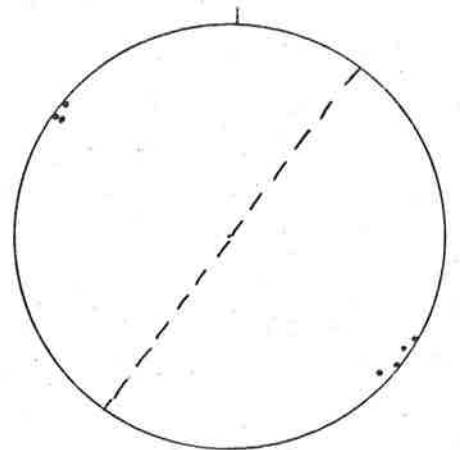
Subarea 18 - see text.

Subarea 19 (Fig. 14E). Poles to  $S_0 + S_1$  define two limbs of an  $F_3$  antiform (dots = western limb, circles = southern limb) folded about an  $F_3$  axis plunging at  $58^\circ$  to  $246^\circ$ . This axis lies within the field of small  $F_3$  folds (crosses) and the field of  $L_1$ .

Subarea 20 (Fig. 14F). Poles to  $S_0 + S_1$  define a girdle around a southwest plunging  $F_3$  axis which lies in the field of small  $F_3$  folds.



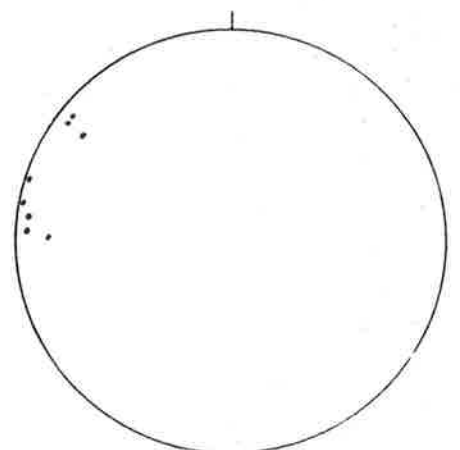
**A**



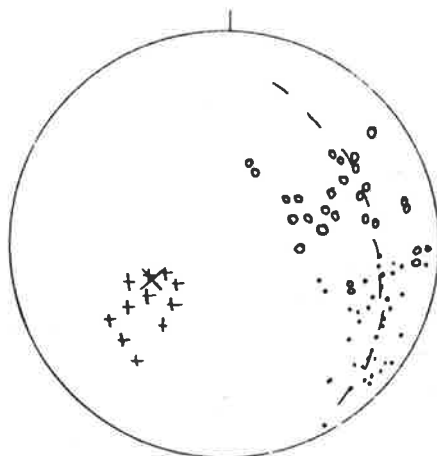
**B**



**C**



**D**



**E**



S<sub>1</sub>P DOMAIN

Subarea 21 (Fig. 15A). Poles to S<sub>0</sub> indicate an orientation of 074° 78° W.  
18 points, contours at 2.09, 4.18, 8.35, 16.70, 32.40; maximum 36.11%.

Subarea 21a (Fig. 15B). Poles to S<sub>1</sub> indicate an orientation of 072° 76° W.  
28 points, contours at 1.45, 2.89, 5.78, 11.56, 23.13; maximum 25.00%.

Subarea 21b (Fig. 15C). Poles to S<sub>0</sub> define a partial girdle about an F<sub>3</sub> axis plunging at 32° to 230°. Despite F<sub>3</sub> folding, the maximum concentration of S<sub>0</sub> poles indicates a dominant orientation of S<sub>0</sub> of 084° 32° S.  
21 points, contours at 1.10, 2.20, 4.40, 8.81, 17.62; maximum at 19.05%.

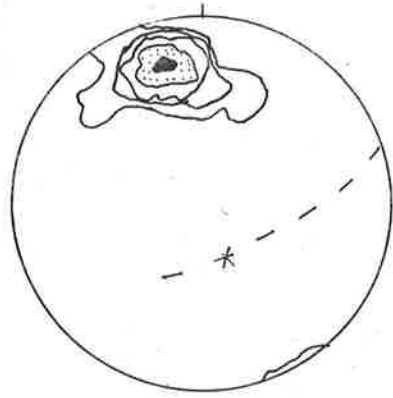
Subarea 21b (Fig. 15D). Poles to S<sub>1</sub> define a girdle about an F<sub>3</sub> axis (33° to 232°). This axis lies in the field of small F<sub>3</sub> folds (crosses) and S<sub>1</sub>/S<sub>3</sub> intersections (dots). The two maxima of S<sub>1</sub> correspond to a long limb orientation (076° 56° S) and a short limb orientation (333° 35° SW).  
25 points, contours at 1.16, 2.31, 4.63, 9.25, 18.50; maximum 20.00%.

Subarea 22 (Fig. 15E). Crosses indicate change of plunge of F<sub>3</sub> folds through the horizontal. Southwest plunging F<sub>3</sub> folds in the south shallow to the northeast to become northeast plunging. Poles to S<sub>3</sub> indicate an orientation of 038° 90°

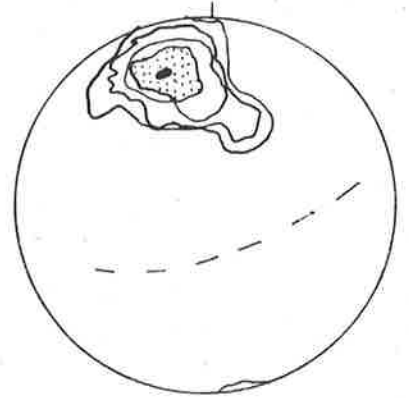
Subarea 23 - see text figures.

Subarea 24 (Fig. 15F). Poles to S<sub>0</sub> define a girdle about an ?F<sub>4</sub> axis plunging at about 50° to 123°  
14 points, contours at .83, 1.65, 3.30, 6.61, 13.21; maximum 14.29%.

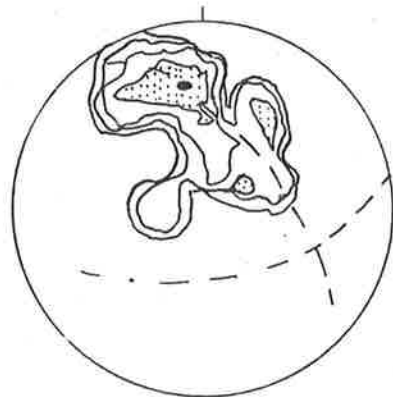
Subarea 24 (Fig. 15G). Poles to S<sub>4</sub>' indicate an orientation of  
18 points, contours at 1.93, 3.85, 7.71, 15.42, 30.83; maximum 33.33%.



**A**



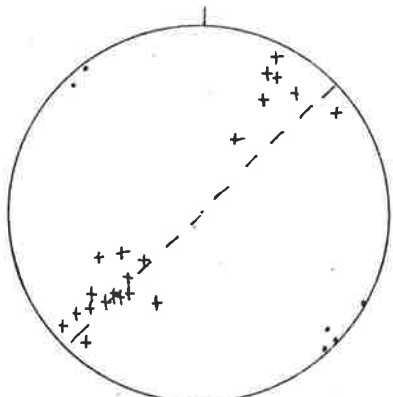
**B**



**C**



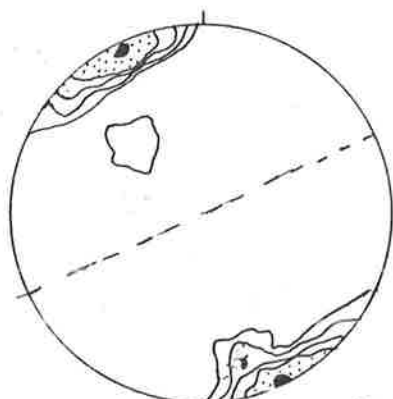
**D**



**E**



**F**



**G**

S<sub>1P</sub> DOMAIN - EASTERN BLOCK

Subarea 25 (Fig. 16A). Poles to  $S_0 + S_1$  in the Parnell Beds indicate a general northeasterly trend and southeasterly dip.  
43 points.

Subarea 25 (Fig. 16B). Plunge of minor  $F_3$  (crosses) and  $F_4$  (circles) folds in Parnell Beds. Trend of  $S_3$  also shown. Note variable plunge of  $F_3$  folds.

Subarea 25 (Fig. 16C). Poles to  $S_0 + S_1$  around a parasitic  $F_3$  hinge in Parnell Beds.  $F_3$  axis plunges at about  $20^\circ$  to  $020^\circ$ .

MT FRANKS RETROGRADE SCHIST ZONE

Fig. 16D. Poles to  $S_R$  in retrograde zone plot as a point maximum, indicating an orientation of  $039^\circ$   $90^\circ$ .

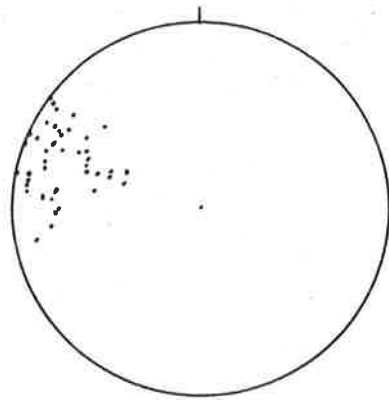
71 points, contours at 2.24, 4.48, 8.96, 17.91, 35.83; maximum 38.73%.

Fig. 16E. Mineral lineation ( $L_M$ ) in  $S_R$  plunges at  $70^\circ$  to  $211^\circ$ .

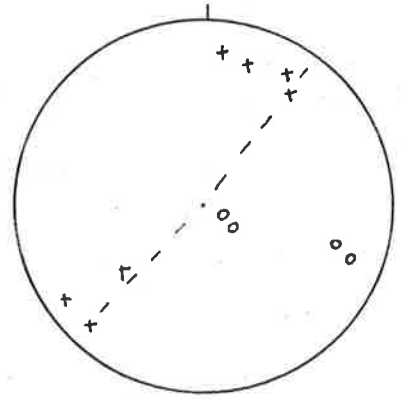
32 points, contours at 1.72, 3.43, 6.87, 13.73, 27.46; maximum 29.69%.

Fig. 16F. Crenulations and folds in  $F_R$  define an elongate maximum. One lobe plunges at  $65^\circ$  to  $106^\circ$ ; the other plunges at  $82^\circ$  to  $248^\circ$ .

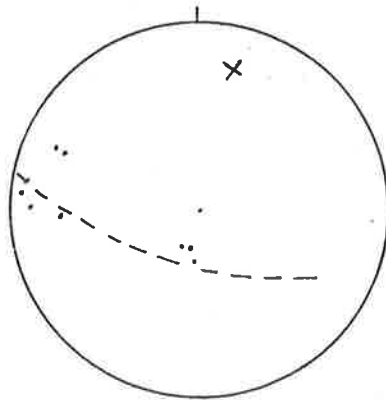
37 points, contours at 1.09, 2.19, 4.38, 8.75, 17.50; maximum 18.92%.



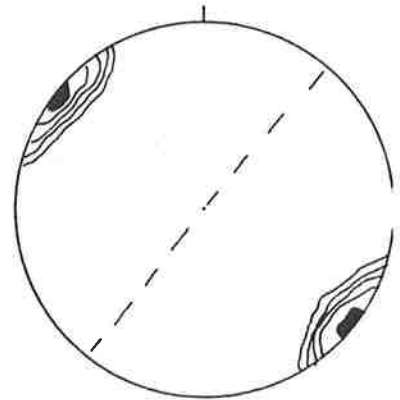
**A**



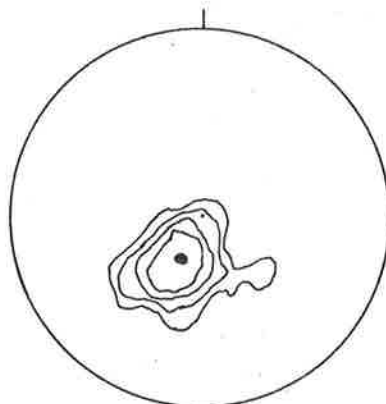
**B**



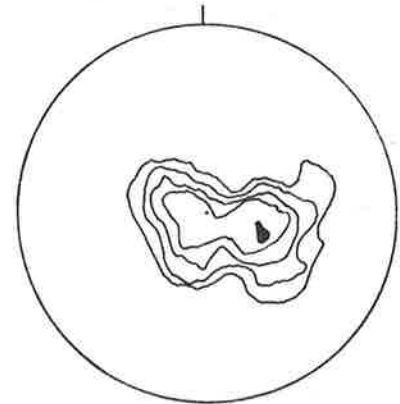
**C**



**D**



**E**



**F**

Glen, R.A. and Laing, W.P.(1975) The significance of sedimentary structures in the Willyama Complex, New South Wales.  
*Australasian Institute of Mining and Metallurgy Proceedings no. 256, pp. 15-20, December 1975.*

NOTE: This publication is included in the print copy of the thesis held in the University of Adelaide Library.